Doctoral Dissertations   Graduate School

Spring 2009

A theoretical study of methanol oxidation mechanisms by methanol dehydrogenase enzymes for fuel cell applications

Nagesh B. Idupulapati
Louisiana Tech University

A THEORETICAL STUDY OF METHANOL OXIDATION

MECHANISMS BY METHANOL DEHYDROGENASE

ENZYMES FOR FUEL CELL APPLICATIONS

by

Nagesh B. Idupulapati, M.S.

A Dissertation Presented in Partial Fulfillment
of the Requirements for the Degree
Doctor of Philosophy

COLLEGE OF ENGINEERING AND SCIENCE

LOUISIANA TECH UNIVERSITY

May 2009

UMI Number: 3358247

INFORMATION TO USERS

The quality of this reproduction is dependent upon the quality of the copy
submitted. Broken or indistinct print, colored or poor quality illustrations
and photographs, print bleed-through, substandard margins, and improper
alignment can adversely affect reproduction.
In the unlikely event that the author did not send a complete manuscript
and there are missing pages, these will be noted. Also, if unauthorized
copyright material had to be removed, a note will indicate the deletion.

UMI®

LOUISIANA TECH UNIVERSITY
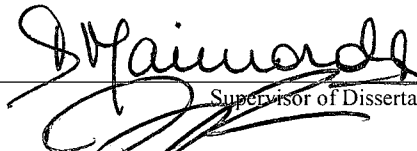
THE GRADUATE SCHOOL

03/31/09
_____
Date

We hereby recommend that the dissertation prepared under our supervision

by____NAGESH BABU IDUPULAPATI_____

entitled____A THEORETICAL STUDY OF METHANOL OXIDATION MECHANISMS

____BY METHANOL DEHYDROGENASE ENZYMES FOR FUEL CELL

____APPLICATIONS_____

_____

_____

be accepted in partial fulfillment of the requirements for the Degree of
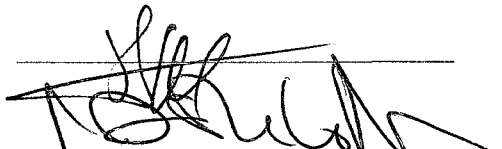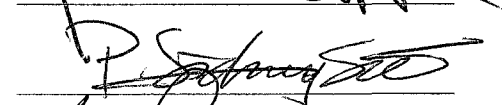
DOCTOR OF PHILOSOPHY

_____
Supervisor of Dissertation Research

_____
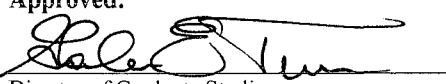Head of Department

ENGINEERING
_____
Department

Recommendation concurred in:
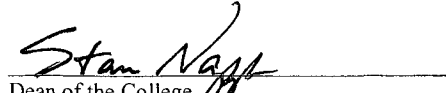
Advisory Committee

Approved:

_____
Director of Graduate Studies

_____
Dean of the College

Approved:

_____
Dean of the Graduate School

GS Form 13a
(6/07)

ABSTRACT

Enzymes are considered for electrochemical generation of power in fuel cells. Methanol dehydrogenase (MDH) is one such enzyme, which has been used as an anodic catalyst for a methanol-fed biofuel cell producing enough power for small electronic device applications. In practice, however, there are power output limitations associated with this MDH fuel cell, which may potentially be eliminated or reduced if the reactivity of this enzyme during the oxidation of methanol at the molecular level is clearly understood.

Two mechanisms for the methanol oxidation process by MDH have been proposed in the literature, Addition-Elimination (A-E) and Hydride Transfer (H-T), but no agreement has been reached about what mechanism actually operates in reality. Also, it was suggested that ion-modified MDH, particularly Ba^{2+}-MDH enzyme, is more active towards oxidation of methanol than Ca^{2+}-MDH from experimental kinetic observations.

In this dissertation, MDH active site models of varying sizes were tested for the A-E and H-T methanol oxidation in the presence of both Ca^{2+} and Ba^{2+}. Potential energy surfaces for the reactions were calculated, and the feasibility of the suggested reaction mechanisms was judged by comparison with available experimental free energy barriers. By systematically increasing the size of the models, deeper insight into the details of the reactions was obtained, and the role of the various active site residues was also analyzed.

Comparison of free energy barriers calculated for the rate-determining steps in this work for the A-E and H-T oxidation mechanisms with experimental Gibbs energy of activation by Ca^{2+}-MDH showed that these two mechanisms may not be correctly proposed in the literature. Also, the reduction of barriers for the rate-determining steps in the presence of Ba^{2+} for A-E and H-T obtained with the best MDH active site model tested here is almost twice as much the experimental free energy reduction with Ba^{2+}-MDH for methanol oxidation.

A modified first step of original H-T resulted in a newly proposed two-step H-T oxidation mechanism, where the barrier for the formation of final product, formaldehyde, during the first step is very much comparable (11.4 kcal/mol) to the experimental Gibbs energy of activation (8.5 kcal/mol). In the case of Ba^{2+} presence during this new mechanism, the free energy barrier is 6.2 kcal/mol, which is comparable to free energy of activation for oxidation of methanol by Ba^{2+}-MDH (3.5 kcal/mol). The second and final step involving proton transfer in this Two-step H-T was observed to be mediated by a water molecule in the presence of both ions.

Moreover, DFT-MD investigations on the reactant complex and necessary intermediates associated with all mechanisms also lead us to the conclusion that oxidation of methanol by MDH has a greater probability of proceeding through the two-step hydride transfer mechanism compared to proposed A-E and H-T.

APPROVAL FOR SCHOLARLY DISSEMINATION

The author grants to the Prescott Memorial Library of Louisiana Tech University the right to reproduce, by appropriate methods, upon request, any or all portions of this Dissertation. It is understood that "proper request" consists of the agreement, on the part of the requesting party, that said reproduction is for his personal use and that subsequent reproduction will not occur without written approval of the author of this Dissertation. Further, any portions of the Dissertation used in books, papers, and other works must be appropriately referenced to this Dissertation.

Finally, the author of this Dissertation reserves the right to publish freely, in the literature, at any time, any or all portions of this Dissertation.

Author _Nagesh Jdnpulupati_

Date _04/22/09_

DEDICATION

Without whom this is not possible

My sweet and loving sister, Swapna and my parents, Uma Maheswari and Madhava Rao.

TABLE OF CONTENTS

LIST OF TABLES

LIST OF FIGURES

ACKNOWLEDGMENTS

CHAPTER 1

INTRODUCTION AND LITERATURE REVIEW

ON METHANOL DEHYDROGENASE

ENZYME

1.1 Enzymatic Catalysts for Fuel Cell
Applications

People are concerned about the high-cost of materials and efficiency limitations

that chemical fuel cells currently have. For a fuel cell to be effective, strong acidic or

alkaline solutions, high temperatures and pressures are needed [1]. Most fuel cells use

platinum as a catalyst, which is expensive, limited in availability, and easily poisoned by

carbon monoxide (CO), a by-product of many hydrogen production reactions in the fuel

cell anode chamber [1, 2]. In proton exchange membrane (PEM) fuel cells, the type of

fuel used dictates the appropriate type of catalyst needed. Within this context, tolerance

to CO is an important issue. It has been shown that the PEM fuel cell performance drops

significantly with a CO concentration of only several parts per million, due to the strong

chemisorption force of CO onto the catalyst [3, 4]. Numerous studies have been aimed

toward reducing the amount of platinum required in current fuel cells [1, 5-11]. For

catalyst materials, tertiary platinum/ruthenium-based alloys seem to offer the best

performance when CO poisoning is of concern [1, 9, 11]. In an attempt to keep reducing

the amount of platinum used, small atomic clusters of platinum deposited

on carbon supports [5, 12] and platinum-based bimetallic catalysts [8-11] were proposed, but metal-metal and metal-adsorbate interactions [13-15] were observed to affect their reactivity [7, 16-19]. In spite of environmental, social, and political concerns surrounding the use of platinum and other more rare and valuable metals in fuel cells, the use of platinum-based alloys has been the focus of study in the last two decades.

Bioelectrochemical generation of power using enzymes has also been considered [20-23]. The use of enzymes as catalysts in fuel cells has been the subject of experimentation [24-27]. Currently some enzymatic fuel cells are being used to produce electricity to power a number of electrical devices, such as pumps, valves, pacemakers; and electronic devices, such as radios, sensors, controllers, and processors [21]. At present, however, enzymatic fuel cells have been reported [21-23, 28, 29] to have power output and stability limitations (0.15 $\mu W/cm^2$ for 30 days of continuous work [28], 50 $\mu W/cm^2$ for two days of continuous operation [29]), which are restricting the use of these kind of fuel cells to high power energy devices.

Enzymes as electro-catalysts are able to improve the performance characteristics of chemical fuel cells since their use avoids the problem of poisoning the fuel cell anode with carbon monoxide present in reforming gas, allowing the use of cheap hydrogen-containing fuels such as methanol and glucose. "The stability of the biological catalysts can be drastically improved by their immobilization on electrode supports, which may provide the development of commercially competitive biofuel cells [21]." Recently, miniature enzymatic fuel cells producing 4.3 μW were built by "wiring" the enzyme using electron-conducting hydrogels, avoiding the need for an electrolyte membrane [22]. This wiring minimizes costs and simplifies the design of bio fuel cells, allowing their

miniaturization. Moreover, an approach to imitate the photosynthetic process that involves a dye-sensitized nanoparticulate semiconductor photo anode working in combination with an enzyme-catalyzed biofuel cell has been proposed in principle to provide more power than either process working independently [23].

1.1.1 Methanol Dehydrogenase Enzyme as an Anodic Catalyst

Recent advances in nano/bio technology are eliminating the past well-known power output limitations that biofuel cells ($\sim\mu W/cm^2$) faced with respect to chemical fuel cells (W/cm^2 to MW/cm^2). For instance, a methanol-fed bio-catalytic fuel cell that uses bacterial methanol dehydrogenase (MDH) enzyme immobilized on N,N,N',N'-tetramethyl-p-phenylenediamine (TPMD)-functionalized carbon paste electrode as the anodic catalyst, produces a continuous power output of 0.25 mW/cm^2 for 30 days of continuous operation [30]. It is believed that the TPMD mediator, responsible for electron transfer resulting from the fuel oxidation by the enzyme to the electrode, is the major factor limiting the power output that deteriorates this fuel cell performance [expected (theoretical) output is 100 mW/cm^2]. The oligomerization (the forming of polymers by the combination of relatively few monomers) of the mediator molecules seems to be increased when stimulating the fuel cell operating conditions by subjecting the mediator to repeated charge-discharge cycles. This oligomerization causes the fuel cell performance to be deteriorated due to reduced electron transfer from the enzyme to the electrode. Moreover, another cause for this bio-fuel cell limited performance is associated to the formation of the by-product formaldehyde (formic acid) as result of methanol (fuel) oxidation by MDH. The continuous accumulation of such a strong acid in the bio-

fuel cell may slowly reduce the activity of the enzyme, thus limiting the overall power output [27].

Providing power output limitations are overcome, enzymatic fuel cells using MDH might offer potentially attractive power sources for some consumer electronic devices. In order to improve these power output limitations, first, the MDH active site and the proposed reaction mechanisms for oxidation of methanol are studied to gain a clear understanding of the reactivity of this enzyme. Next, detailed theoretical investigations are carried out at the molecular level concentrating on the active site of the enzyme to unravel secrets of its catalytic activity and to observe whether simple modifications would make it a better catalyst towards methanol electro-oxidation.

1.2 Methanol Dehydrogenase Enzyme

Methanol dehydrogenase (MDH) enzyme is a water soluble pyrroloquinoline quinone (PQQ)-containing protein found in the periplasm of methylotrophic bacteria such as methylobacterium extorquens [31, 32] and methylophilus W3A1 [33-36], and plays a crucial role in the metabolism of these organisms [37]. This bacterium can be found mostly in soils, on leaves, and in other parts of plants, and it is a highly studied organism [37]. These bacteria grow on methylamine, methanol, and C_2, C_3, and C_4 compounds, and also on the methanol emitted by the stomata of plants [38]. It oxidizes methanol (and other primary alcohols) to the corresponding aldehydes with the release of two protons and two electrons [37, 39]. Pyrroloquinoline quinone (PQQ) acts as the cofactor and cytochrome C_L, as its natural electron acceptor for this enzyme. Phenazine ethosulphate (PES) and *N,N,N',N'*-tetramethyl-*p*-phenylenediamine (TMPD) have also been used as artificial electron acceptors even though cytochrome C_L is the physiological electron

acceptor associated with MDH [37]. The main disadvantages of using these alternative electron acceptors are that, at high pH values (above 9), PES acts as an inhibitor, and TMPD is not commercially available and must be synthesized [37]. In the presence of these artificial electron acceptors, it has been suggested that the methanol oxidation by MDH requires ammonia or ammonium salts as activators [37]. However, low concentrations of ammonia or ammonium salts help the activity of the enzyme (< 4 mM), but higher concentrations may cause inhibitory effects (> 20 mM) [37].

1.2.1 <u>MDH Active Site</u>

Apart from the PQQ cofactor, MDH active site center contains a divalent calcium cation for its catalytic activity [37, 39]. The X-ray structure of methanol dehydrogenase from the methylophilus methylotrophus W3A1 (M.W3A1) and methlylobacterium extorquens were obtained at various resolutions, and unequivocally determined that the enzyme structure consists of a $\alpha_2\beta_2$ heterotetramer in which molecular masses of the two subunits α and β are 62 and 8 kDa, respectively [31-36]. Each heavy subunit contains a Ca^{2+} cation and a PQQ cofactor not covalently bound to the protein, and there is a binding pocket right above the top of the active site, where the analytes could get attached to the enzyme (Figure 1.1(a)). The view of the active site from the binding pocket is shown in Figure 1.1(b). From X-ray studies, it was observed that the oxygen atoms of the PQQ are involved in several hydrogen bonds with the residues GLU55, ARG109, THR159, SER174, ARG331 and ASN394 (Figure 1.1(b)) [31-36]. Additionally it was found that there are several water molecules present near the active site of MDH, of which the ones nearer to the PQQ and catalysis area are shown here (Figure 1.1(b)). Water molecules W362, W615, and W213 form hydrogen bonds with Ca^{2+}, PQQ, and GLU171 in the active site, while water molecules W130, W131, W134, and W198 form a

cluster on the left upper portion of PQQ and form hydrogen bonds with oxygens of PQQ

(Figure 1.1(b)) [31-36]. Coordination of Ca^{2+} in the active site has been under debate

because of these several X-ray studies. The coordination of the ion with O5, N6, and O10

atoms of PQQ was consistent with all studies with distances in the 2.32-2.47, 2.25-2.77,

and 2.30-2.44 Å range, respectively. The other interactions of Ca^{2+} have been suggested

to be with O12 of GLU171 (2.33-2.74 Å), O11 of ASN 261 (2.27-2.48 Å), O14 of

ASP303 (2.37-2.54 Å), and with the oxygens of waters W362 (2.51 Å), W615 (2.62 Å)

[31-36].

(a)   (b)
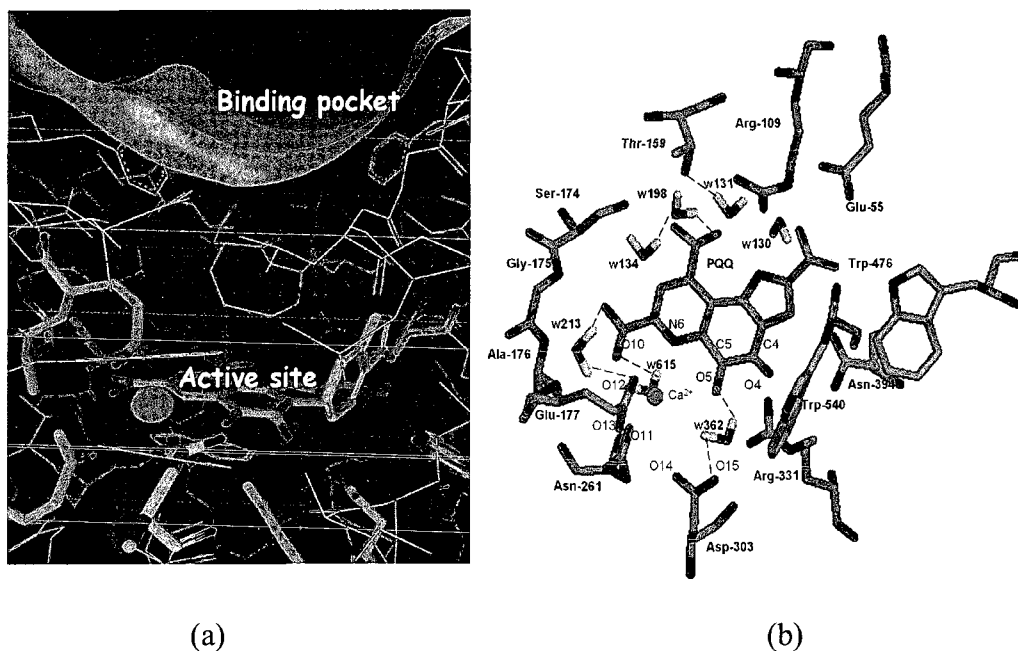
Figure 1.1 (a) View of the inside of the methanol dehydrogenase (MDH) enzyme with the active site in stick model. The solid surface represents the solvent-accessible MDH external surface showing the binding pocket. (b) View from the binding pocket of the entire MDH active site. Amino acids labels denote their location in the sequence obtained from the entry 1W6S (Methylobacterium Extorquens W3A1 [32]) of the Protein Data Bank.

1.2.2 Methanol Electro-Oxidation by Methanol Dehydrogenase Enzyme

Two possible mechanisms for methanol oxidation by MDH enzymes have been proposed in the literature, the addition-elimination (A-E) and the hydride transfer (H-T) mechanisms [37, 39, 40]. The A-E is a three-step mechanism (Figure 1.2(a)) that involves a proton transfer from methanol to an active site base, which is proposed to be ASP303. It is believed that the presence of this catalytic base at the MDH active site initiates the oxidation reactions by subtracting a proton (H16) from methanol (Figure 1.2(a)).

(a)

(b)
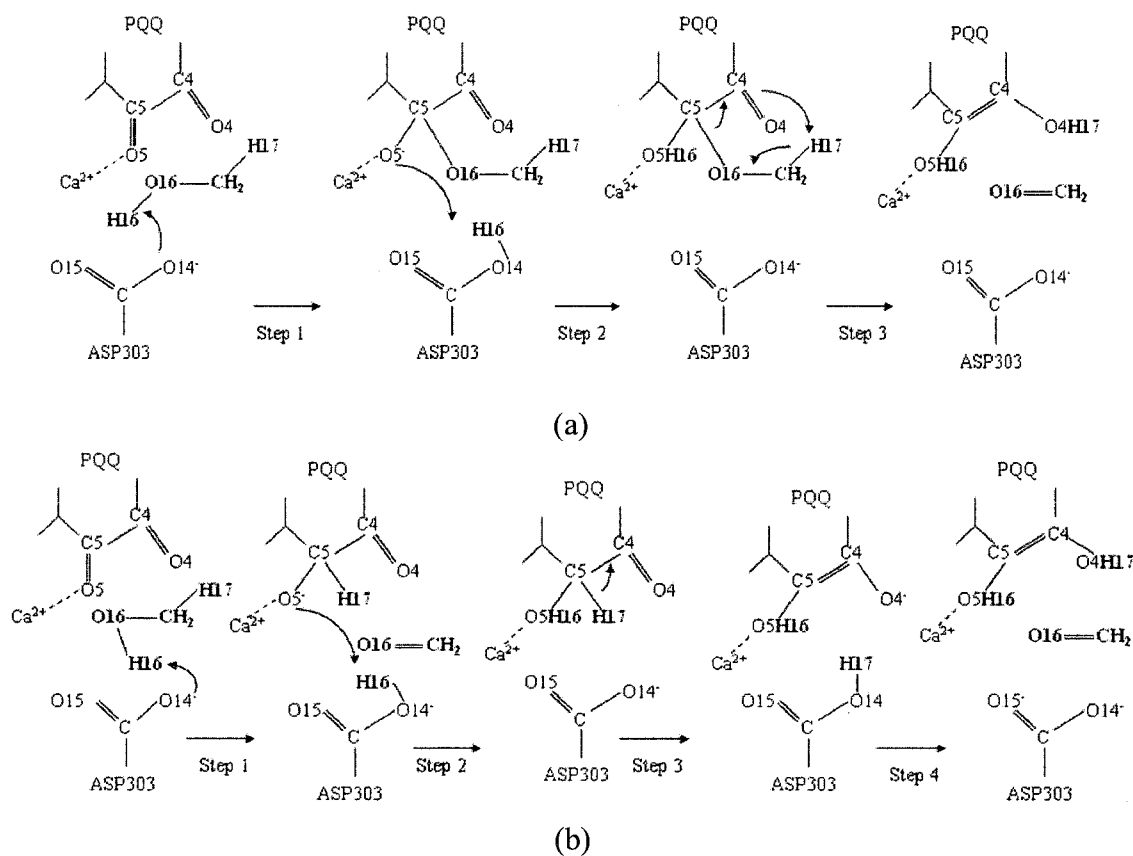
Figure 1.2 (a) Addition-elimination (A-E) and (b) Hydride-transfer (H-T) methanol electro-oxidation mechanisms by methanol dehydrogenase enzyme proposed in the literature [37, 39, 40].

This proton "addition" to ASP303 leads to the formation of a covalent hemiketal intermediate, since the resulting oxyanion (O16⁻) in the methanol molecule is then attracted to the C5 of PQQ. The second step consists of the proton (H16) "elimination" from ASP303 and transfer to O5 of PQQ, and the final step is characterized by a second proton (H17) transfer from the methanol molecule to the O4 of PQQ [Figure 1.2(a)], resulting in the formation of the by-product formaldehyde (CH₂O) [37, 39, 40].

The hydride transfer (H-T) is proposed to be a four-step mechanism (Figure 1.2(b)). The first step involves one proton and one hydride transfer: H16 and H17 from the methanol molecule to ASP303 and C5 of PQQ, respectively, resulting in the formation of the by-product formaldehyde. In the second step, there is a proton (H16) transfer from ASP303 to the C5 of PQQ. The third step involves the proton (H17) transfer from the C5 of PQQ to ASP303, and the final step consists of the transfer of H17 from ASP303 to the O4 of PQQ (Figure 1.2(b)) [37, 39, 40]. Irrespective of the mechanism under consideration, the rate-determining step for methanol oxidation by MDH is believed to be the breaking of the C_{met}-H17 bond leading to the second proton transfer in A-E and hydride transfer in H-T, which occurs in Steps 3 and 1 (Figure 1.2) of these mechanisms respectively [37, 39, 40].

Several experimental and theoretical studies were conducted for the elucidation of the preferred methanol electro-oxidation mechanism by methanol dehydrogenase enzymes. Experimental studies by Frank et al. [41] suggested that the C5 carbonyl (which participates in the oxidation process) of the isolated PQQ molecule is very reactive towards nucleophilic reagents, suggesting that a covalent PQQ-substrate complex (hemiketal intermediate) formation would be possible [41]. This hemiketal complex

formation was also anticipated since the spectra of the MDH-methanol complexes are almost identical to the absorption and fluorescence spectra of covalent adduct of PQQ and methanol, which is in favor of the A-E over the H-T mechanism [42, 43]. Itoh et al. [44, 45] from their theoretical and spectroscopic measurements, reported that the crystal structure of one of the isolated hemiketal adducts showed methanol bound to C5 of PQQ [44, 45] and also, demonstrated that PQQ systems in organic solution can oxidize methanol, ethanol, and 2-proponal to their corresponding aldehydes via A-E mechanism. Crystallographic studies by Xia et al. [36] on MDH from Methylophilus W3A1 in the presence of methanol indicated that in the MDH-PQQ-methanol complex, the methanol hydroxyl group is closer to the PQQ C5 atom (3.1 Å) than the methyl group (3.9 Å). According to these authors [36], the hydride ion transfer (H17 to C5 of PQQ) from the more distant methyl group of methanol would not be possible, also supporting the formation of a hemiketal intermediate as suggested by the A-E mechanism.

Oubrie et al. [46, 47] obtained the crystal structure of soluble GDH at 1.9 Å resolution in which the carbon atom in glucose was observed to be in good position for hydride transfer to C5 of PQQ. These authors suggested that hydride transfer could be the mechanism in operation for all dehydrogenase family [46, 47]. Zheng et al. [48] reported several theoretical structures representing an MDH active site, postulating the hydride-transfer mechanism to be the preferred one. Quantum mechanics/molecular mechanics and molecular dynamics calculations by Reddy et al. and Zhang et al. [49-51] supported the hydride-transfer mechanism rather than the addition–elimination by looking at the conformational variations of the active site residues of MDH enzyme. From their calculations [51], the free energy barrier for the first step of H-T was calculated to be

11.7 kcal/mol, which they compared to experimental Gibbs energy barrier for oxidation of methanol by wild–type Ca^{2+}-MDH (8.5 kcal/mol) [52]. This experimental Gibbs energy barrier for methanol oxidation is not specified for a particular step or rate-determining step as proposed in the oxidation mechanisms, but the comparison by Zhang et al. [51] with free energy barrier of the first step of H-T was performed as the by-product formaldehyde is formed by the end of this first step itself as proposed in the literature. Recently, Kay et al., conducted electron paramagnetic resonance (EPR) studies on binding of substrate to PQQ-Ca^{2+} in ethanol dehydrogenase. Their results indicated a strong coordination of the substrate to the cation in the active site, which should be broken if the oxidation process goes through the addition–elimination, for which reason, that mechanism could be unlikely [53].

In recent investigations on elucidating several enzyme catalysis, a common procedure is to use relatively small models of enzyme active sites and apply quantum chemical methods to study their reaction mechanisms [54-61]. According to this approach, a homogeneous polarizable medium with some assumed dielectric constant is used for treating the neglected enzyme environment and density functional theory calculations are performed to obtain reaction barriers. The calculated reaction energies from various studies [54-61] are often sufficient to confirm or rule out a suggested reaction mechanism, and a well-chosen quantum model representing the enzyme active site is able to reproduce the chemistry taking place to such a high degree that it can provide detailed insight and observations about the mechanisms.

In 2007, Leopoldini et al. [58] theoretically investigated the two proposed A-E and H-T mechanisms using the procedure described in the last paragraph, at the B3LYP

density functional theory level and 6-31+G* basis set for all atoms except calcium (LANL2DZ was used). Their model for the MDH active site included the PQQ cofactor, the Ca^{2+} ion, the amino acids having coordination with the calcium ion (GLU171, ASN261, ASP303), and also five nearby amino acids which form a sphere around the PQQ molecule (ARG331, GLU55, ARG109, THR153, SER174). In their calculations, however, only the reactive groups (CH_3COO^- and NH_3COCH_3) of the amino acids having coordination with the calcium ion and the PQQ molecule were considered, and hydrogen atoms of each reactive group were frozen to prevent unreliable expansion of model during the optimization procedure [58]. Their calculated energy barriers for the rate-determining step, i.e. for the cleavage of C_{met}-H17 bond of methanol for the two proposed mechanisms (34.6 kcal/mol for A-E, 32.3 kcal/mol for H-T), were observed to be well above the general kinetic requirements of an enzymatic catalytic process [58]. So, Leopoldini et al. [58] postulated an alternative mechanism, the "addition-elimination-protonation", in which the first step is the same as in the A-E mechanism (Step 1), but the second step consists of the proton (H17) "elimination" from the hemiketal methyl group and transfer to O4. The final step in their mechanism is characterized by the proton transfer (H16, "protonation") from the ASP303 to the O5 of PQQ. This new proposed mechanism reduced the energy barrier of the rate-determining step to 16 kcal/mol [58].

1.2.3 Role of the Ion in the Active Site of MDH

The role of Ca^{2+} in the active site is not well understood. It has been suggested that apart from holding the PQQ molecule in place in the active site, the calcium ion might have an important role in the electro-oxidation reaction mechanism. It was proposed previously that the Ca^{2+} ion acts as a Lewis acid (electron pair acceptor)

contributing to the oxidation mechanism by its coordination with the C5 carbonyl oxygen of PQQ, thus providing the electrophilic C5 for attack by an oxyanion or hydride in addition to a structural role in maintaining PQQ in the active site configuration. Several experimental and theoretical studies have been conducted in order to elucidate the function of the Ca^{2+} ion.

Itoh, Kawakami and Fukuzumi [44] performed semi-empirical molecular orbital calculations to characterize and study the alkali metal ion (Ca^{2+}, Ba^{2+}, Sr^{2+}) binding to the PQQ coenzyme in the active site of MDH. Their results showed that the hemiketal stabilization improved in the presence of Ca^{2+} and suggested that the binding constant of Ca^{2+} to PQQ is stronger than that of Sr^{2+} and Ba^{2+}. Theoretical DFT calculations were performed on the MDH active site as a part of our previous work where the binding of both Ca^{2+} and Ba^{2+}, with respect to the models representing the active site, has been evaluated. The binding of Ca^{2+} is calculated to be 0.2-1.0 eV more stable than that of Ba^{2+}. The reason was attributed to the size of Ca^{2+}, which best fits in the binding pocket of PQQ in the enzyme [62]. Harris and Davidson [63] replaced Ca^{2+} by Sr^{2+} in the MDH active site and observed two-fold increase in specific activity towards methanol oxidation due to increased kinetic properties of Sr^{2+}-modified methanol dehydrogenase. Goodwin et al. [52] have also replaced the Ca^{2+} ion in the wild-type MDH active site with Ba^{2+} and Sr^{2+} in order to observe the kinetics of the modified MDH enzyme on methanol oxidation. These authors reported that the Gibbs energy of activation for the oxidation of methanol was found to be smaller in the case of Ba^{2+}-MDH (3.4 kcal/mol) than that in Sr^{2+}-MDH (7.6 kJ/mol) and Ca^{2+}-MDH (8.5 kJ/mol). This result was not expected by them, since the replacement of Ca^{2+} with Ba^{2+}, a weaker Lewis acid, should decrease the

activity of the enzyme, and therefore its activation energy should be larger. From their experimental calculations, the decrease in the activation energy was attributed to 1200-fold decrease in affinity for methanol of Ba^{2+}-MDH, which corresponded to decreased free energy of substrate binding ($\sim$ 4.5 kcal/mol) [52].

To the best of our knowledge, there are two popular mechanisms (A-E and H-T) proposed in the literature regarding the oxidation of methanol by MDH, but still no consensus has been reached about which one actually operates. Hence, a detailed theoretical investigation is conducted on the proposed mechanisms (A-E and H-T) by using extended MDH active site models in gas phase and protein environment. The theoretical methodology behind the calculations such as density functional theory and transition state theory are outlined in Chapter 2. Chapter 3 discusses the ideas behind modeling an MDH enzyme active site for quantum chemical calculations and how the surrounding protein environment is considered by following specific guidelines as set forth in the literature.

Chapters 4 and 5 discuss in detail the theoretical investigation carried on the proposed A-E and H-T using smaller and bigger active site models in gas phase and dielectric solvation (protein environment).

As suggested by Goodwin et al. [52] if Ba^{2+}-MDH requires only half the activation energy for the oxidation of methanol than Ca^{2+}-MDH, then we hypothesize that ion modified MDH (Ba^{2+}-MDH) enzymes can function as better anodic catalysts for fuel cell applications. But no specific mechanism(s) for this Ba^{2+}-MDH oxidation of methanol by identifying the transition states and intermediates involved, were suggested by Goodwin et al. [52] or any other researchers. So the Ca^{2+} is replaced by Ba^{2+} in the

MDH active site models selected and tested on the A-E and H-T mechanisms proposed for Ca^{2+}-MDH, which is explained in detail in Chapter 6. Also, the comparison between structure and energetics for both ions for the best active site model were discussed.

Chapter 7 contains information on other suggested mechanisms that were shown to be possible by considering different reaction pathways for the original A-E and H-T. This chapter also outlines DFT-MD calculations on a much bigger active site model to validate the findings from the already proposed and suggested new mechanisms.

Finally, Chapter 8 outlines the conclusions and future work that can be done on this topic of MDH enzyme catalysis.

CHAPTER 2

THEORETICAL BACKGROUND

Theoretical chemistry is the field used to study chemical problems, where mathematical methods are combined with fundamental laws of physics/chemistry. The most powerful theory used to describe the microscopic chemistry, in particular the motion of electrons in a molecule is the quantum mechanics. In quantum mechanics, the general equation is the time-dependent Schrödinger equation, by solving which we can in principle obtain all properties of a system, such as energy. For the enzymatic reactions studied in the present dissertation which involves ground-state chemistry, it is sufficient to use the time-independent form of the Schrödinger equation ($\hat{H}\Psi = E\Psi$) as the base. Obtaining the exact solution of the Schrödinger equation encounters great difficulty. The only systems that can be solved exactly are those composed of only one electron. A number of approximations are necessary to solve the equation for many-particle systems.

2.1 Electronic Structure Methods

All properties of a molecular system are in principle derived from the motion of electrons and nuclei in the molecules, which can generally be described by the Schrödinger equation.

The time-independent non-relativistic Schrödinger equation is shown in Eq. (2.1) [64],

for a molecular system containing N electrons and M nuclei.

$$\hat{H}\Psi_i(\vec{r}_1,\vec{r}_2......\vec{r}_N,\vec{R}_1,\vec{R}_2.....\vec{R}_N) = E_i\Psi_i(\vec{r}_1,\vec{r}_2,....\vec{r}_N,\vec{R}_1,\vec{R}_2,....\vec{R}_M)$$ (2.1)

In Eq. (2.1), $\hat{H}$ is the Hamilton operator representing the total energy of a system

as given in Eq. (2.2), $\Psi_i(\vec{r}_j,\vec{R}_k)$ is the wave function which represents the i-th state of the

system, and E_i is the numerical value of the energy of the state described by $\Psi_i(\vec{r}_j,\vec{R}_k)$,

$\vec{r}_j$ represents the coordinates of electron j, and $\vec{R}_K$ represents the coordinates of nucleus

K.

$$\hat{H} = \sum_i^{electrons} \frac{-\hbar^2}{2m_e}\nabla_i^2 + \sum_A^{nuclei} \frac{-\hbar^2}{2m_A}\nabla_A^2 + \sum_i^{electrons}\sum_A^{nuclei} \frac{-e^2 Z_A}{r_{iA}} + \sum_{i>j}^{electrons} \frac{e^2}{r_{ij}} + \sum_{A>B}^{nuclei} \frac{e^2 Z_A Z_B}{r_{AB}}$$

(2.2)

The first term in Eq. (2.2) represents the kinetic energy of the electrons; the second term

represents the kinetic energy of the nuclei; the third term represents the electrostatic

interaction between the electrons and the nuclei (attractive); the fourth one represents the

electrostatic interaction between the electrons (repulsive); and the fifth term represents

the electrostatic interaction between the nuclei (repulsive). Eq. (2.2) written in atomic

units (Planck's constant $\hbar = 1$, $m_e = 1$, $e = 1$) is shown in Eq. (2.3) [64]

$$\hat{H} = \sum_i^{electrons} \frac{-1}{2}\nabla_i^2 + \sum_A^{nuclei} \frac{-1}{2m_A}\nabla_A^2 + \sum_i^{electrons}\sum_A^{nuclei} \frac{-Z_A}{r_{iA}} + \sum_{i>j}^{electrons} \frac{1}{r_{ij}} + \sum_{A>B}^{nuclei} \frac{Z_A Z_B}{r_{AB}}$$

(2.3)

Solving the Schrödinger equation consists of finding the values of E_i and Ψ_i so that

when the wave function is operated upon by the Hamiltonian, it returns the wave function

multiplied by energy [64].

Beyond H_2^+, this Eq. (2.3) is too complicated to be solved exactly [65-67]. Therefore, some approximations/simplifications have to be introduced. As a first approximation, the most fundamental Born-Oppenheimer approximation is made. This approximation is based on the fact that electrons move much faster than the nuclei, and their motions can be separated. The kinetic energy of nuclei can thus be ignored, and for certain geometry, the nucleus-nucleus repulsion is constant. The Schrödinger equation can thus be separated into two parts which describe the electronic and nuclear wave functions, respectively [65-67]. Calculating the electronic energies for different nuclear arrangements as a solution to the electronic Schrödinger equation, leads to a potential energy surface (PES). The minima of this PES determine the equilibrium geometries of a molecule [65-67]. The electronic Schrödinger equation is still too complicated to be solved for a many-particle system, so additional approximations are needed [65-67]. Second and the most important approximation is the Hartree-Fock (HF) method. This method is based on the independent-particle model, where each electron is considered to move in the mean field of all other particles. Each electron is thus related with a one-electron wave function called as the molecular orbital (MO), which is the combination of a spin function that depends on its spin and a spatial function that depends on the coordinate of the electron. According to *Pauli Principle*, the wave function has to satisfy the anti-symmetry and must change sign if the coordinates of two electrons are interchanged. A Slater determinant is used to build the wave function of the N one-electron orbitals (N is the number of electrons). Now, the N-particle problem is transformed to a set of N-one-particle problems as shown in Eq. (2.4) [68]

$$\hat{F}\chi_i = \varepsilon_i\chi_i \tag{2.4}$$

where $\hat{F}$ is an effective one-electron operator, in which the electron-electron repulsion is treated in an average way. χ_i is the corresponding eigenfunction (i.e. MO) and the electron in the MO has the orbital energy ε_i [67]. This Eq. (2.4) is non-linear and a self-consistent field (SCF) method has to be used to solve it iteratively. The single Slater determinant orbitals can then be optimized to minimize the energy. However, in practice, the molecular orbitals in a molecule are usually constructed as a linear combination of the atomic orbitals (LCAO) of the corresponding atoms [67, 68].

Since the motion of all electrons are correlated in a real system, the HF method based on the independent-particle model results in an inherent limitation. Large deviations from experimental values results in neglecting correlation energy, which makes the HF method a poor choice for exploring chemical reactions. A number of approaches, collectively called *post-Hartree-Fock* methods [67, 69] have been developed to correct this weakness by including the electron correlation. For example, multi-configurational self-consistent field (MCSCF), configuration interaction (CI), coupled cluster (CC), and complete active space SCF (CASSCF) expand the "true" multi-electron wave function in terms of a linear combination of Slater determinants [67, 69]. These approaches become computationally much more demanding even though they improve the level of accuracy and, thus are only suitable for relatively small systems at the moment. To investigate large systems, as the enzymatic reactions in this dissertation, a "computationally cheaper" alternate method is needed [67, 69].

2.2 Density Functional Theory

Density functional theory (DFT) approach comes as a fruitful alternative to the wave function methods. The basis of DFT is the Hohenberg-Kohn theorem [70], which shows that the total energy of a non-degenerate ground state is a unique functional of the electron density of the system, given by, $E = E[\rho(r)]$ [70]. According to this theory, all properties of a system can be deduced from the ground-state density and the determination of the complicated many-electron wave function can thus be avoided. However, a fundamental difficulty emerges here with the exact functional as the dependency of the energy on the given electron density is unknown. Several approximations and attempts have been made and the energy functional is initially expressed as shown in Eq. (2.5) [71]

$$E[\rho] = T[\rho] + E_{ee}[\rho] + E_{ne}[\rho], \qquad (2.5)$$

where T is the kinetic energy, E_{ee} the electron-electron repulsion, and E_{ne} the nuclei-electron attraction. Gradually, Kohn and Sham contributed a significant development, with their orbital-based scheme, where independent particles move in an effective potential (the non-interacting one electron orbitals are called Kohn-Sham orbitals, φ_i) [72]. Now, the real system of interacting electrons can be described through a system of non-interacting particles by expressing the electron density as the sum of the squared orbitals. So, the total kinetic energy (T) is divided into two parts, the kinetic energy of non-interacting system of n-electrons (T_s) and a missing fraction (T_c) of kinetic energy relative to the real interacting system as shown in Eq. (2.6) [72]

$$T[\rho] = T_s[\rho] + T_c[\rho] \qquad (2.6)$$

The second functional in Eq. (2.5) regarding the electron-electron repulsion ($E_{ee}[\rho]$) can be divided into the classical Coulomb interaction (J) and a non-classical part containing correlation and exchange ($E_{ncl}[\rho]$). So the total new energy by combining Eqs. (2.5) and (2.6) can now be written as Eq. (2.7) [72]

$$E[\rho] = T_s[\rho] + T_c[\rho] + J[\rho] + E_{ncl}[\rho] + E_{ne}[\rho] \qquad (2.7)$$

Now, the missing fraction of the kinetic energy ($T_c[\rho]$) and the correlation and exchange part ($E_{ncl}[\rho]$) are combined to form a new term known as the exchange-correlation functional ($E_{xc}[\rho]$). The total energy can finally be represented as shown in Eq. (2.8) [72]

$$E[\rho] = T_s[\rho] + J[\rho] + E_{ne}[\rho] + E_{xc}[\rho] \qquad (2.8)$$

The first three terms in Eq. (2.8) can be calculated explicitly. All problems have now been centralized on the exchange-correlation term, $E_{xc}[\rho]$, which incorporates all unknown contributions to the total energy and how to accurately describe it. Using the normalization constraints together with the variational principle and minimizing the total energy of a determinant constructed by Kohn-Sham orbitals results in the Kohn-Sham equation as shown in Eq. (2.9) (similar to the Hartree-Fock Equation) [72]

$$\hat{h}_{ks}\varphi_i(r) = \varepsilon_i\,\varphi_i(r), \qquad (2.9)$$

where $\hat{h}_{ks}$ is the one-electron operator and depends on the electron density. If the exact form of the $E_{xc}[\rho]$ functional is known, the exact total energy of the many-electron system can be obtained by iteratively solving the Eq. (2.8). The precision of a DFT method relies on how accurate the form of $E_{xc}[\rho]$ is [73, 74].

Various DFT methods differ from one another in the way they describe the kinetic energy term and the exchange and correlation term [73, 74]. DFT methods compute

electron correlation using general functionals of the electron density [75, 76]. There are three types of functional used. The first one is the local spin density approximation (LSDA) functional, which uses only the values of electron spin densities. The second one is the Generalized Gradient approximation (GGA) functional, which involves both values of the electron spin density and its gradient. These functionals are also referred to as non-local functional. The third kind of functional is known as the hybrid functional. Hybrid functionals describe exchange function as a linear combination of Hartree-Fock, local and gradient-corrected exchange term [75, 76]. This exchange term is then combined with local or gradient corrected correlation term [71, 75, 76].

Most widely used GGA exchange-correlation combinations in literature are BP86, BLYP and BPW91 [64,77]. Of them, the most popular one, BLYP exchange-correlation functional as employed in the DMOL^3 module of Materials Studio$^®$ software [78,79] is used to perform calculations as a part of this dissertation. A BLYP calculation combines Becke's GGA exchange (usually abbreviated simply as 'B') with the GGA correlation functional of Lee, Yang, and Parr (LYP). The LYP functional seems to be the better one of the above noted correlation functional because of the better handling of the self-interaction error in many-electron systems [64, 77].

2.3 Basis Sets

A basis set is a mathematical representation of the atomic orbitals [64]. An atomic or molecular orbital is a function that restricts each electron to a particular region of space. All quantum mechanical calculations use a basis set expansion to express the unknown molecular orbitals (MO) that are commonly expressed as a linear combination of atomic orbitals (LCAO) as shown in Eq. (2.10) [64, 66]

$$\Psi_i = \sum_{\mu=1}^{K} C_\mu \varphi_\mu ,$$

(2.10)

where Ψ_i is a spatial molecular orbital MO, and φ_μ is one of K atomic orbitals (H-like functions; these are the basis functions), and C_μ are coefficients. However, basis functions φ_μ need not be H-alike. Larger basis sets more accurately approximate the orbitals by imposing fewer restrictions on the locations where an electron can be present, but require higher computational power and longer time to perform the calculations [64, 66].

The way these basis functions are defined as analytical functions are known as Gaussian-type basis sets, and where they are defined numerically, they are known as numerical basis sets. A numerical basis function is essentially a table of the values that an atomic orbital wavefunction has at many points around the nucleus, with empirical functions fitted to pass through these points [66, 69]. These empirical functions are used in calculations instead of the analytical Gaussian-type functions. Also, the use of these functions has several advantages such as, the molecule can be dissociated exactly to its constituent atoms (within the DFT context). Basis set superposition effects are minimized, and it is possible to obtain an excellent description, even for weak bonds [66, 69].

One such numerical basis set used for our calculations is double numerical plus polarization (DNP) [66, 69] This basis set considers a polarization d function on heavy atoms and a polarization p function on hydrogen atoms. It compares to the split-valence double zeta 6-31G** in size; however, it is more accurate than the Gaussian basis sets of the same size [78, 79]. Also this basis set is the best available for the calculations

involving ions in their geometries, and it is used in conjunction with density functional theory calculations in this work.

2.4 Transition State Theory and Reaction Rates

The present dissertation deals with studying the catalytic reaction mechanisms of the MDH enzyme. This process is characterized by reaction rates and involves continuous chemical and potential energy changes. How quickly reactants change into products in a chemical reaction is defined by a reaction rate. Some of the important quantities used in the characterization of uncatalyzed and enzyme catalyzed reactions, are shown in Figure 2.1.

For an uncatalyzed reaction, the relative free energy of the transition state (TS) to the reactant (S) is defined by the reaction barrier, ΔG. With respect to the enzymatic reaction, the substrate first binds to the enzyme to form an enzyme-substrate complex (ES), and then the reaction proceeds via one or several transition state(s) resulting in an enzyme-product complex (EP), from which the product (P) is finally released so that the enzyme is set free again. So, in the enzyme-catalyzed case, the reaction barrier (ΔG_{cat}) is the relative energy between the ES complex and the transition state. The rate of the overall reaction is consequently accelerated by the presence of the enzyme, which provides the catalytic power to make $\Delta G_{cat} < \Delta G$ [67].
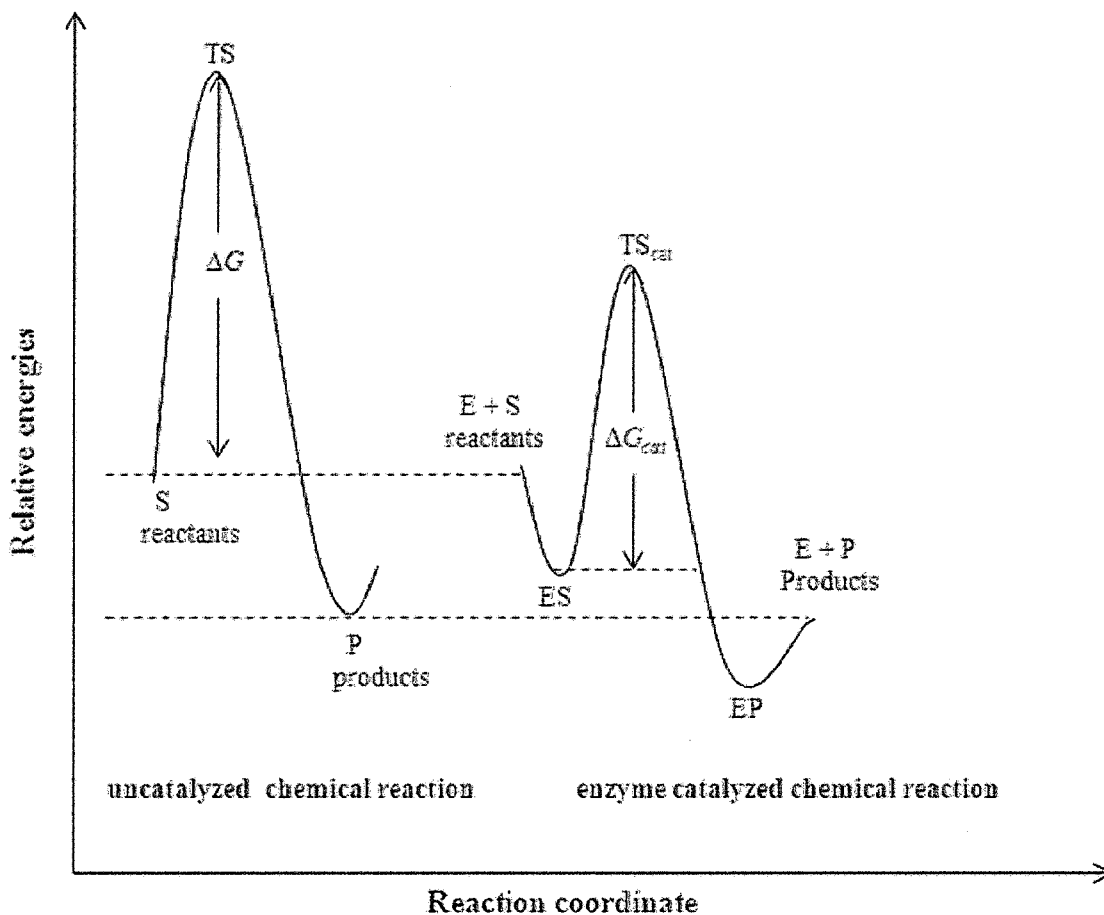
Figure 2.1 Schematic free energy profile for uncatalayzed and enzyme catalyzed chemical reactions.

Potential energy surfaces and the relative free energies between different states can be computed using the quantum chemistry while reaction rates are determined experimentally. Classical transition state theory (TST) can be used to connect these two concepts. This theory postulates an equilibrium (Boltzmann) energy distribution at all stable and unstable states along the reaction coordinates, leading to the following expression for the rate constant k

$$k = \frac{k_B T}{h} \exp(-\frac{\Delta G}{RT}),$$

(2.11)

where k the first order rate constant (s^{-1}), k_B is the Boltzmann's constant (1.38×10^{-23} J/K), h is the Planck's constant (6.626×10^{-34}J s), T is the absolute temperature (298.15 K at room temperature), R is the universal gas constant (8.314 J K^{-1} mol^{-1}), and ΔG is the Gibbs free energy of activation. Gibbs free energy consists of enthalpic and entropic terms, $\Delta G = \Delta H - T\Delta S$ [67].

According to the Eyring Eq. (2.11), one can estimate that a reaction with a rate constant of 1 s^{-1} at room temperature (298.15 K) gives a barrier of approximately 18 kcal/mol. So, one can use this relationship to quickly convert between rates and energies. However, it is important to note that, due to the exponential nature of the equation, a calculated energy barrier with an error bar of 2-3 kcal/mol, which is considered to be good, leads to an error in the rate of two orders of magnitude. It is therefore not possible with the methods used in this work to determine accurate reaction rates. However, comparison with experimentally determined rate constants or free energy barriers is suitable in order to evaluate the feasibility of a certain reaction mechanism. For a multistep mechanism, the step involving the transition state with the highest energy barrier is known as the rate-limiting (determining) step. So for any step(s) taking place in an enzymatic reaction, the reaction free energy barriers are supposed to be less than or around 18 kcal/mol (obtained from theoretical methods) to be in the acceptable reaction rates of enzymatic catalytic process [54-58, 60, 61]. So if the barriers for the rate-limiting or any steps is much higher than 18 kcal/mol, then that proposed mechanism is not feasible.

2.4.1 Obtaining Transition States as Implemented in DMOL³

Transition state calculations conducted as a part of this dissertation work are performed using the DMOL³ module of the Materials Studio® [78, 79] software using synchronous transit methods (linear synchronous transit or LST, and quadratic synchronous transit or QST [80, 81]). Appropriate optimized geometries of reactants and products involved in each reaction step are considered for defining atom pairing according to $r_{ab}^i(f) = (1-f)r_{ab}^R + fr_{ab}^P$, so that a 3D trajectory file representing the reaction path is generated using the reaction preview tool of the Materials Studio® software [80, 81]. In the equation specified above, r_{ab}^R and r_{ab}^P are the inter-nuclear distances between the pair of atoms a and b in the reactant and the product, respectively and f is an interpolation parameter that varies between 0 and 1 [80, 81]. For a molecule with N atoms, the number of distinct inter-nuclear separations is N(N-1)/2, which is greater than 3N Cartesian degrees of freedom of the system by which the interpolation equation over specifies the geometry.

Once these trajectory files are obtained, they are used as inputs to obtain the corresponding transition states, using the linear synchronous transit and quadratic synchronous transit (LST/QST) calculation with conjugate gradient (CG) minimization using the transition state search tool in DMOL³. This methodology starts with a LST/optimization (bracketing the maximum between the reactant and product and performing energy minimization of the obtained maximum in the reaction pathway). The transition state thus obtained is used as starting point for performing a finer search with the QST/optimization followed by a conjugate gradient (CG) minimization [80, 81]. This cycle is repeated until a stationary point with only one imaginary frequency is found.

Then this imaginary mode is selected to perform transition state optimization. But in some cases several imaginary frequencies were found by the end of LST/QST/CG. In such situations, the corresponding (imaginary) modes of vibrations are animated in order to visualize the mode that would eventually follow the intended step from a particular reactant to product. That particular mode is then selected to perform the transition state optimization to verify whether the obtained geometry is indeed a transition state.

The transition state finally obtained by the LST/QST/CG method may not be the transition state connecting the intended reactant and product for a particular reaction step. Therefore, in order to thoroughly investigate the reaction paths, the intrinsic reaction coordinate (IRC) analysis is performed. In DMOL^3, the IRC calculations are included in the transition state confirmation tool. This tool starts at the transition state and locates successive minima in the direction of the reactant and product paths. This path is known as the minimum energy path which should connect the supposed transition state to the presumed reactants and products. It uses the nudged elastic band method to validate a transition state by introducing a fictitious spring force which connects the neighboring points to ensure continuity of the path, and then it projects the force so that the system converges to the minimum energy path [80, 81].

2.5 Molecular Dynamics

Classical molecular dynamics (MD) is a computer simulation technique where the time evolution of a set of interacting atoms is followed by integrating their equations of motion using $F_i = m_i a_i$, where F_i is the force exerted on particle i, m_i is the mass of particle i, and a_i is the acceleration of particle i. Knowing the force on each atom, it is possible to determine the acceleration of each of the atoms in the system [65]. Integration

of the equations of motion then yields a trajectory that describes the positions, velocities, and accelerations of the particles as they vary with time. From this trajectory, the average values of properties can be determined. The equations of motion are deterministic, i.e. the positions and the velocities at time zero determine the positions and velocities at all other times, t. The initial positions could be either arbitrary or obtained from experimental data. The initial distribution of velocities is usually determined from a random distribution with the magnitudes conforming to the required temperature and corrected, so there is no overall lineal momentum [65]. The velocities are often chosen randomly from a Maxwell-Boltzmann or Gaussian distribution at a given temperature, which gives the probability of an atom with a velocity in a particular x, y or z direction [65].

The way inter-atomic interactions (potential energy) are represented is through a "force field." The force field is a function of the atomic positions (3N) of all the atoms in the system. Every force field includes terms related to the bond stretching energy, the angle bending energy, the torsion term, and the interactions between the bonded and non-bonded atoms. Forces are then derived as the gradients of the potential with respect to atomic displacements. Due to the complicated nature of this function and the large number of particles usually involved, there is no analytical solution to the equations of motion; they must be solved numerically, for which a large number of numerical algorithms such as verlet, velocity-verlet, predictor-corrector, leap-frog, and Beeman algorithms have been developed for integrating the equations of motion [65].

MD simulations carried out in this work using DMOL[3] is similar to classical force-field based MD with the main difference being that the atomic forces are derived by solving DFT equations rather than from empirical potentials of inter-atomic interactions.

This methodology is called DFT based MD.[82] Electrons are kept on the Born-Oppenheimer surface by means of explicit electronic structure optimization after each MD step. The disadvantage of this procedure is that it is computationally much more expensive than the classical MD due to energy and force evaluation using DFT after each step. Velocity-verlet algorithm is used for integrating equations of motion in MD as implemented in $DMOL^3$. This algorithm uses the position, acceleration, and velocities at time 't' to compute the position, acceleration, and velocities at time 't + δt'. Even though this algorithm is computationally expensive, it is more precise than other algorithms stated above [65].

Micro-canonical (NVE- constant energy and constant volume) and canonical (NVT- constant temperature and constant volume) ensembles available in $DMOL^3$ are used in this dissertation work [78, 79]. The NVE ensemble is obtained by solving the standard Newton equation without any temperature and pressure control. Energy is conserved when this (adiabatic) ensemble is generated [78, 79]. NVT is an isothermal ensemble where heat is exchanged with a temperature bath to maintain a constant thermodynamic temperature. These ensembles can be used to calculate various structural, energetic, and dynamic properties of the systems under study.

CHAPTER 3

MODELING OF ENZYMATIC REACTIONS

Quantum chemical studies of enzyme reaction mechanisms come with many obstacles and limitations. The main problem is that the systems are too big for quantum mechanical treatment. With the computer power of today, DFT methods allow us to treat up to 150 atoms quite routinely at a reasonable level of accuracy. So, it allows us to treat only a very small portion of the enzyme, but how can we study the reaction mechanism of an enzyme consisting of thousands of atoms? Obviously, a number of approximations have to be made. In this context, a quite powerful methodology has been developed that uses the DFT methods to treat the critical parts of the active site of the enzyme and make much cruder approximations about the rest of the enzyme environment. In this chapter, this methodology will be briefly outlined.

3.1 Construction of the Active Site Model

The basic idea when modeling the enzyme is to construct a best-fit model that can reflect the main features of the active site of the enzyme. The first step is to start from an experimentally-determined X-ray crystal structure of the enzyme whose coordinates are commonly deposited in online libraries, such as the Protein Data Bank (PDB). The active site of the enzyme is located from that crystal structure and, important amino acid

residues which have some kind of role are selected to be included in the computational model (Figure 3.1). Sometimes, due to the resolutions of protein crystal structures, hydrogen atoms are not visible and have to be added manually to the model. For most groups this procedure is quite simple.
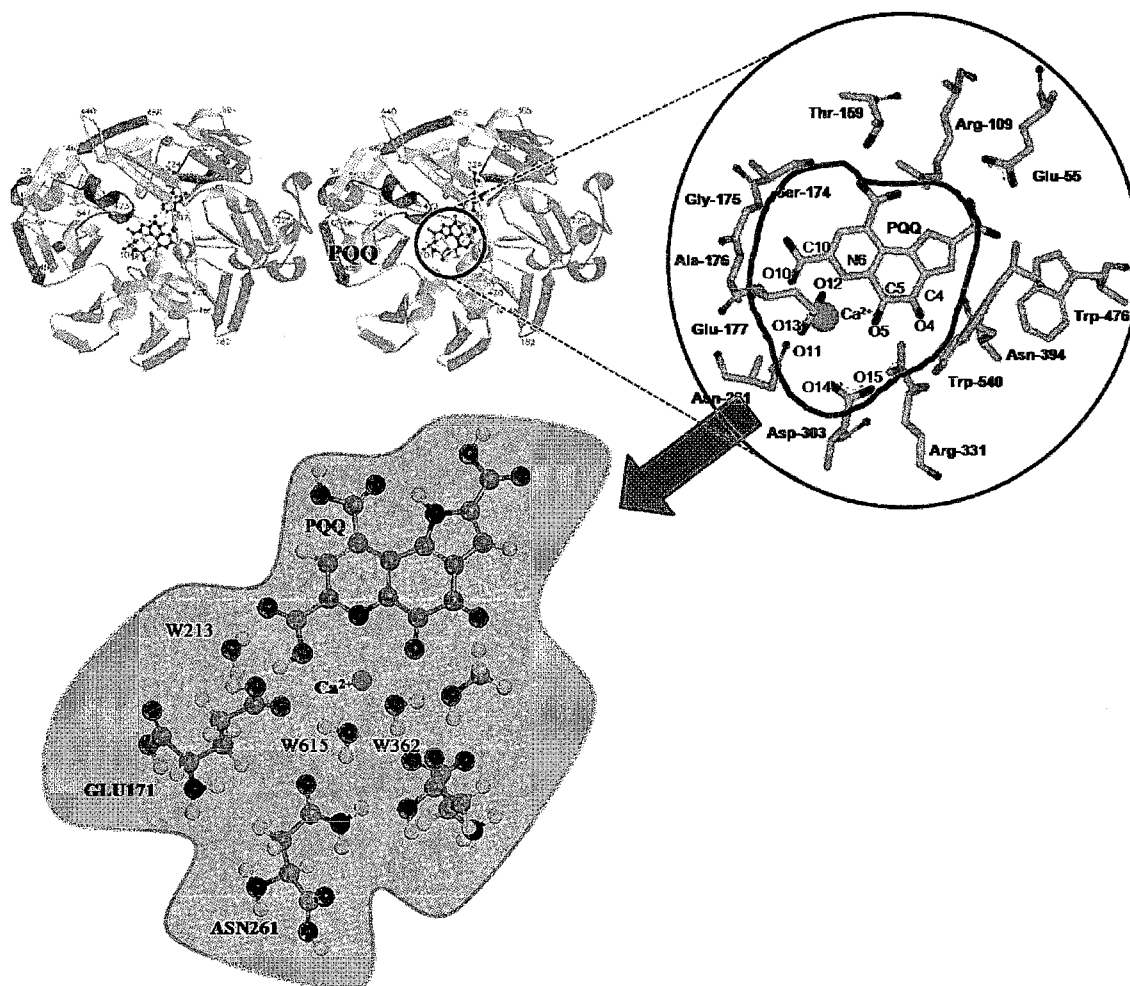
Figure 3.1 Construction of a model by identifying important groups from MDH active site (highlighted in black circle). Missing enzyme surrounding modeled by a continuum solvation around the selected model.

However, when histidine residues are present in the active site, considerations based on the pKa values and the pH of the solution have to be made to assign the protonation state of the group or one might design separate models with different

protonation states and test the effects on the barriers and energies of the reactions [54-61]. In MDH active site, no histidine groups are present, so this situation was not a problem while building our model.

The second step is building the substrate into the selected model. The substrate is not always present in the crystal structure and in some cases inhibitors or products are part of the structure instead. In such cases, superimposition of the substrate based on the position of either the inhibitor or the product has to be done [54-61]. In cases where substrate is not present such as ours, it is built into the model based on knowledge of the active site crystal structure predictions, like proximity to certain atoms and residues of the enzyme suggested to be the acid/base catalysts during oxidation.

The model should be constructed in such a way that the main focus is on the active site, where the actual chemistry takes place. In most cases there is experimental support to what residues are specifically important in the reaction mechanism. In other cases educated guesses have to be made by visually studying the active site and include the residues which could possibly interact with the substrate. The third step is to keep the size of the model as small as possible. So, if there are large numbers of residues to be considered, truncations can be made. The residues can be truncated in such a way, so that they are big enough to keep their chemical properties but small enough to keep the size of the model at its minimum [54-61]. While constructing our models, no truncations were made, since the total number of residues considered were not that large.

The idea to keep the size of the model as small as possible is important because computational costs can be reduced and also, there won't be a problem with the local minima. Geometry optimization of bigger models has a higher risk of converging to local

minima that are not actually global minima. So, the easiest way to avoid this problem is to keep the models as small as possible but still retain the chemical features that are important for the reaction.

The final step in the construction of an active site model is to construct a small model, conduct theoretical calculations, evaluate the results, and then go back to the x-ray crystal structure and construct a bigger model by considering more residues. By following this scheme, information about the enzyme active site chemistry can be obtained at a much lower computational cost initially, and a larger model can be constructed based on the results obtained from the smaller model. Also, when results from two different model sizes are obtained, the importance of specific residues in the larger model can be seen in a more direct way and useful mechanistic information at the active site can be obtained [55-57, 59-61].

3.2 Surrounding Effects

As discussed in Section 3.1, it is natural to construct a model with the active site of enzyme in focus as it is the place where the actual reaction takes place. However, the surrounding enzyme environment does influence the reaction with its steric and polarization effects [54-61].

In non-metalloenzymes, these steric effects are predominant because the enzyme surrounding has to keep the active site groups in certain positions relative to the substrate and relative to each other. Also, these effects are very large when there are no bonds or hydrogen bonding to other groups in the active site to keep things in place. In such cases, by locking certain atoms where the truncations are made to the residues at their crystallographic positions, these steric effects can be taken into account. This way, very

large and unrealistic movements of the various groups can be avoided. However, the structure and energetics are most affected as this procedure leads to a too rigid model [54-61].

But in the case of enzymes containing a metal ion in the active site, such as ours where the ion coordinates with the important residues to keep them in place and the presence of bonding and/or hydrogen bonding between residues is present, this steric effect is less of a problem. So no atoms were constrained in the selected active site models.

The polarization effects caused by the surrounding protein environment are implemented with a continuum solvation model known as COSMO (Conductor-Like Screening Model) in the DMOL^3 module. This theory treats the surrounding enzyme environment as a continuous homogeneous electrostatic medium with a dielectric constant chosen such that the environment of both neglected protein and water are replicated. The COSMO model works in such a way that the solute molecule forms a cavity within the dielectric continuum of permittivity, ε, that represents the solvent [83, 84]. The dielectric medium is polarized by the charge distribution of the solute. The response of the dielectric medium is described by the generation of screening (or polarization) charges on the cavity surface. The dielectric constant (ε) was chosen to be four, which is the standard value used in modeling protein surroundings and also, by giving accurate solvent effect. Geometry optimizations were performed in the presence of this solvation model so that the final total energy includes the DMOL^3/COSMO electrostatic energy [83, 84].

Usually the COSMO calculations have an effect of a few kcal/mol on the relative energy of the reaction. Very large solvation effects usually indicate that the active site model is too small and misses some important groups.

3.3 Computational Details

All the computations reported in this dissertation were performed with generalized gradient approximation (GGA) within the density functional theory formalism as implemented in DMOL^3 in Materials Studio® software by Accelrys Inc [78, 79]. All geometry optimization calculations are performed using the Becke-Lee-Yang-Parr BLYP exchange correlation functional and the double numerical with polarization (DNP) basis set, which is the best set available in DMOL^3. Harmonic vibrational frequency calculations are performed to ensure that stationary points on the potential energy surface of the systems are in fact local minima (all real frequencies) or transition states (only one imaginary frequency) and also to obtain thermal corrections to free energies at 298.15 K. The transition states obtained by the DMOL^3 may not be the transition state connecting the intended reactant and product for a particular reaction step. Therefore, in order to thoroughly investigate the reaction paths, the intrinsic reaction coordinate (IRC) analysis was performed.

DFT-MD investigations were also carried out on bigger active site model geometries to see the conformational fluctuations using NVT/NVE ensembles available in DMOL^3 module. The homogeneous polarizable medium is considered with a continuum solvation model known as COSMO as implemented in the DMOL^3 module. The dielectric constant (ε) was chosen to be four, which is the standard value used in

modeling protein surroundings. Geometry optimizations were performed in the presence

of this solvation model for the obtained gas phase geometries.

CHAPTER 4

INVESTIGATION OF ADDITION-ELIMINATION

OXIDATION MECHANISM BY MDH

The A-E is a three-step mechanism (Figure 4.1) that involves a proton transfer from methanol to an active site base, which is proposed to be ASP303. It is believed that the presence of this catalytic base at the MDH active site initiates the oxidation reactions by subtracting a proton (H16) from methanol (Figure 4.1). This proton "addition" to ASP303 leads to the formation of a covalent hemiketal intermediate, since the resulting oxyanion (O16⁻) in the methanol molecule is then attracted to the C5 of PQQ. The second step consists of the proton (H16) "elimination" from ASP303 and transfer to O5 of PQQ. The final step is characterized by cleavage of C_{met}-H17 bond resulting in a second proton (H17) transfer to the O4 of PQQ (Figure 4.1), and the formation of the by-product formaldehyde (CH_2O). This final step is considered to be the rate-determining one according to the literature.
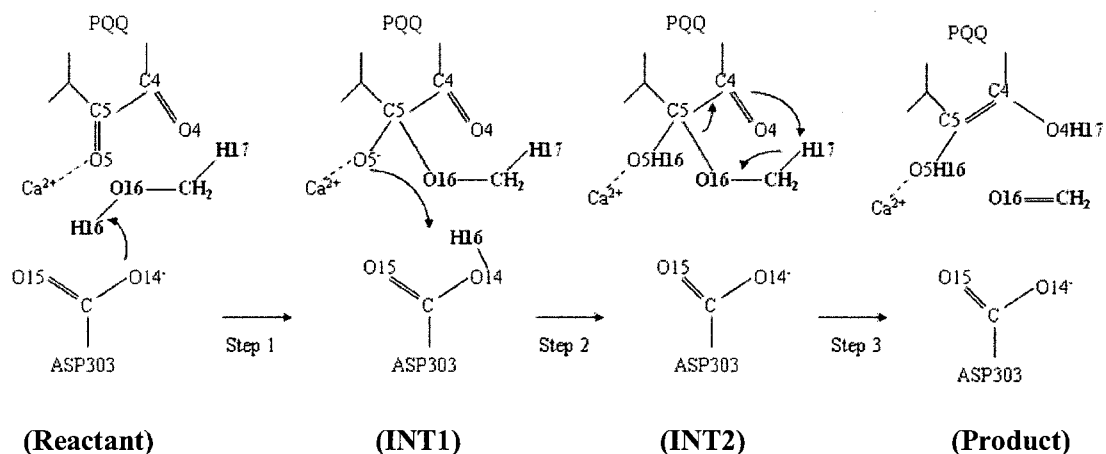
Figure 4.1 Addition-elimination (A-E) methanol electro-oxidation mechanisms by methanol dehydrogenase enzyme proposed in the literature.

4.1 Methanol Dehydrogenase Active Site Models

In order to investigate the A-E mechanism, relevant portions (models) of the complete MDH active site are considered to reduce the number of atoms to conduct accurate electronic structure calculations as explained in Chapter 3. The two MDH active site models selected in this work (Models A and B) consisted of the Ca^{2+} ion, since it is part of the active site and its role is still unknown; the PQQ molecule, since it is MDH's co-factor; and relevant amino acids carefully selected based on the current state of knowledge on methanol oxidation by MDH. Model A consists of the PQQ molecule, the Ca^{2+} ion, and aspartic acid (ASP303); Model B contains glutamic acid (GLU177) and asparagine (ASN261), in addition to the contents of Model A. Then, three water molecules (W362, W615, W213) identified near the catalysis area of the enzyme were also taken into account by adding them to the contents of Model B to see whether they have any influence on the reaction mechanism. All the active site models are tested with and without the presence of dielectric solvation (for neglected protein environment) to provide extended analysis on the oxidation mechanisms.

MDH active site models were geometry minimized at the BLYP/DNP level with no constraints, and further tested upon methanol oxidation as explained in the following sections. As discussed earlier in Chapter 3, to estimate the energetic effects of the protein environment not included in the chosen quantum chemical model, solvation effects were employed on the model with a dielectric constant of four. The choice of dielectric constant value is somewhat arbitrary, but a value of four was used frequently in similar enzymatic studies [55-57, 59-61]. Free energies of the reactant, all intermediates, and corresponding transition states for each step are obtained from our calculations.

4.2 <u>Model A</u>

In Model A, the system representing MDH is formed by PQQ, Ca^{2+}, and ASP303. For step one, a methanol molecule is added to that system according to Figure 4.2 to represent the reactant (total number of atoms in the model is 52), and the complete complex is geometry optimized at the BLYP/DNP theory level [85, 86]. The Ca^{2+} coordination with the nitrogen and oxygen atoms of PQQ (at 2.62, 2.45, and 2.52 Å respectively, Figure 4.2) is well preserved with respect to the X-ray crystal structures [31-36]. Also, the ion coordinates with carboxylic oxygen of the ASP303 (2.41 Å). The four coordination of the ion in this model is not consistent with the six coordination of the ion as illustrated in the X-ray structures because of other missing amino acids. As seen from Figure 4.2, the methanol molecule is in a perfect position (O14-H16 = 2.18 Å) for initial proton abstraction by ASP303. However, C5 of PQQ to O16 of methanol distance appear a little longer.
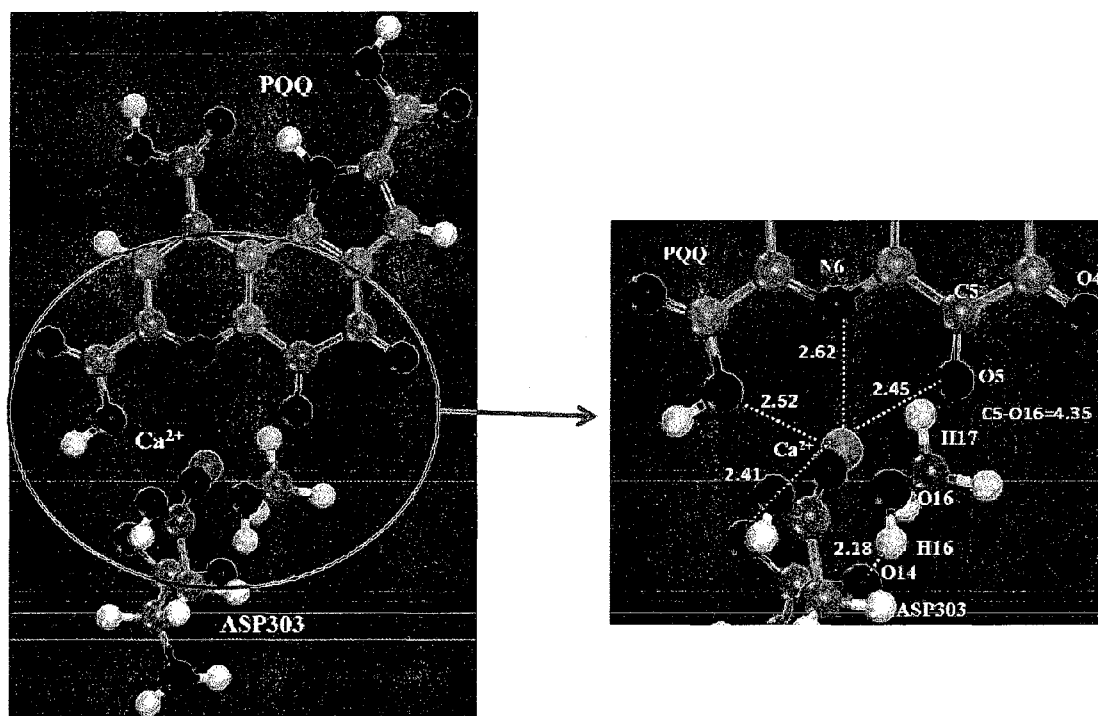
Figure 4.2 Optimized reactant complex for Model A. Reactive portion of the structure is highlighted and the distances are in Å.

4.2.1 Step 1: Proton Abstraction by ASP303 from Methanol and Nucleophilic "Addition" of Hemiketal Complex to PQQ

In Step 1 of A-E (Figure 4.1), a proton (H16) transfer from methanol to ASP303 and the nucleophilic addition of the CH_3O^- complex to the C5 of PQQ is proposed to take place. The O14-H16 distance reduces from 2.18 (reactant) to 1.01 (transition state TS1) and to 0.98 Å (INT1), and the C5-O16 bond distance changes from 4.35 (reactant) to 2.96 (TS1) and to 1.46Å (INT1) indicating that the formation of O_{met}-C5 and the shift of proton from alcoholic OH group of methanol to ASP303 occurs in a concerted way (Figure 4.3). The imaginary frequency (~95 cm^{-1}) of TS1 corresponds to the translational motion of the CH_3O^- towards the C5 of PQQ and the proton (H16) transferred to the ASP303. The methoxide (CH_3O^-) addition to the PQQ results in the formation of first intermediate (INT1) where the O_{met}-C5 bond is completely formed (1.46 Å) [85, 86].

In the gas phase, the free energy barrier for TS1 from the reactant is 29.5 kcal/mol, and the INT1 is calculated to lie above 17.1 kcal/mol with respect to the reactant complex [85, 86]. In the presence of dielectric solvation, the barrier is decreased to 22.6 kcal/mol, and the energy of the intermediate is lowered from 17.1 to 10.2 kcal/mol. It is easy to rationalize these results considering that the reaction step under study is a proton transfer that results in a positive charge on the aspartic acid and an additional negative charge on the CH_3O^-, which attacks the C5 of PQQ resulting in negative charge on the O5 of INT1. Therefore, solvation lowers the energy of transition and intermediate states compared to the reactant species.

4.2.2 Step 2: Proton "Elimination" from ASP303 and Transfer to PQQ

For Step 2, a proton (H16) transfer is proposed to occur from ASP303 to the O5 of PQQ via a transition state (TS2). The proton is shared between the oxygen atoms of PQQ (at 1.23 Å) and the ASP303 (at 1.24 Å), respectively (Figure 4.3). This transition state imaginary frequency (~700 cm^{-1}) corresponds to the symmetrical stretching of the O5-H16 and H16-O14 bonds. The proton transfer leads to the formation of second intermediate (INT2) along the overall reaction profile. The C5-O16 distance lengthens from 1.46 at INT1 to 1.58 Å at INT2. Also, the CH_3 group of attached methanol orients towards O4 of PQQ, so that the latter is in a good position in breaking the $H-CH_2$ bond (the distance from H17 to O4 of PQQ is 2.51 Å) [85, 86].
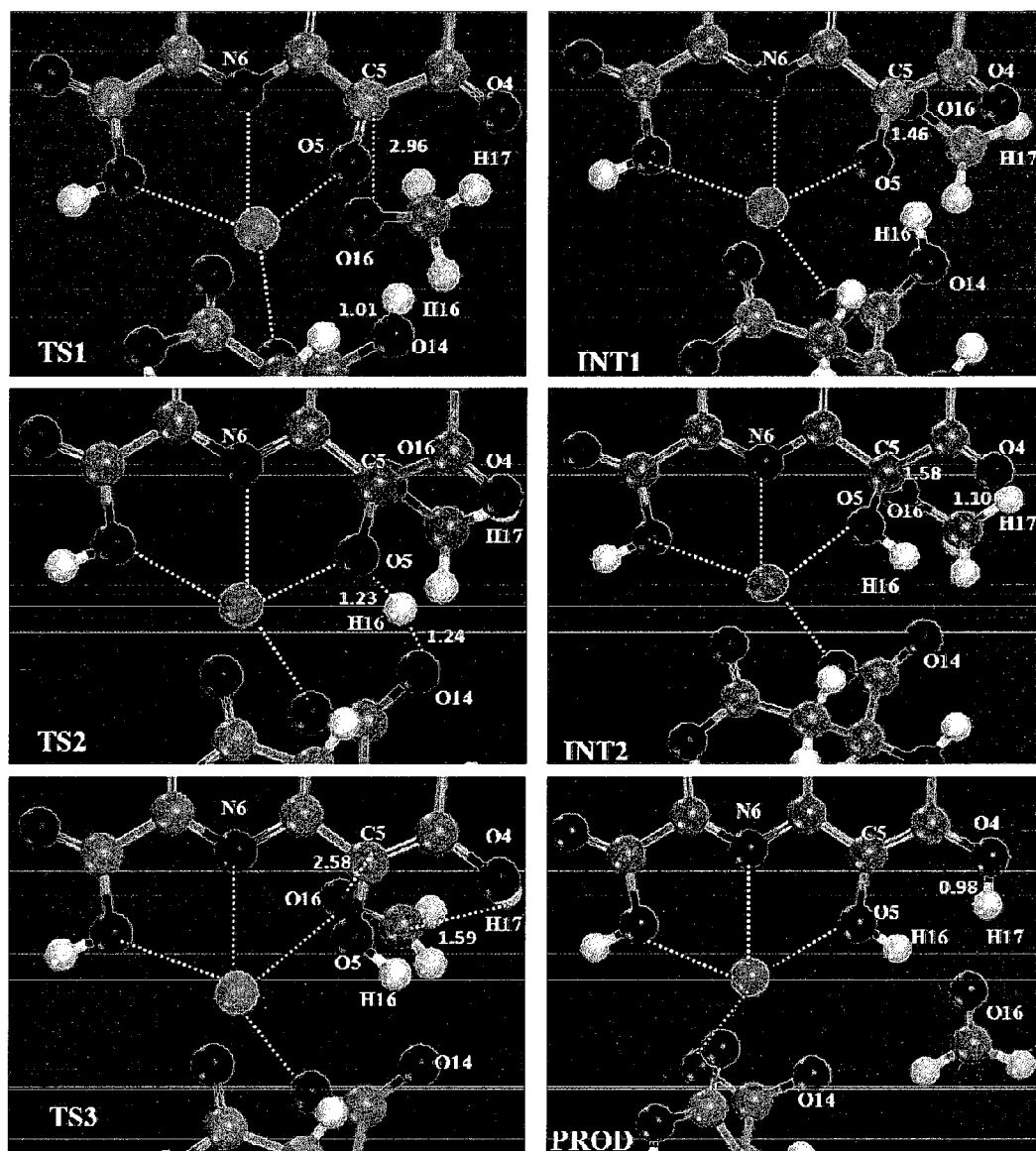
Figure 4.3 Reactive portions of geometry optimized structures involved in A-E methanol oxidation mechanism by MDH active site Model A. Distances are in Å.

The gas phase energy barrier of TS2 with respect to INT1 is calculated to be 7.7 kcal/mol, and the energy of the intermediate INT2 is 11.9 kcal/mol with respect to the reactant [85, 86]. Dielectric solvation lowers the barrier by 3.2 kcal/mol, while the energy of INT2 is lowered by 8.1 kcal/mol with respect to the gas phase. The presence of a

negative charge on both O5 of PQQ and O14 of ASP303 during TS2 is largely stabilized by the solvation compared to the negative charge on just the ASP303 in INT2.

4.2.3 Step 3: Formation of Formaldehyde and Reduced PQQ

The final transition state TS3, which leads to the formation of $PQQH_2$ reduced species, is located in this step. The cleavage of the carbon atom in the methanol molecule and H17 is observed since the C_{met}-H17 bond length evolves from 1.10 (INT2) to 1.59 (TS3) to 2.58 Å (product), and the corresponding H17-O4 distances reduces from 2.51, to 1.01, and to 0.98 Å, respectively. The bond between O16 and C5 of PQQ lengthens up to 2.58 Å indicating the breakage to form the by-product formaldehyde (Figure 4.3). TS3 imaginary frequency (~430 cm^{-1}) corresponds to the movement of the H17 between the methyl carbon (C_{met}) and O4 of PQQ.[85,86] Even though the O4 of PQQ and H17 of methanol appear close to each other during the previous steps, in reality they are not close until this step takes place.

The free energy required to overcome the transition state for this step is 17.7 kcal/mol with respect to INT2 [85, 86]. The energy of the final product is below 1.6 kcal/mol with respect to the reactant. There is not any change in the barrier even though the INT2 and transition state TS3 are much stabilized in the presence of solvation.

By looking at the potential energy curve of full reaction for Model A from Figure 4.4, we can say that Step 1 is the slowest (rate-determining) and Step 2 is fastest in the gas phase [85, 86] and even in solvation. There appears a contradiction because according to the literature [37, 39, 58], Step 3 was indicated as the rate-determining for this mechanism. The energies of the transition states and intermediates associated with all steps are much lowered in the presence of dielectric solvation, thereby lowering the free

energy barriers in case of Steps 1 and 2. In gas phase, Steps 2 and 3 are plausible from their barriers, but the barrier for Step 1 is perhaps too high to be possible for a general enzymatic catalytic process (greater than 18 kcal/mol). Since solvation has a more pronounced effect on the reaction mechanism energies tested with this model, we can say that some groups that should be explicitly present to account for stabilization are absent. So, we devised an even bigger Model B by adding some more residues to validate the results obtained from Model A.
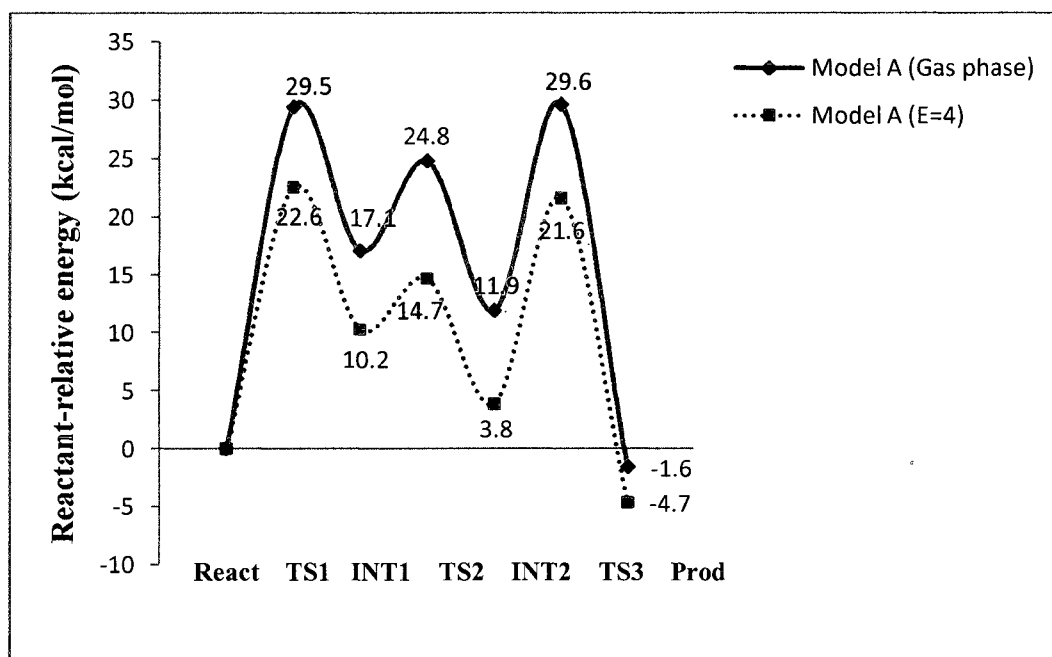
Figure 4.4 Potential Energy Surface (PES) for methanol A-E oxidation mechanism by MDH active site Model A. Reactant-relative energies calculated at the BLPY/DNP theory level are in kcal/mol.

4.3 Model B

Model B consists of glutamic acid (GLU177) and asparagine (ASN261) in addition to the contents of Model A. The total number of atoms present in this model are 88. Also the six-coordination of the Ca^{2+} neglected in Model A is considered here with

the presence of other amino acids. The minimum energy reactant complex in the presence of methanol for Model B is shown in Figure 4.5. The Ca^{2+} coordinates with the nitrogen and oxygen atoms of PQQ (at 2.64, 2.52, and 2.72 Å, respectively), the carbonyl oxygen atoms of ASN261 (at 2.38 Å), GLU177 (at 2.37 Å), and ASP303 (at 2.33 Å) . The methanol and ASP303 orient better in this case for the first step to occur with distances O14-H16 =1.69 (2.18), C5-O16 = 3.10 (4.35) Å compared to Model A (parenthesis) [85, 86].
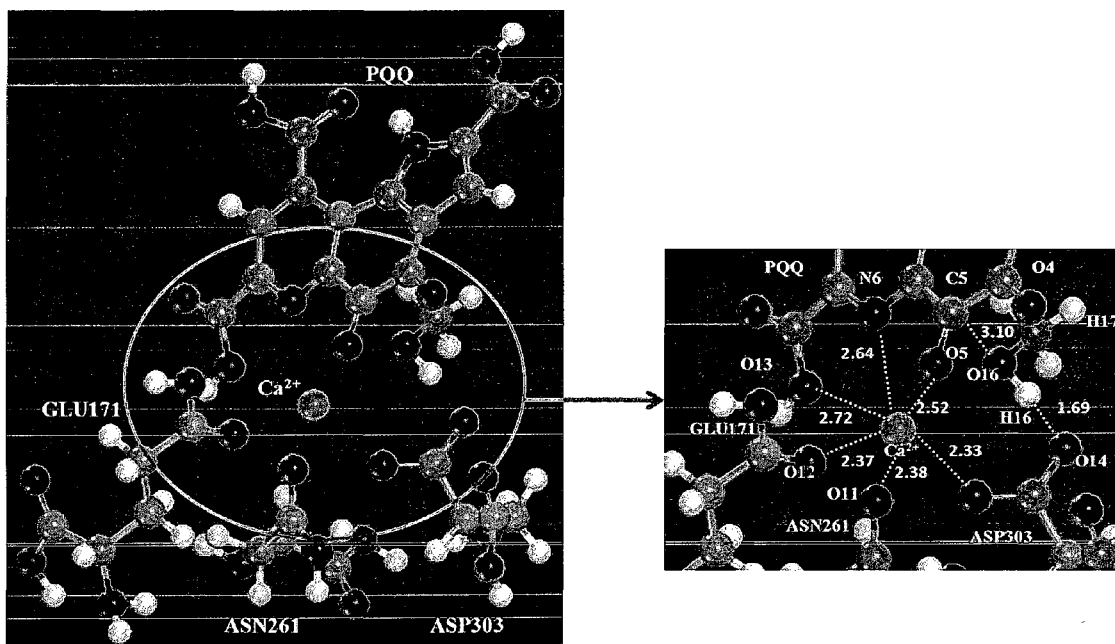
Figure 4.5 Optimized reactant complex for Model B. Reactive portion of the structure is highlighted and the distances are in Å.

Similar to Model A, we have optimized all stationary points (React, TS1, INT1, TS2, INT2, Prod) for this model. Important structural parameters are shown in Figures 4.5 and 4.6, and potential energy curves in both the gas phase and protein environment in Figure 4.7. We note that some critical distances with respect to the transition states and intermediates changed compared to those in Model A.

From transition state TS1 to INT1, the C5-O16 distance changes from 2.76 to 1.40 Å (Figure 4.6) compared to 2.96 to 1.46 Å in Model A. O14-H16 distance remains the same. This change in distance didn't affect the gas phase free energy barrier for this transition state to occur for this step (28.5 kcal/mol, 29.5 for Model A). Even in the presence of solvation the TS1 energy remains almost the same. However, the energy of INT1 is calculated to be 22.5 kcal/mol with respect to the reactant, higher by 5.4 kcal/mol than INT1 of Model A in gas phase. Even the presence of solvation had a greater impact on the energy of this intermediate, accounting for the negative charge on O5 of PQQ as we observed for Model A [85, 86].

TS2 seems to be later with Model B than A. The O14-H16 and O5-H16 distances are 1.58 and 1.21 Å, Figure 4.6 (compared to 1.24 and 1.23 Å in Model A). The gas phase free energy barrier for this step is lowered by 3 kcal/mol compared to Model A. The energies of the TS2 and INT2 are lowered by 6.4 and 4.5 kcal/mol in solvation compared to the gas phase. The solvation effects for this step with Model B were less pronounced than with Model A [85, 86].
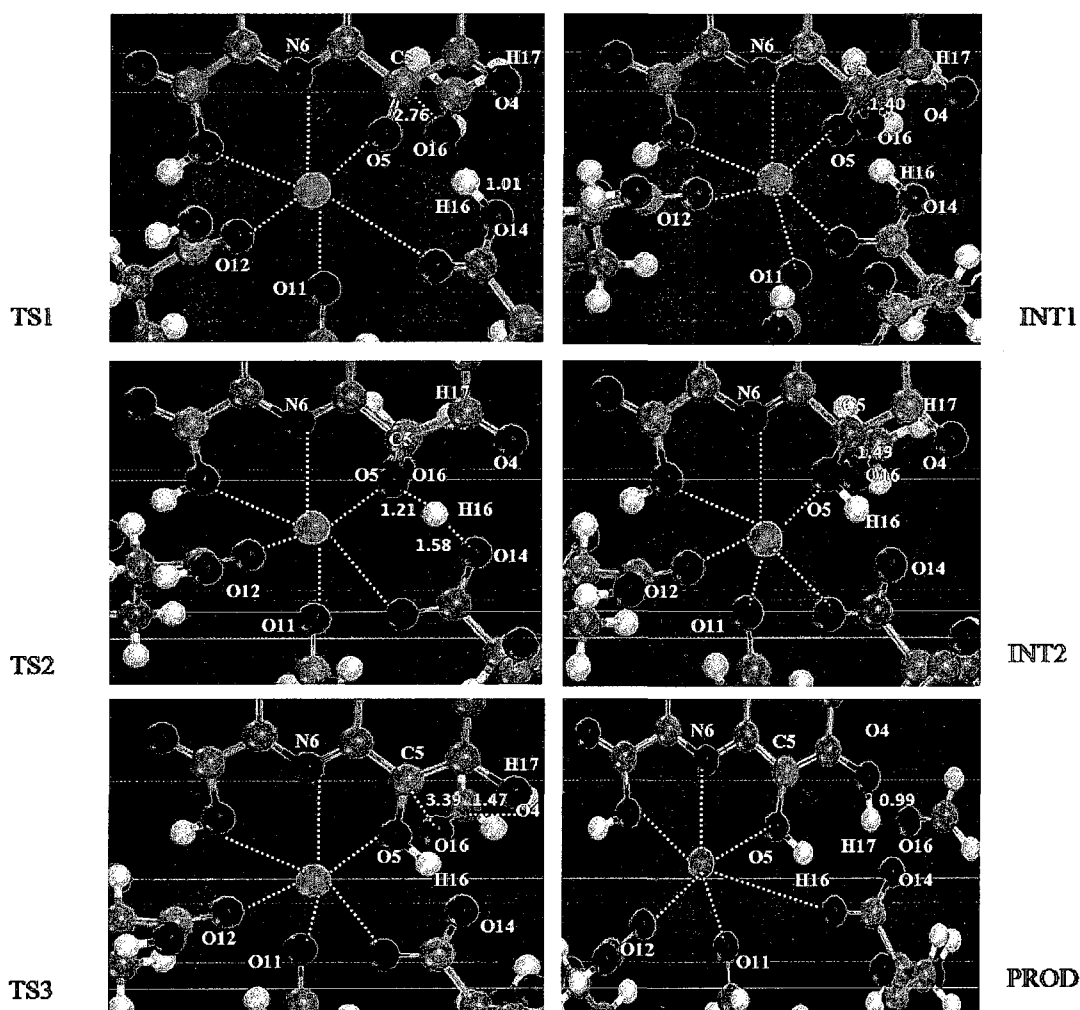
Figure 4.6 Reactive portions of geometry optimized structures involved in A-E methanol oxidation mechanism by MDH active site Model B. Distances are in Å.

The third transition state, TS3, forms a little earlier in case of Model B. The C_{met}-H17 distance is 1.47 compared to 1.59 Å in Model A. The bond between O16 and C5 of PQQ breaks, and the distance increases up to 3.39 Å, indicating the formation by-product formaldehyde (Figure 4.6). The final product is 1.1 kcal/mol lower than the reactant, and the free energy barrier for this step is almost the same (~1 kcal/mol difference) as that of Model A in gas phase. Dielectric solvation increases the barrier by 4.3 kcal/mol and lowers the energy of the product by 5.1 kcal/mol [85, 86].
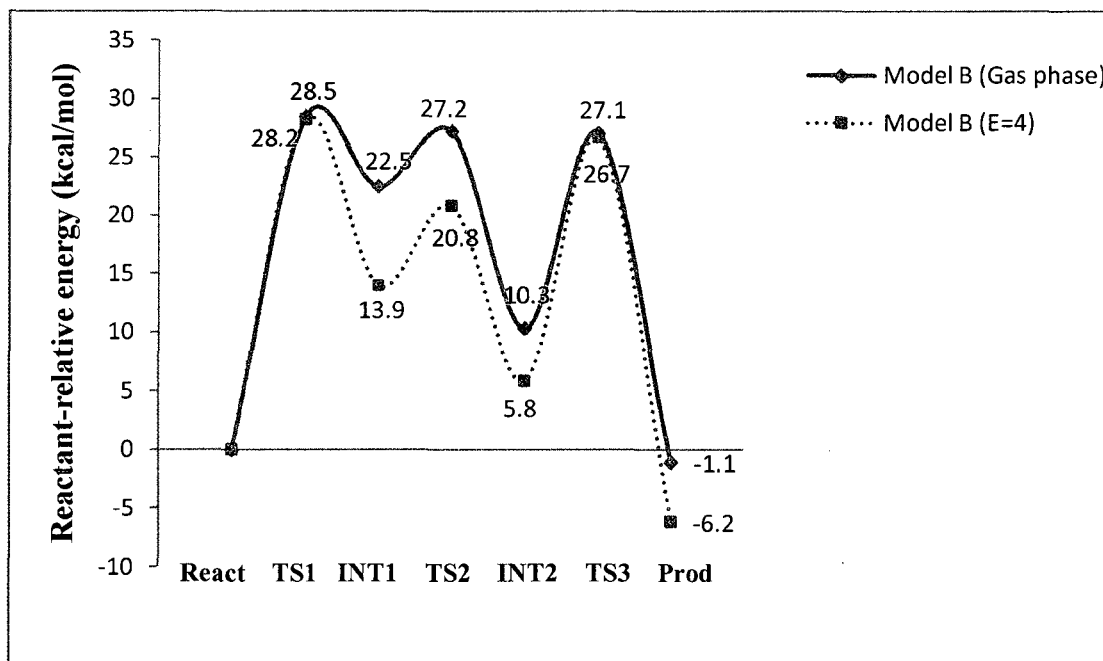
Figure 4.7 Potential energy surface (PES) for methanol A-E oxidation mechanism by MDH active site Model B. Reactant-relative energies calculated at the BLPY/DNP theory level are in kcal/mol.

From the potential energy curves of Model B in gas phase (Figure 4.7), we can see that the barriers for Steps 1 and 3 were almost the same as observed for Model A. The barrier for Step 2 was only reduced by three kcal/mol compared to Model A. The presence of solvation lowered the energies of the components of Step 2 and the final product only, but Model B still showed that there is a need to add some more explicit groups. The energies of TS1 and TS3 didn't change that much when compared to Model A, and the barrier for Step 1 is still high for an enzymatic catalytic process. The same contradiction with the literature appears here as in Model A concerning the rate-limiting step [85, 86]. So we tried to improve Model B by considering also the water molecules in the catalysis area in addition to the residues.

4.4 <u>Model B + Three Water</u>

This model consists of three waters W362, W615, and W213 in addition to the contents of Model B. The total number of atoms present in the model are 97. Also the six-coordination of the Ca^{2+} as in Model B is replicated here with the presence of water. The minimum energy reactant complex in the presence of methanol for this Model is shown in Figure 4.8. In this case, the Ca^{2+} coordinates with the nitrogen and oxygen atoms of PQQ (at 2.57, 2.41, and 2.56 Å, respectively), the carbonyl oxygen atom of GLU177 (at 2.86 Å); and both oxygen atoms of water molecules W362 and W615 (at 1.94 and 2.24 Å), respectively. Also W615 and W213 maintain hydrogen bonding with PQQ, PQQ, and GLU177, respectively, in accordance with the literature. The methanol and ASP303 orient better in this case for the first step to occur with distances O14-H16 =1.74, C5-O16 = 4.10 Å, compared to Model A [86].

Similar to Models A & B , we have optimized all stationary points (React, TS1, INT1, TS2, INT2, Prod) for this model. Important structural parameters are shown in Figures 4.8 and 4.9, and potential energy curves for both gas phase and protein environment in Figure 4.10. As we observed for Models A and B, we noticed that some critical bond distances with respect to the transition states and intermediates change compared to those in Model B without water. Important distances are tabulated for this model in Table 4.1.

For TS1 of Step 1, the C5-O16 distance is 2.78 Å, almost same as that of Model B without water but less than that of Model A (2.96 Å). The O14-H16 distance remains the same in all three cases.
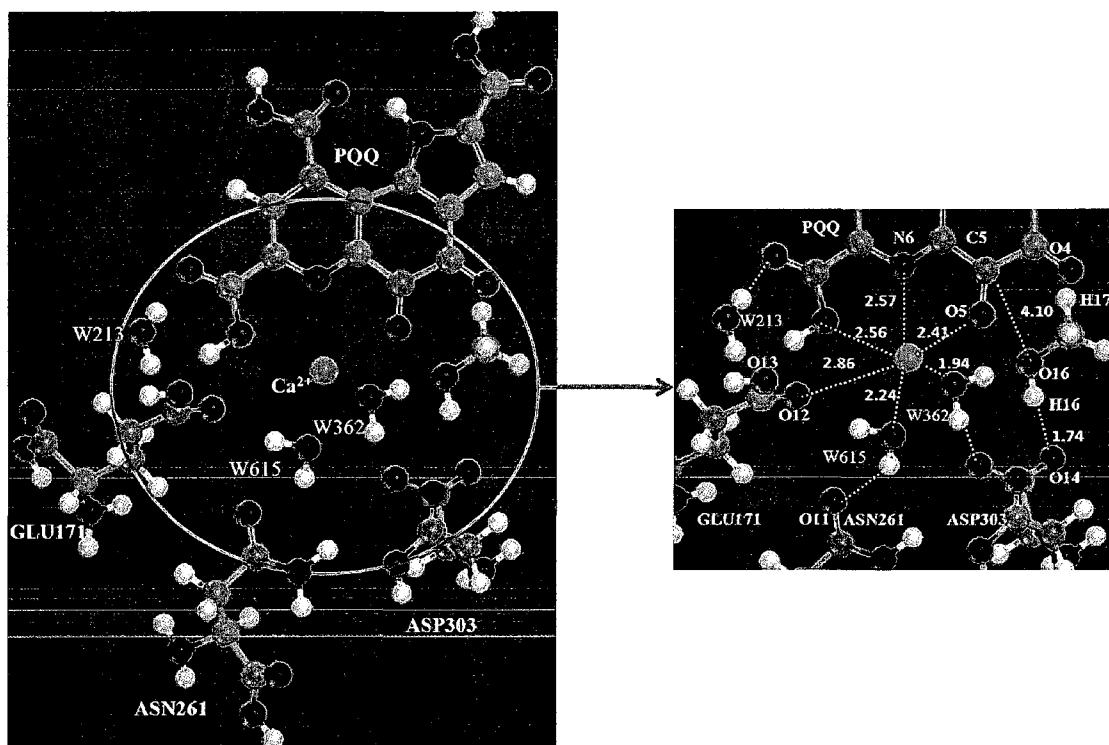
Figure 4.8 Optimized reactant complex for Model B + 3W. Reactive portion of the structure is highlighted, and the distances are in Å.

Table 4.1 Selected bond distances corresponding to the optimized structures of reactant, transition states and intermediates during the methanol A-E oxidation mechanism from MDH Model B with water.

Bond Length (Å)	Reactant	TS1	INT1	TS2	INT2	TS3	Product
O14-H16	1.74	1.01	0.98	1.58	2.60	2.89	2.60
C5-O16	4.10	2.78	1.54	1.48	1.89	3.47	4.33
O5-H16	3.55	3.53	3.43	1.40	1.03	1.00	1.00
O4-H17	5.21	4.91	2.83	2.51	2.51	1.01	0.99
C_{met}-H17	1.10	1.11	1.10	1.10	1.10	1.47	2.82

The C5-O16 for INT1 in this case is 1.54 Å, higher than both previous models (Figure 4.9). In the gas phase, the free energy barrier calculated for this step is 19.5 kcal/mol, and the energy of INT1 is 14.1 kcal/mol with respect to the reactant, almost lowered by 10 kcal/mol with respect to the barrier from Model A. There can be two

reasons for this reduction in the barrier and also the energy of INT1 for this step. The first reason can be that the coordinating distance between $O5\text{-}Ca^{2+}$ reduces as the reaction proceeds from 2.41 (Reac) to 2.35 (TS1) to 2.29 Å (INT1). The second reason can be that the hydrogen bonding of water molecule (W362) to O5 of PQQ gradually decreases from 2.50 to 2.30 to 1.98 at INT1, thereby making more stable the negative charge on O5 of PQQ (Figure 4.9). Also, the presence of solvation did not have any effect on the energetics of TS1 and INT1. So we can say that the ion and the water suffice in stabilizing these species, thereby lowering the barrier [86].

TS2 and INT2 appears to form earlier in this case than in Model B without water. The O5-H16 and C5-O16 distances increase to 1.40, 1.89 compared to 1.21, 1.49 Å, respectively (Table 4.1), and also the energies are lower with respect to the reactant compared to the previous models. The hydrogen bonding of W362 slowly deteriorates with O5 of PQQ and improves with ASP303 as the reaction proceeds. The gas phase energy barrier is increased by 2.1 kcal/mol in this case compared to Model B without water. However, with the solvation effects, the barrier is reduced back to 3.8 kcal/mol [86].

Figure 4.9 Reactive portions of geometry optimized structures involved in A-E methanol oxidation mechanism by MDH active site Model B + 3W. Distances are in Å.

For Step 3, the third transition state, TS3 appears the same as that of Model B without water and of Model A. The formation of formaldehyde is observed with the breakage of the bond between O16 and C5 of PQQ (3.47 Å) (Figure 4.9). Water molecules W615 and W362 maintain their coordination with calcium, ASP303, and calcium, respectively throughout this proposed reaction path until the formation of the final product. However, the free energy barrier for this step increased by 3.7 kcal/mol compared to both previous models, and dielectric solvation does not change this barrier but lowers the energy of the product by 4.4 kcal/mol [86].
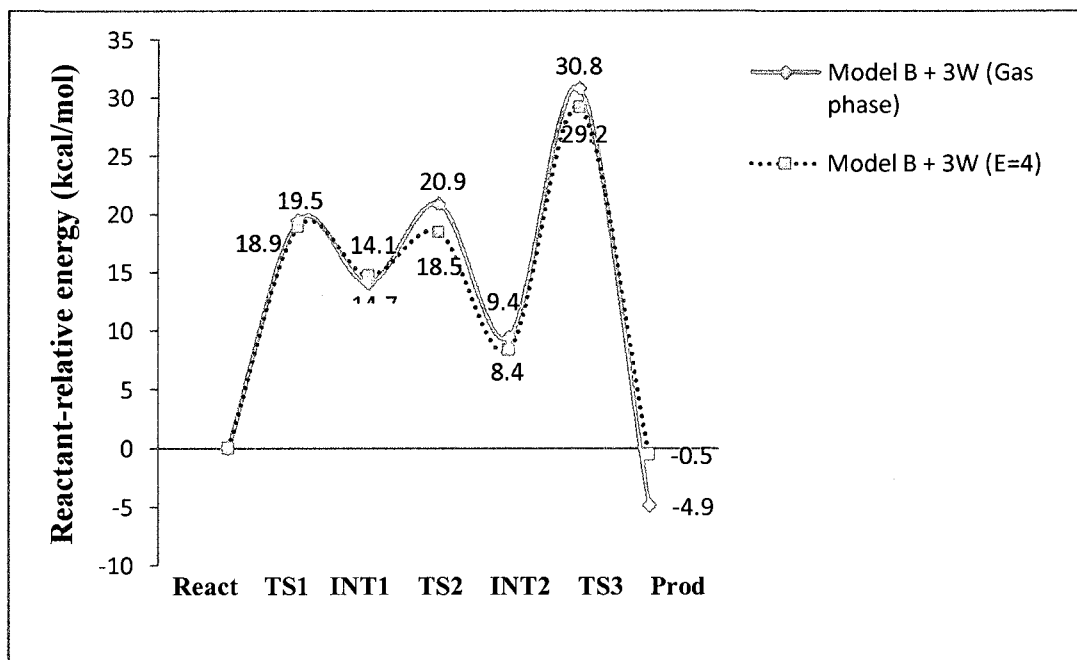
Figure 4.10 Potential energy surface (PES) for methanol A-E oxidation mechanism by MDH active site Model B + 3W. Reactant-relative energies calculated at the BLPY/DNP theory level are in kcal/mol.

Table 4.2 Energy barriers (kcal/mol) corresponding to Steps 1 to 3 of the methanol A-E oxidation mechanism calculated at the BLPY/DNP theory level for Models A, B, and B + 3W in Gas Phase (GP) and solvation (E=4).

	Model A (GP)	Model A (E=4)	Model B (GP)	Model B (E=4)	Model B + 3W (GP)	Model B + 3W (E=4)
Step 1	29.5	22.6	28.5	28.2	19.5	18.9
Step 2	7.7	4.5	4.7	6.9	6.8	3.8
Step 3	17.7	17.8	16.8	20.9	21.4	20.8

4.5 Discussion and Summary

The PES of Model B + 3W is shown in Figure 4.10. Dielectric solvation doesn't

have much of an impact on the model energetics as we observed for the other two models

because most of solvation to stabilize the charged species is already included explicitly in

the Model with the presence of water. In the gas phase, there is a major decrease in the free energy barrier for Step 1 (~10 kcal/mol), making it kinetically plausible in this case. There is also a slight increase in the free energy barrier for Step 3 (~ 3.7 kcal/mol) compared to the other two models. The barrier for Step 2 remains the same as in Model B without water and with an increase of 2.3 kcal compared to Model A (Table 4.2). Step 2 is the fastest in this case, consistent with the previous results, but the barriers for Steps 1 and 3 make both of these rate-limiting ones as opposed to Models A and B where only Step 1 was found to be kinetically slower [86]. The A-E seems to be more plausible with all free energy barriers less than or nearer (~ 2 kcal/mol) to 18 kcal/mol when the MDH model consisted of PQQ, Ca^{2+}, ASP303, GLU171, ASN261 and three waters W362, W615, and W213 (Model B + 3W) [86].

From theoretical calculations by Leopoldini et al. [58] there is only one rate-determining step for A-E (34.6 kcal/mol for Step 3 of A-E), and it is not kinetically favorable according to the general kinetic requirements of an enzymatic catalytic process. Step 1 was observed to proceed normally from their calculations with a barrier of 11.4 kcal/mol. However, from our calculations with Model B + 3W, there appears a contradiction with the literature with step 1 being rate-determining along with Step 3 (Step 1, 19.5 kcal/mol & Step 3, 21.4 kcal/mol). Even for the new "addition-elimination-protonation" proposed by Leopoldini et al. [58], the barrier for the rate-limiting step has been reduced to 16 kcal/mol; however, Step 1 remains the same as that of A-E, which was found to be kinetically slower from our calculations. From experimental kinetics on methanol oxidation by wild-type Ca^{2+}-MDH, Goodwin et al. [52] reported Gibbs free energy of activation to be 8.5 kcal/mol, and this calculation was not related to a particular

step of A-E. if we compare our rate-determining steps free energy barriers with this Gibbs activation (as done by Zhang et al. [51] for H-T), they are higher by approximately 11-13 kcal/mol. This indicates, from our DFT calculations, that A-E may not be the mechanism under operation for oxidation of methanol.

CHAPTER 5

INVESTIGATION OF HYDRIDE TRANSFER

OXIDATION MECHANISM

The Hydride transfer (H-T) is proposed to be a four-step mechanism (Figure 5.1). The first step involves a proton and hydride transfer: H16 and H17 from the methanol molecule to ASP303 and C5 of PQQ respectively, resulting in the formation of the by-product formaldehyde. In the second step, there is a proton (H16) transfer from ASP303 to the C5 of PQQ. The third step involves the proton (H17) transfer from the C5 of PQQ to ASP303, and the final step consists of the transfer of H17 from ASP303 to the O4 of PQQ, thus getting PQQ reduced (Figure 5.1). The rate-determining step is proposed to Step 1 which involves the cleavage of C_{met}-H17 thereby transferring the hydride (H17) to C5 of PQQ.
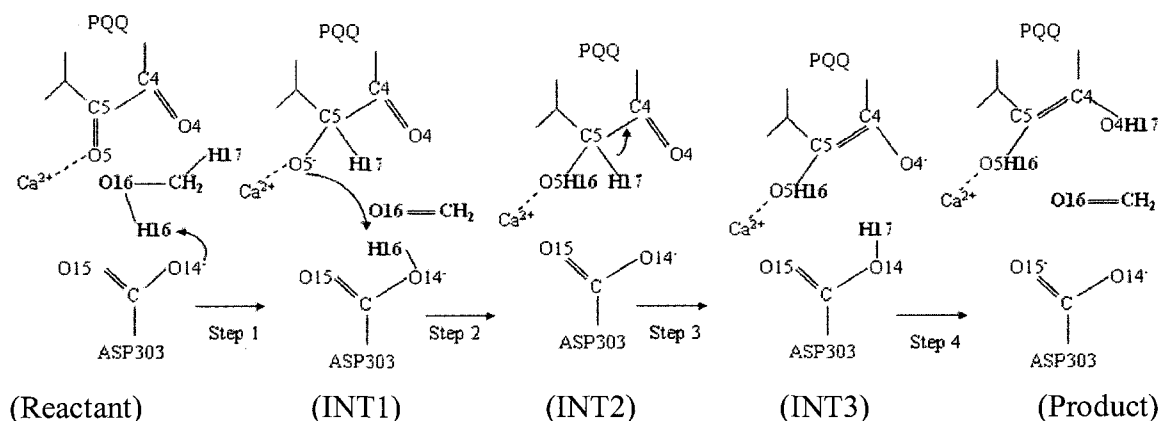
Figure 5.1 Hydride-Transfer (H-T) methanol electro-oxidation mechanism by methanol dehydrogenase enzyme proposed in the literature.

5.1 MDH Active Site Models

As we did for the A-E mechanism, to investigate the H-T mechanism we used the same kind of active site models. Model A (PQQ, Ca^{2+}, ASP303); Model B (Model A + GLU177 + ASN261); and Model B + 3W (W362, W615, W213). These active site models were geometry minimized with methanol at the BLYP/DNP level with no constraints, and further tested upon methanol oxidation as explained in the following sections. Dielectric solvation is also applied to estimate the energetic effects of the protein environment not included in the quantum chemical model chosen, with a dielectric constant of 4 [86].

5.2 Model A

The minimum energy reactant complex obtained for Step 1 of this mechanism is the same as that of A-E as shown in Figure 5.2. Coordination of ion with atoms of PQQ and Asp303 are already discussed in Chapter 4. The methanol molecule is in a good position for proton transfer (O14-H16 = 2.18 Å), whereas H17 is farther away from C5 of PQQ, C5-H17 = 4.55 Å.
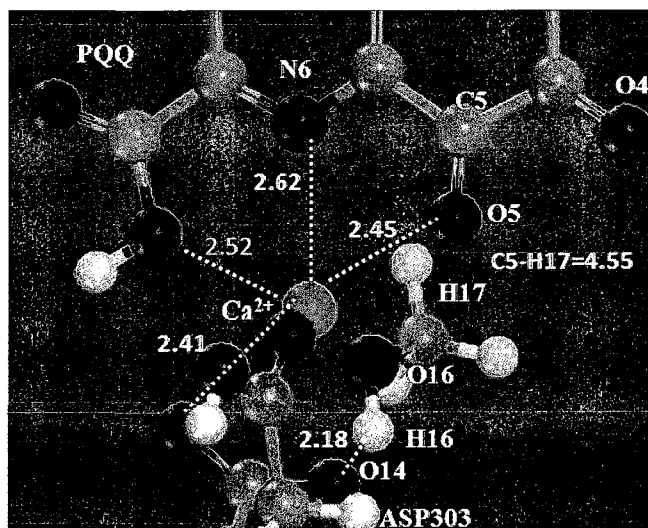
Figure 5.2 Reactive portion of the reactant complex and the distances are in Å.

5.2.1 Step 1: Formaldehyde Formation

According to Step 1 of the H-T methanol oxidation mechanism (Figure 5.1), there should be a direct hydride transfer (H17) from methanol to C5 of PQQ in concert with proton abstraction (H16) by O14 of ASP303. Hence, the first transition state from the reactant complex evolves into the first intermediate (INT1), where the by-product formaldehyde formed leaves the active site. From our calculations at the BLYP/DNP level, it is found that O14-H16 bond length evolves from 2.18 (reactant) to 1.12 (TS1) to 1.00 (INT1) Å (Figure 5.3), showing the binding of the H16 proton to ASP303. The C5-H17 distance from the initial reactant is reduced from 4.55 to 1.83 and finally to 1.21 Å, evidencing the hydride transfer to the C5 of PQQ. The single imaginary frequency ($\sim$1089 cm^{-1}) of TS1 corresponds to the symmetrical stretching of the C5-H17 and C_{met}-H17 bonds.

The gas phase energy barrier obtained from TS1 to reactant is 29.2 kcal/mol, and the first intermediate obtained as a product for this step lies at 17.3 kcal/mol above the

reactant. When dielectric solvation is applied, the barrier and the energy of the intermediate are lowered by 4.6 and 2.0 kcal/mol respectively. Ca^{2+} polarizes the C5-O5 bond, making C5 more positive and O5 more negative with ASP303 essentially protonated during this step. So the solvation effects provides the electrostatic stabilization lowering the energies of TS1 and INT1 [86].

5.2.2 <u>Step 2: Proton Transfer from ASP303 to PQQ</u>

According to the proposed Step 2 in the H-T mechanism, there should be a proton transfer from ASP303 to the O5 of PQQ, thus resulting in the formation of a second intermediate (INT2). Our calculations found that the transition state for this step (TS2) shows an intermediate location of H16 on its way from O14 of ASP to the PQQ carbonyl oxygen O5, with H16-O5 = 1.31 Å, and H16-O14 = 1.21 Å, Figure 5.3. This transition state imaginary frequency ($\sim$1009 cm^{-1}) corresponds to the symmetrical stretching of the O5-H16 and H16-O14 bonds. This proton transfer leads to the formation of a second intermediate (INT2) along the overall reaction profile.

The gas phase energy barrier of TS2 with respect to INT1 is calculated to be 14.2 kcal/mol and the energy of the intermediate INT2 is 15.1 kcal/mol with respect to the reactant. Applied solvation decreases the energy of TS2 by almost 10 kcal/mol without much change in INT2 energy. So the barrier is reduced by more than half from the gas phase. The developing charge on both ASP303 and O5 of PQQ during this TS2 could be the reason for huge stabilization during solvation [86].
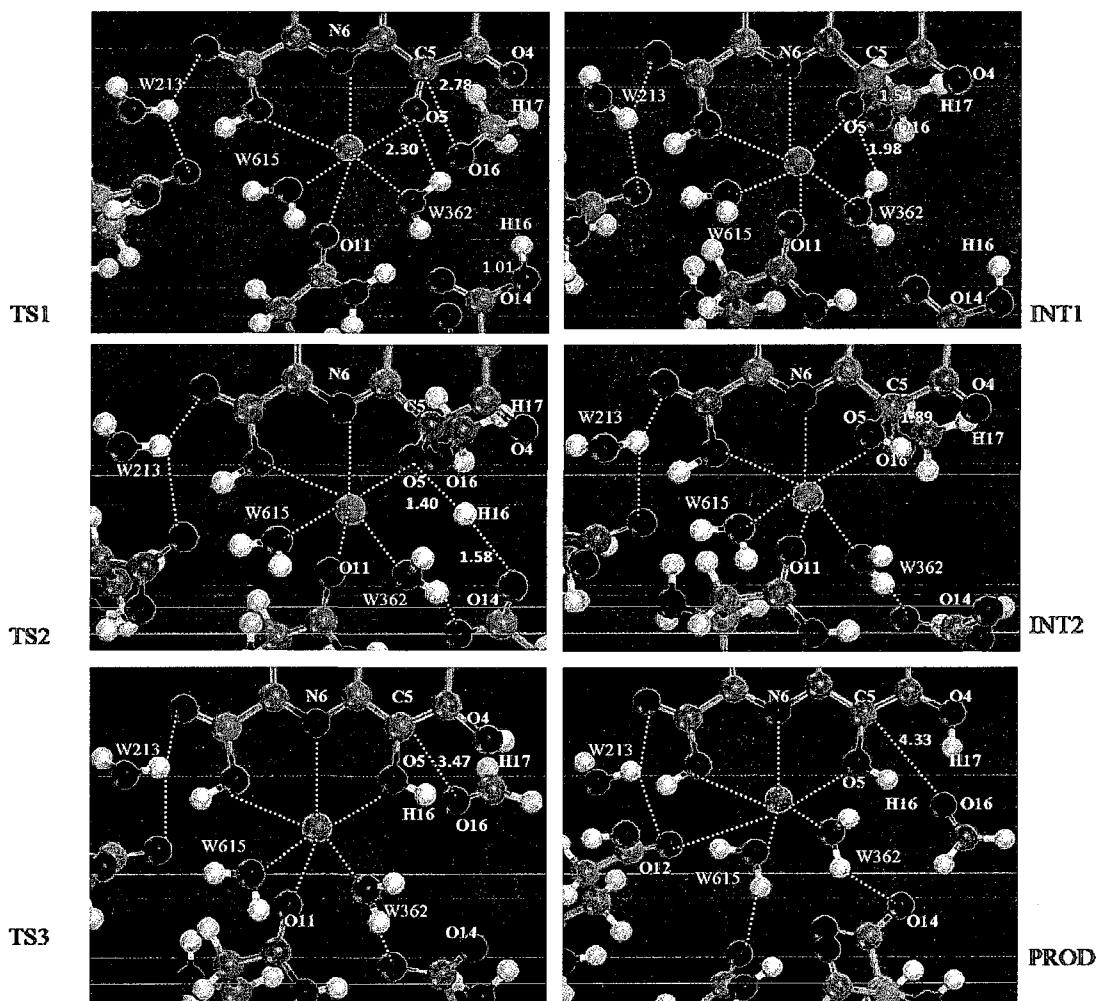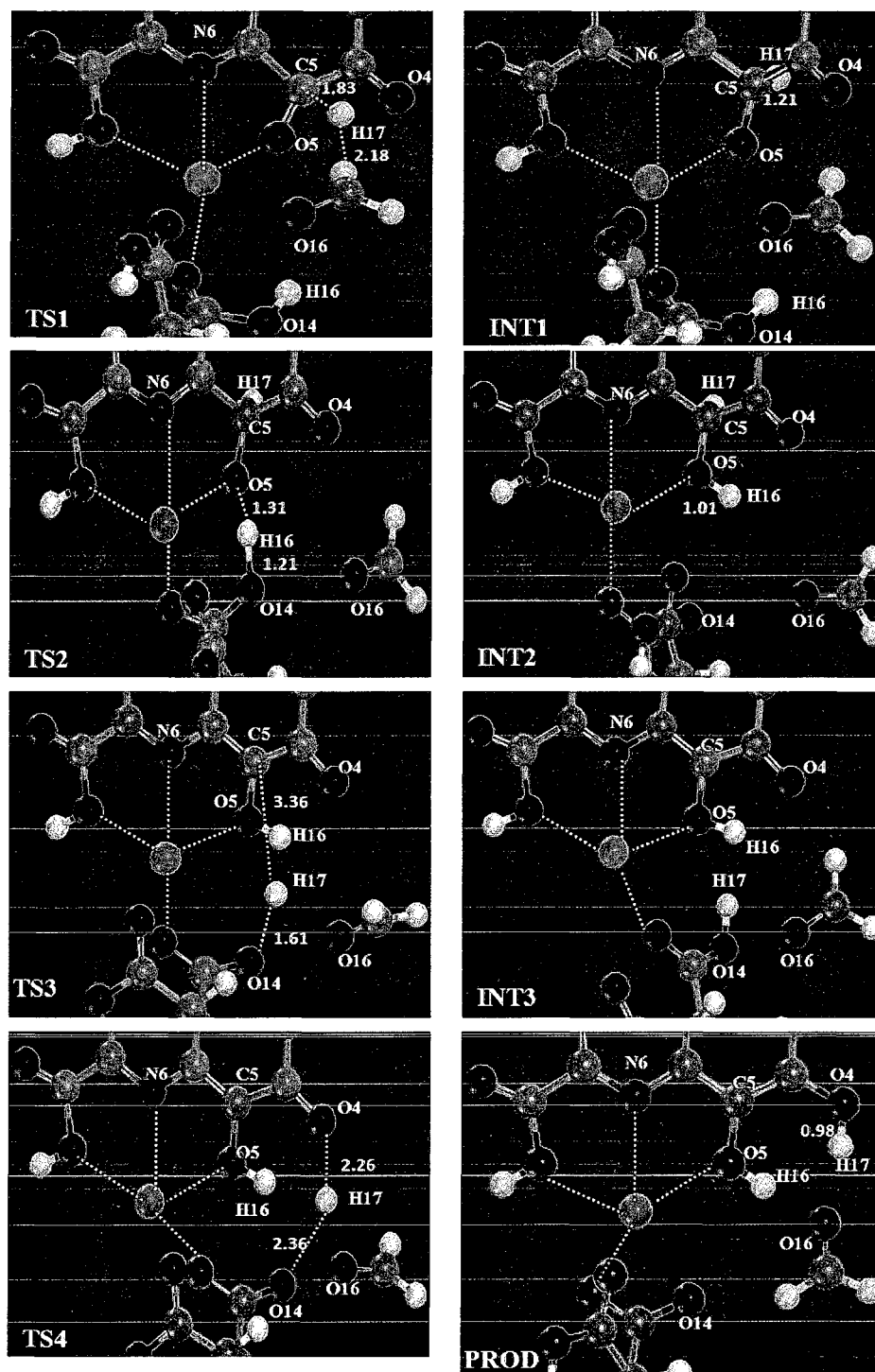
Figure 5.3 Reactive portions of geometry optimized structures involved in H-T methanol oxidation mechanism by MDH active site Model A. Distances are in Å.

5.2.3 Steps 3 and 4: Proton Transfer from PQQ to ASP303 (Step 3) and back to PQQ (Step 4)

Proposed Steps 3 and 4 of the methanol H-T mechanism involve the transfer of a proton (H17) from C5 to O4 of PQQ mediated by ASP303, emphasizing the role of this amino acid as the base catalyst. Step 3 shows the breaking of the C5-H17 bond and the formation of the O14-H17 bond. For this step, the transition state shows an intermediate location of H17 on its way from PQQ carbon C5 to the O14 of ASP, with H17-C5 = 3.36 Å and H17-O14 = 1.61 Å (Figure 5.3). TS3 imaginary frequency ($\sim$454 cm^{-1}) corresponds to the symmetrical stretching of the C5-H17 and H17-O14 bonds. The gas phase free energy required to overcome the transition state for this step is 12.9 kcal/mol with respect to INT2, and energy of the INT3 is 13.2 kcal/mol above the reactant. As observed for the second transition state, the energy of TS3 is lowered in the presence of dielectric effects, thereby reducing the barrier more than half [86].

During the final step, the distance O14-H17 has been increased from 1.02 (INT3) to 1.40 (TS4) to 1.72 (Product) Å, and O4-H17 decreased from 1.67 (INT3) to 1.50 (TS4) to 1.01 (Product) Å respectively, indicating that PQQ is finally reduced (Figure 5.3). Single imaginary frequency ($\sim$426 cm^{-1}) of TS4 corresponds to the movement of the H17 between the O14 of ASP303 and O4 of PQQ [86]. There is not much change in the barrier for this final proton transfer in gas phase and solvation (6-7 kcal/mol), even though the energies of corresponding species are more stabilized in presence of protein environment.

By looking at the potential energy curve of H-T for Model A from Figure 5.4, we can say that the energies of the transition states are much stabilized than the intermediates associated with all steps in the presence of dielectric solvation, thereby predominantly

lowering the free energy barriers in case of Steps 2 and 3. In the gas phase, Step 4 is observed to be the fastest. The barrier for Step 1 is very high for a general enzymatic process (greater than 18 kcal/mol) to be kinetically plausible, even though the barriers for remaining steps are well within the limits [86]. Since solvation has a more pronounced effect on the transition energies tested with this model as observed for A-E, the same mechanism is tested with an even larger Model B to validate the results obtained from Model A.

Figure 5.4 Potential energy surface (PES) for methanol H-T oxidation mechanism by MDH active site Model A. Reactant-relative energies calculated at the BLPY/DNP theory level are in kcal/mol.

5.3 Model B

The reactive portion of minimum energy reactant complex obtained with bigger active site model in the presence of methanol is shown in Figure 5.5. Coordination distances within the complex are already discussed in Chapter 4. O14-H16 distance

reduced further to 1.69 compared to 2.18 Å for Model A, and H17 is also much nearer to

C5 of PQQ than Model A (C5-H17 = 4.55 Å). Similar to Model A, all stationary points

(React, TS1, INT1, TS2, INT2, Prod) are obtained for this model. Important structural

parameters are shown in Figures 5.5 and 5.6, and potential energy curves for both gas

phase and solvation are shown in Figure 5.7.
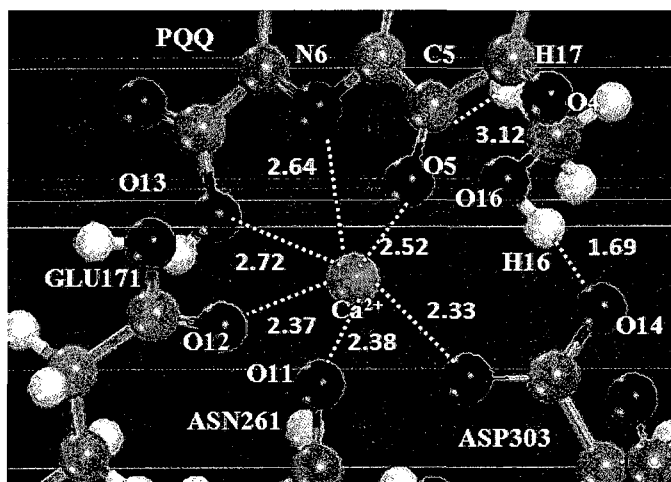
Figure 5.5 Reactive portion of the Model B reactant complex highlighted, and the distances are in Å.

Transition state TS1 obtained using this model is late (C5-H17 = 1.32 Å, Figure

5.6) compared to the one obtained from Model A (1.83 Å). So the TS1 is placed at 32.8

kcal/mol above the reactant (higher by 3.6 kcal/mol than TS1 for Model A) in gas phase.

There is not any change in the O14-H16 distance. INT1 is much more stable in this case

(reduced by 2.6 kcal/mol) with the C5-H17 bond completely formed. As observed for

Model A, solvation has a much more pronounced affect on TS1 than INT1 in this case.

The carboxylic group of the ASP303 with H16 is aligned very well towards the

O5 of PQQ in INT1 for Model B. This alignment makes the proton transfer easier in this

case compared to Model A with the barrier for the step reduced by 6.2 kcal/mol. Even the

energy of the intermediate INT2 is lowered by 9 kcal/mol making the reaction even more facilitating. There is approximately 4 kcal/mol change in the energy of TS2 without any change in INT2 in the presence of solvation.

TS3 also forms earlier with O14-H17 distance at 1.83 compared to 1.61 Å in Model A. This formation is reflected in the energy of TS3 lowered by 8.3 kcal/mol. However, there is not much change in the gas phase free energy barrier in both cases. Dielectric solvation has less effect on the barrier value here compared to Model A.

Similar to INT1, INT3 formed by the end of Step 3 is in a much more favorable position for the final proton transfer to O4 of PQQ in this model. This condition was indicated by the decrease in the energy of this intermediate by 7.8 kcal/mol as compared to Model A. The TS4 is also formed early in this case thereby reducing the barrier for this step. INT3 is hugely stabilized by solvation in this case.
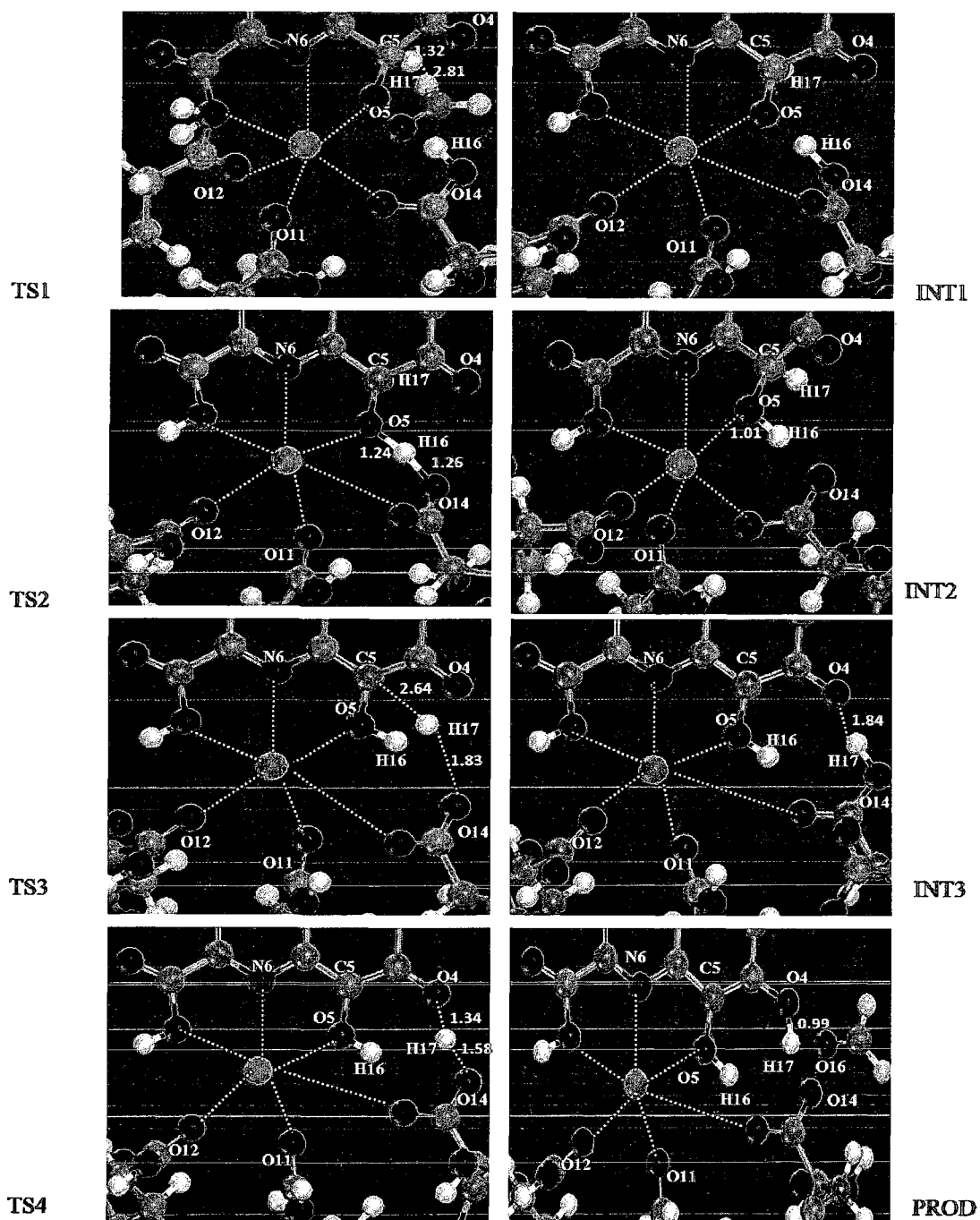
Figure 5.6 Reactive portions of geometry optimized structures involved in A-E methanol oxidation mechanism by MDH active site Model B. Distances are in Å.
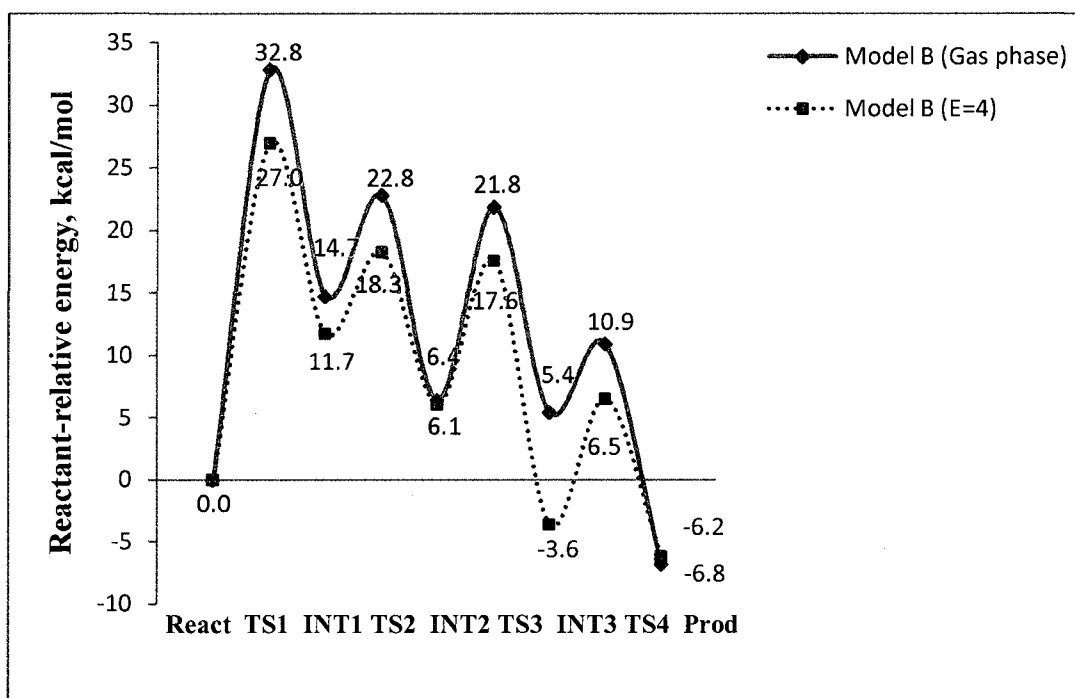
Figure 5.7 Potential energy surface (PES) for methanol H-T oxidation mechanism by MDH active site Model B. Reactant-relative energies calculated at the BLPY/DNP theory level are in kcal/mol.

From the PES of H-T obtained using Model B (Figure 5.7), we can say that the energies of TS2, TS3, and TS4 are lowered significantly with Model B in the gas phase itself. TS1 energy is little higher than that in Model A. The gas phase free energy barriers for Steps 2 and 4 are reduced than others in Model B compared to A because the intermediates corresponding to these steps INT1 and INT3 are in a more favorable position here to stimulate the reaction. The energies and, therefore, the barriers are lowered in the presence of solvation for all steps, but the change is not that much as observed for Model A, thereby accounting for some explicit solvation. However, the barriers for all steps except Step 1 are favorable according to the general kinetic requirements for this model and also for that of A [86]. We tried to do what we did in

case of A-E to see if Model B + 3W can change the barrier for Step 1 and keep the same trend for remaining steps.

5.4 Model B + Three Water

The reactive portion of the reactant complex of Model B + 3W in the presence of methanol is shown in Figure 5.8. As referred to in the Model A reactant complex discussion, the O14-H16 distance was reduced by 0.44 Å and C5-H17 by 0.86 Å. The coordination of ion and hydrogen bonding of water with various species is already discussed in Chapter 4. Important distances between the species for this model are tabulated in Table 5.1.

For TS1 of step 1, the C5-H17 distance is 1.22 Å (Figure 5.9), reduced more than that of Model B without water (1.32 Å) and that of Model A (1.86 Å). The O14-H16 distance remains the same in all three cases. For INT1, the C5-H17 bond is completely formed as previously, so there is no change in energy of this species with respect to the reactant in both cases. In the gas phase, energy of TS1 is reduced by 8.5 and 12.1 kcal/mol with respect to TS1 of Model A and Model B without water. The reason for reduction in the barrier can be the same as discussed for Step 1 of A-E with the same model.
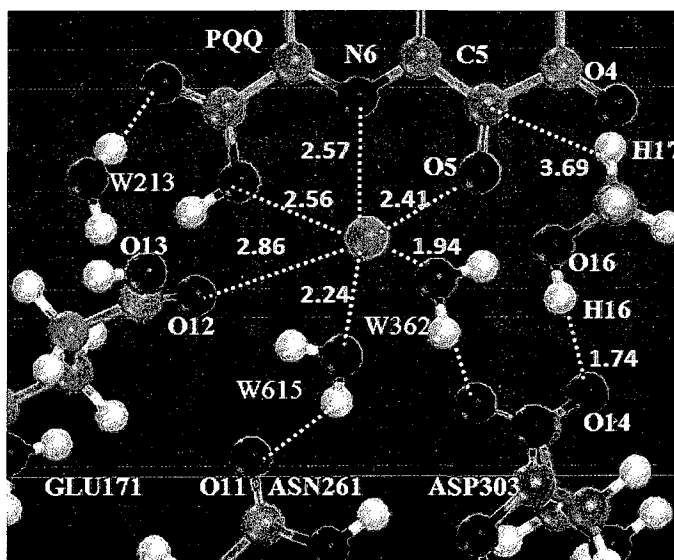
Figure 5.8 Reactive portion of the reactant complex. Distances are in Å.

The interaction between O5 and Ca^{2+} reduces as the reaction proceeds from 2.41 (Reac) to 2.29 (TS1) to 2.24 Å (INT1), and the hydrogen bonding of the water molecule (W362) with respect to O5 of PQQ gradually decreases from 2.50 to 2.10 to 1.98 at INT1, thereby stabilizing more the negative charge on O5, with the hydride attraction to C5 of PQQ (Figure 5.9). Also the presence of solvation did not have any effect on the energetics of TS1 and INT1. From this, we can say that the ion and the water play a major role in stabilizing these species, thereby lowering the barrier.

TS2 is more stabilized in this model compared to Model B without water. The hydrogen bonding of W362 is still maintained with O5 of PQQ but deteriorates as the reaction proceeds and improves with ASP. The barrier is reduced by 4.1 kcal/mol in this case. As observed for Step 1, the energies of the species didn't change that much with solvation.
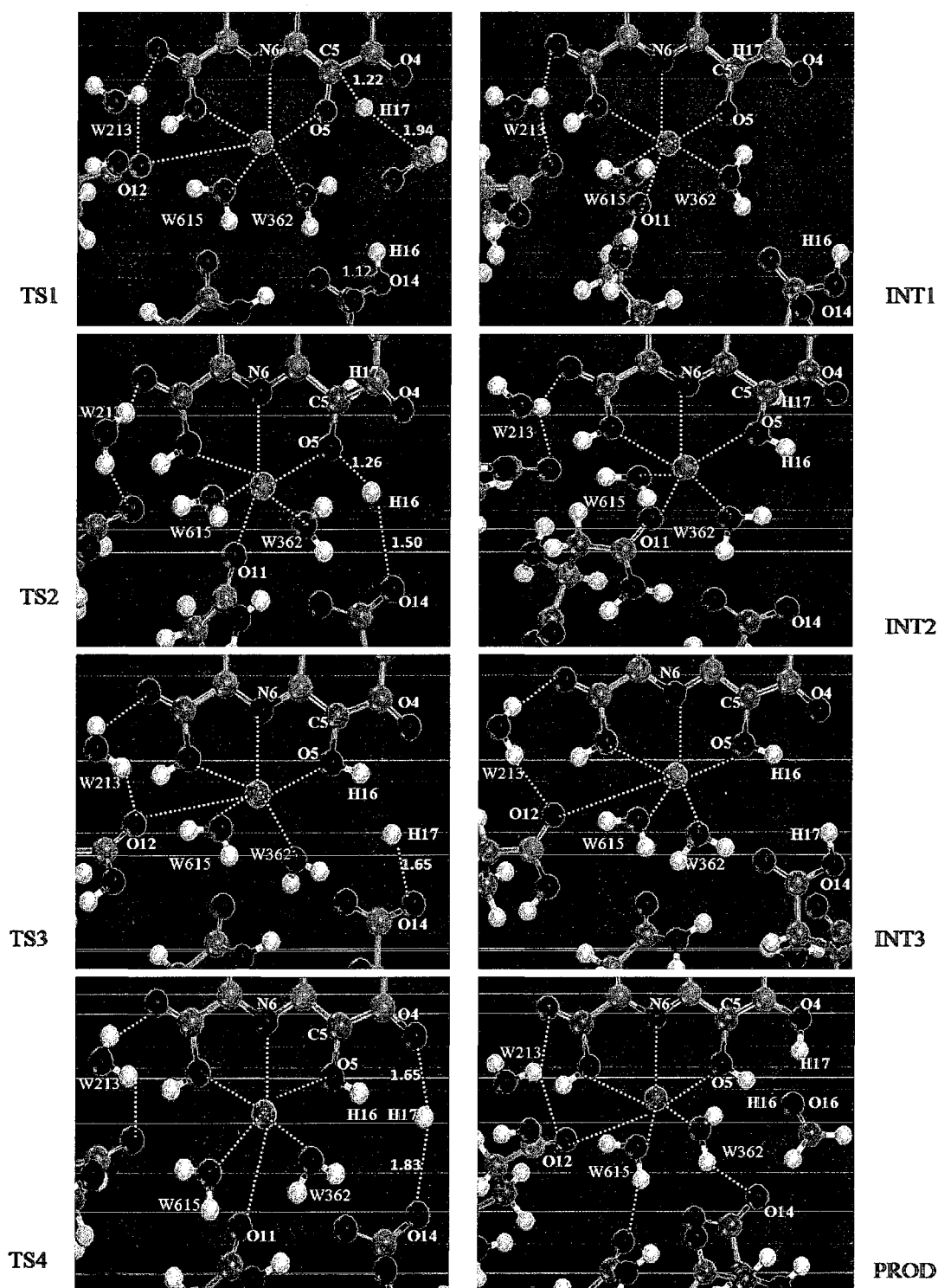
Figure 5.9 Reactive portions of geometry optimized structures involved in H-T methanol oxidation mechanism by MDH active site Model B + 3W. Distances are in Å.

Table 5.1 Selected bond lengths corresponding to the optimized structures of reactant, transition states and intermediates during the methanol H-T oxidation mechanism by MDH Model B with water.

Bond Length (Å)	Reactant	TS1	INT1	TS2	INT2	TS3	INT3	TS4	Product
O14-H16	2.00	1.12	1.00	1.26	1.53	2.37	3.01	2.94	2.98
O5-H16	3.39	2.58	1.36	1.30	1.04	1.05	1.04	1.04	1.04
O14-H17	4.23	3.28	3.53	3.54	2.98	2.65	1.02	1.40	1.72
C_{met}-H17	1.10	2.81	4.50	6.05	5.67	5.03	5.12	3.47	3.52

As the reaction proceeds from INT2 to INT3, there is not much change in the energy barrier compared to Model B without water. W362 is more coordinated with the ion rather than having any hydrogen bonding with the charged species. Solvation stabilized the TS3 species as it did for Model B without water. INT3 of Model B without water and with water doesn't have the same conformation, as the former is in a superior position for the final proton transfer. This disadvantage is evident by the increase in the energy of INT3, TS4 in this case, thereby increasing the barrier by 4.3 kcal/mol. Solvation improves the energy of TS4 and reduces the barrier by 2.2 kcal/mol. Also, the energy of final product increased in the presence of solvation [86].

We attempted to see whether Steps 3 and 4 can be combined into a single step, where the H17 proton is transferred directly from C5 to O4 carbonyl oxygen of PQQ (i.e. INT2 to final product), thereby not involving ASP303 for this direct step. A transition state is obtained for this step (TS3`), where the C5-H17 and O4-H17 distances are found to be 1.47 and 1.32 Å, respectively (not shown in Figure 5.9). However, the gas phase free energy barrier for this transition state to occur was calculated to be 45.4 kcal/mol, which is much higher than the free energy barriers of original Steps 3 and 4 combined (22.5 kcal/mol). Also, this barrier is energetically prohibitive as per the kinetic

requirements of enzymes. We decided it is meaningless to apply solvation to this TS3` as its high gas phase relative energy cannot undergo significant change. This calculation emphasizes the role of ASP303 as a base catalyst for this particular proton transfer from C5 to O4 of PQQ.
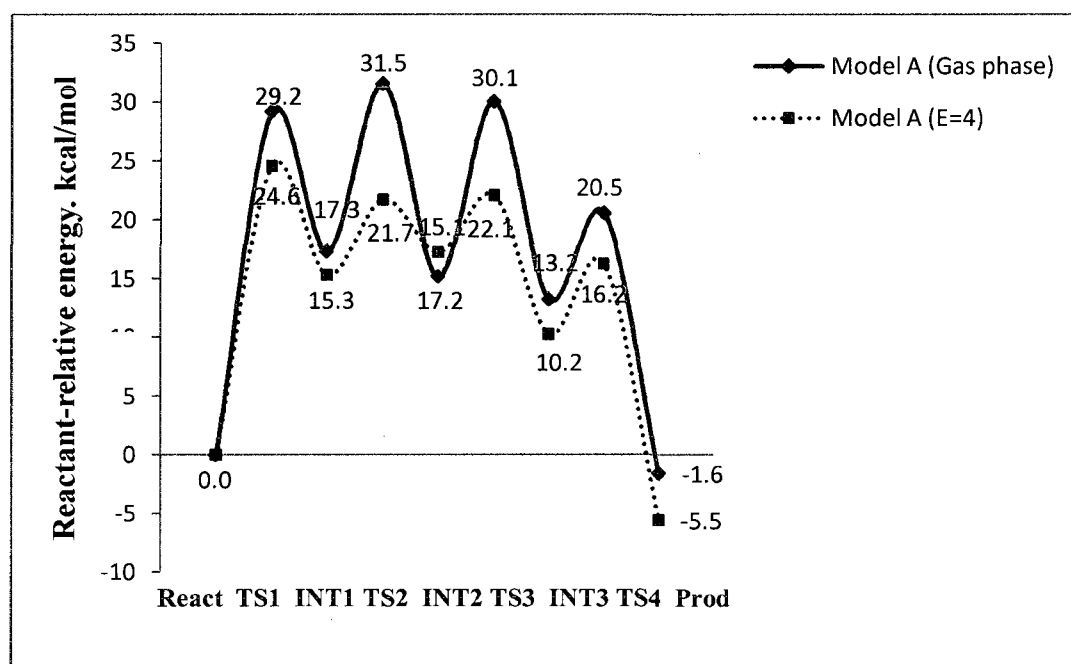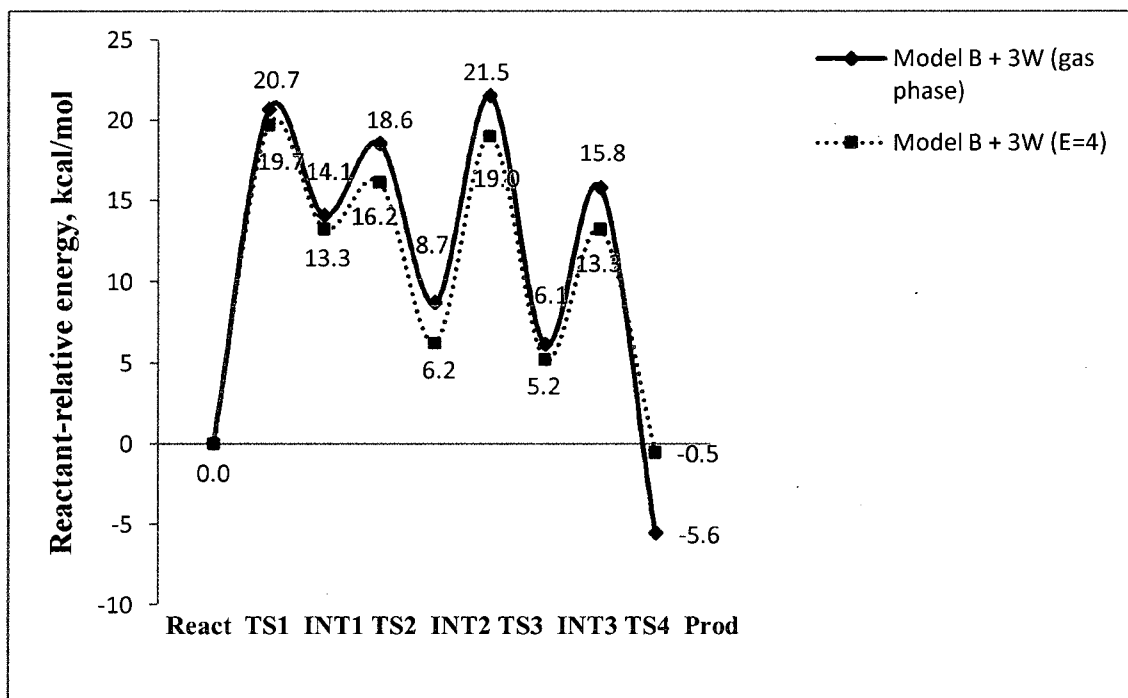

Figure 5.10 Potential energy surface (PES) for methanol H-T oxidation mechanism by MDH active site Model B + 3W. Reactant-relative energies calculated at the BLPY/DNP theory level are in kcal/mol.

Table 5.2 Energy barriers (kcal/mol) corresponding to Steps one to four of the H-T methanol oxidation mechanism calculated at the BLPY/DNP theory level for Models A and B in Gas Phase (GP) and solvation (E=4).

	Model A (GP)	Model A (E=4)	Model B (GP)	Model B (E=4)	Model B + 3W (GP)	Model B + 3W (E=4)
Step 1	29.2	24.6	32.8	27.0	20.7	19.7
Step 2	14.2	6.4	8.1	6.6	4.5	2.9
Step 3	15.0	7.0	15.4	11.5	12.8	12.8
Step 4	7.3	6.0	5.5	10.1	9.7	8.1

5.5 <u>Discussion and Summary</u>

From the PES of Model B in the presence of water (Figure 5.10), we can see that the gas phase barrier for the Step 1 is largely reduced compared to Models A and B without water, making it kinetically plausible. Also the barriers for Steps 2 and 3 reduced mildly whereas for Step 4, there is a moderate increase by 4.3 kcal/mol. So in gas phase, Step 2 is observed to be the fastest here whereas Step 4 was observed to be the fastest one from Models A and B (Table 5.2). Solvation didn't have any major impact on the energies here thereby confirming that all necessary groups for charge stabilization are accounted for in this model. Now the reaction is favorable with barriers for all steps within the general kinetic requirements of an enzymatic process (less than or nearer to 18 kcal/mol).

The free energy barrier for Step 1 is observed to be the rate-limiting one with all models and kinetically plausible with Model B + 3W, which is in accordance with the literature. However, the barrier obtained by Leopoldini et al. [58] for this step in H-T is 32.3 kcal/mol, and these authors opposed this mechanism by comparison with general enzyme requirements. From QM/MM calculations, Zhang et al. [51] obtained a free energy barrier of 11.7 kcal/mol for this first step of H-T. The free energy barrier from our best model, which is kinetically plausible, is found to be higher by 9 kcal/mol with respect to Zhang et al. [51] and less by 11.6 kcal/mol than Leopoldini et al. [58] Also, it is higher by 12.2 kcal/mol than the Gibbs free energy barrier from experimental kinetics on methanol oxidation by Goodwin et al. [52] which Zhang et al. [51] compared with their free energy barrier. This increase in barrier from H-T in our case can be related to

the same reason as observed from our A-E calculations: H-T may not proceed as proposed in the literature for oxidation of methanol.

CHAPTER 6

SUBSTITUTING Ca^{2+} WITH Ba^{2+} IN THE MODELS

AND EXPLORING A-E AND H-T

It was reported in the literature that various bivalent metal ions can replace the natural ones in the active site of enzymes in the reconstitution of apo-enzymes (enzymes without a cofactor) to holo-enzymes (functional enzymes with a co-factor) [40, 52, 63]. In the case of the MDH enzyme also, people tried to replace the Ca^{2+} with Sr^{2+} and Ba^{2+}. Kinetic analysis on these modified enzymes as detailed in the introduction (Chapter 1) showed that the Gibbs energy of activation for oxidation of methanol is less in the case of Ba^{2+}-containing MDH than Ca^{2+} and Sr^{2+}-containing MDH [52, 63]. But researchers reported no detailed information on why this is happening or what the oxidation mechanism(s) of Ba^{2+}-MDH were.

By replacing the Ca^{2+} with Ba^{2+} in the active site models previously used to test the A-E and H-T (Model A, B and Model B + 3W), we repeated the calculations to carry out a detailed theoretical investigation to obtain the stationary points corresponding to the potential energy surface for both these mechanisms. Comparison of the energetic profiles for the reaction paths with both ions allowed us to assess possible effects of the metal center substitution in the active site on the structure and energetics. For both ions Ca^{2+} and Ba^{2+}, the same set of minima and transition state structures were found for A-E and

H-T. Certain changes in equilibrium geometry configurations as well as in reaction free energy barriers were noticed for the different ions, but qualitatively the structures were the same. For Model A, dielectric solvation had pronounced effects on the energetics of all steps obtained from gas phase as observed for this model with Ca^{2+} (Chapters 4 and 5). So only gas phase calculations are reported here for this Model A. For Model B, both gas phase and solvation calculations were performed, and the results showed that energetics were affected only for rate-determining steps in solvation. For Model B with three water molecules with Ba^{2+} in the model, both gas phase and solvation calculations indicated that there was not much of a difference in the energetics (~ 2 kcal/mol) with solvation when compared to gas phase as exactly found for Ca^{2+} in this model (Chapters 4 and 5). In this chapter, detailed discussion with respect to change in distances and energetics is done with this best model, Model B + 3W in gas phase, and free energy barriers with respect to all models are reported.

6.1 Addition-Elimination

The initial reactant in both, the A-E and H-T methanol oxidation mechanisms by MDH are the same complex. Hence, a methanol molecule is added to the Model B + 3W with Ba^{2+}, and the complete complex is geometry optimized at the same BLYP/DNP theory level. The ground state geometry of the Ba^{2+}-containing complex agree with the configuration of the Ca^{2+}-complex in coordination with atoms of PQQ and water molecules. Ba^{2+} coordinates with the nitrogen and oxygen atoms of PQQ (at 3.16, 2.83 and 3.05 Å, respectively); ASN261 (at 2.80 Å); and both oxygen atoms of water molecules W362 and W615 (at 2.80 and 2.85 Å), respectively (Figure 6.1). Ba^{2+} also coordinates with O16 of methanol (2.89 Å), which was not observed with Ca^{2+} in place.

Also W615 and W213 maintain hydrogen bonding with respect to PQQ, PQQ, and GLU177, respectively. There is an increase in bond distances with respect to Ba^{2+} coordination (~ 0.3-0.5 Å than Ca^{2+} coordination), which can be mainly due to the ionic size of the element i.e., Ba ionic radius (1.34 Å) is larger than that of Ca ion (0.99 Å) and also due to the distortion introduced by the replacement of ion. Coordination and binding of these two ions in representative models of MDH active sites and their interaction with methanol were previously studied by us, where the same kind of increase in bond distances with respect to Ba^{2+} and Ba^{2+}-O16 coordination was observed [62]. The free energy of substrate (methanol) binding to the active site model has been obtained for both Ca^{2+} and Ba^{2+} containing clusters. It was observed that binding energy of methanol is less by 8.6 kcal/mol for Ba^{2+} model as compared to Ca^{2+} model. A decrease of 4.5 kcal/mol was obtained by Goodwin et al. [52] for the whole Ba^{2+}-enzyme when investigating the oxidation of methanol.

6.1.1 Step 1: Proton Abstraction by ASP303 from Methanol and Nucleophilic "Addition" of Hemiketal Complex to PQQ

As seen from the optimized structure of the reactant species (Figure 6.1), the active site is nicely set up for a proton (H16) transfer from methanol to ASP303 and the nucleophilic addition of the CH_3O^- complex to the C5 of PQQ. Optimum transition state (TS1) for this step is obtained characterized by a single imaginary frequency and presented in Figure 6.1. The O14-H16 distance reduces from 1.64 (Reactant) to 1.01 (transition state TS1) and to 0.98 Å (INT1), and the C5-O16 bond distance changes from 4.07 (Reactant) to 2.42 (TS1) and to 1.52 Å (INT1) indicating that the formation of O_{met}-C5 and the shift of proton from alcoholic OH group of methanol to ASP303. The

methoxide (CH_3O^-) addition to the PQQ results in the formation of first intermediate (INT1) where the O_{met}-C5 bond is completely formed (1.52 Å). The resulting oxyanion of the carbonyl group (O5) binds more to the Ba^{2+} with a bond length of 2.42 Å (2.83, 2.71Å at reactant and TS1, respectively). The hydrogen bonding of water molecule (W362) with respect to O5 of PQQ improves as the reaction proceeds to INT1 (1.91 compared to 3.18, 2.83 Å at reactant and TS1, respectively).
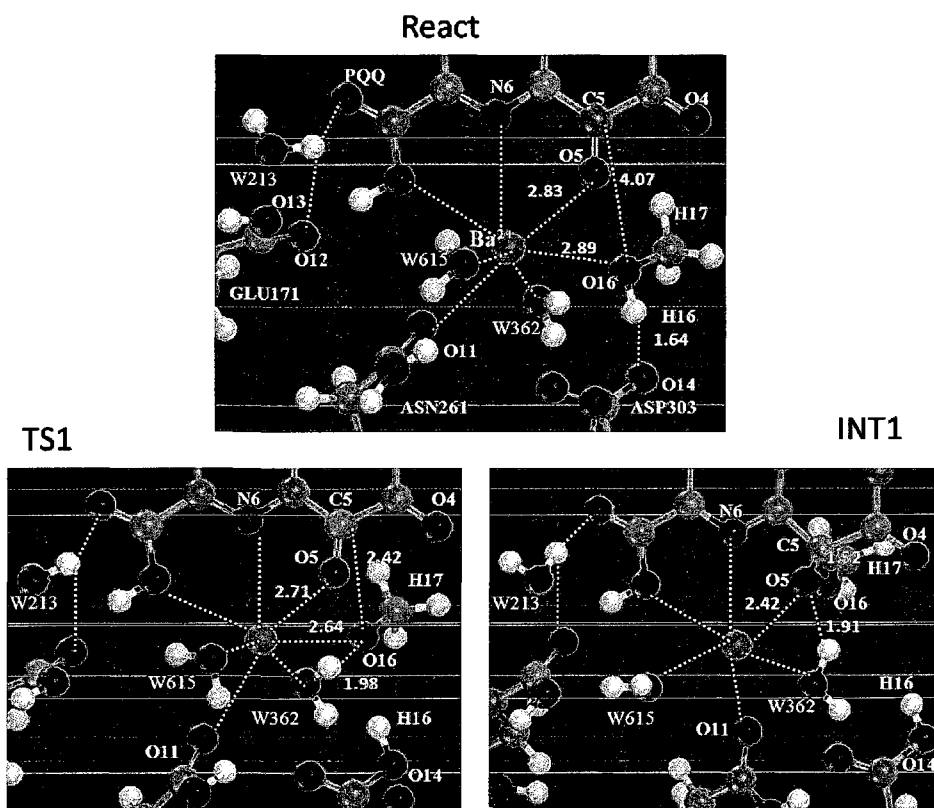
Figure 6.1 Geometry optimized structures involved in Step 1 for the A-E methanol oxidation mechanism by MDH active site Model B + 3W with Ba^{2+}.

The free energy barrier for this step is calculated to be 10.8 kcal/mol (19.5 kcal/mol with respect to Ca^{2+}-cluster) in gas phase. Once the proton is abstracted by ASP303, the coordinating distance of O16 with ion reduces to 2.64 Å (2.89 Å at reactant), and there is hydrogen bonding with W362 at TS1. Also, the resulting negative

charge on O5 of PQQ as the reaction proceeds to INT1 is more electro stabilized by interaction with Ba^{2+} and W362 (Table 6.1), thereby lowering the energy of the INT1 and barrier for this step compared to Ca^{2+} presence. This reaction is less endothermic in this case, by 7.9 kcal/mol (14.7 kcal/mol for Ca^{2+}-case), as the energy of the first intermediate is lowered by 6.8 kcal/mol when Ba^{2+} is present compared to the Ca^{2+}case, relative to the reactant energy.

Table 6.1 Comparison of selected parameters for TS1 of A-E.

Parameter	Ca^{2+}	Ba^{2+}
O14-H16, Å	1.01	1.01
$C5-O_{met}$, Å	2.78	2.42
Ion-O16	3.38	2.64
W362-O5	2.58	2.38
W362-O16	2.62	1.98

6.1.2 Step 2: Proton "Elimination" from ASP303 and Transfer to PQQ

Having established that the first proton transfer and nucleophilic addition to PQQ are energetically feasible, the next step is a proton (H16) transfer from ASP303 to the O5 of PQQ. At this transition state (TS2), the proton is shared between the oxygen atoms of PQQ (at 1.23 Å) and the ASP303 (at 1.50 Å), respectively. The hydrogen bonding of the W362 to the O5 of PQQ is completely lost as the reaction proceeds to INT2 as observed for the Ca^{2+}case, but the bonding with respect to ASP303 remains intact thereby stabilizing the negative charge on the residue.

There is not much change in the free energy barrier for this step in the gas phase with respect to both ion clusters (~1.2 kcal/mol). This reaction is exothermic by 4.7 kcal/mol

for the Ca^{2+}- containing case whereas here it is exothermic by only 0.5 kcal/mol as there is not much change in the energy of the first and second intermediates.

6.1.3 Step 3: Formation of PQQH₂ and Formaldehyde

The proton transfer leads to the formation of a second intermediate (INT2) along the overall reaction profile. For this INT2, the CH_3 group of attached methanol orients towards O4 of PQQ, so that the latter is in a good position in breaking the $H-CH_2$ bond (C5-O16 bond lengthens up to 1.98 Å, Figure 6.2). The final transition state TS3, which leads to the formation of PQQH₂ reduced species and formaldehyde, is located with C_{met}-H17 and O4-H17 distances at 1.68 and 1.04 Å, respectively. At TS3, the bond between O16 and C5 of PQQ lengthens up to 3.92 Å, indicating the breakage to form by-product formaldehyde (Figure 6.2). Water molecules W362 and W615 maintain their coordination with calcium, and ASP303 and calcium, respectively throughout this proposed reaction path until the formation of the final product.

INT2   TS3   Prod
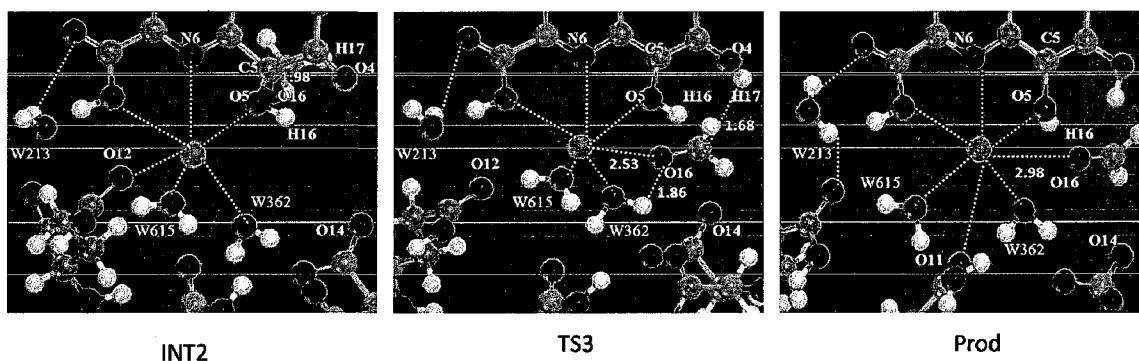
Figure 6.2 Geometry optimized structures involved in step 3 for A-E methanol oxidation mechanism by MDH active site model.

The gas phase free energy barrier for this step is 13.2 kcal/mol compared to 21.4 kcal/mol with respect to the Ca^{2+}-cluster. The reason for the larger stability of TS3 is the

coordination of O16 of resulting formaldehyde with Ba^{2+} and W362, which was not observed for Ca^{2+} case (Table 6.2). This reaction is also exothermic in both cases with a difference of only 1.2 kcal/mol (Table 6.3). Also the cleavage of C_{met}-H17, formation of O4-H17 bond, and detachment of HCHO to form formaldehyde is almost completely formed at the transition state itself in the presence of Ba^{2+}, and it is more stabilized than Ca^{2+} in place (Table 6.2). The product formed in this case is almost the same as the transition state obtained with the particular difference of formaldehyde moving away from the ion (Figure 6.2).

Table 6.2 Comparison of selected parameters for TS3 of A-E.

Parameter	Ca^{2+}	Ba^{2+}
C_{met}-H17	1.44	1.68
C5-O16	3.47	3.92
Ion- O16	4.42	2.53
W362-O16	3.98	1.86

Table 6.3 Reactant-relative free energies of the critical points along the PES of A-E tested with Model B + 3W in kcal/mol.

Point	Ca^{2+}	Ba^{2+}
Reac	0.0	0.0
TS1	19.5	10.8
INT1	14.1	7.9
TS2	20.9	10.6
INT2	9.4	8.4
TS3	30.8	21.6
Prod	-0.5	-4.5

Table 6.4 shows the free energy barriers for all steps involved in A-E for all models. For all the models, the gas phase barriers obtained with Ba^{2+} in place are within or nearer to the general requirements of enzymes. For Model B in the gas phase, the

barriers for Steps 1 and 3 increased by 3 kcal/mol over Model A. There is a huge decrease in the barrier for Step 1 for Model B in solvation. As observed in case of Ca^{2+}, the rate-limiting one is Step 1 in case of Models A and B in gas phase, whereas for Model B in solvation and Model B + 3W in gas phase, Steps 1 & 3 are observed to be rate-limiting. Also, the barriers for all steps are less in case of Model B + 3W, and negligible solvation effects as indicated earlier makes it a better model compared to others.

Table 6.4 Free energy barriers for all the steps involved in A-E with Ba^{2+} in Model A (Gas phase) and Model B (Gas phase, solvation), Model B + 3W (gas phase) in kcal/mol. Values in the parenthesis are for Ca^{2+} in the Models.

	Model A (Gas Phase)	Model B (Gas Phase)	Model B (E=4)	Model B + 3W (Gas phase)
Step 1	19.6 (29.5)	22.7 (28.5)	12.5 (28.2)	10.8 (19.5)
Step 2	3.5 (7.7)	3.1 (4.7)	5.1 (6.9)	2.7 (6.8)
Step 3	10.6 (17.7)	13.6 (16.8)	10.8 (20.9)	13.2 (21.4)

6.2 Hydride Transfer Mechanism

6.2.1 Step 1: Hydride Transfer to PQQ and Proton Abstraction by ASP303 from Methanol and Formaldehyde Formation

According to Step 1 of the H-T methanol oxidation mechanism, the initial reactant complex evolves in first intermediate through TS1, with a direct hydride transfer (H17) from methanol to C5 of PQQ in concert with proton abstraction (H16) by O14 of ASP303, thus resulting in the formation of the by-product formaldehyde. From our calculations at the BLYP/DNP level, we found that O14-H16 bond length evolves from 1.64 (reactant) to 1.05 (TS1) to 1.00 (INT1) Å, showing the binding of the H16 proton to ASP303 (Figure 6.3). The C5-H17 distance from the initial reactant is reduced from 3.69 to 1.22 and finally to 1.12 Å, evidencing the hydride transfer to the C5 of PQQ. The C5

of PQQ changes its hybridization from sp^2 to sp^3 and establishes a covalent bond with H17 at 1.12 Å. The hydrogen bonding of water molecule (W362) with respect to O5 of PQQ decreases as the reaction proceeds to INT1 (1.88 compared to 3.18 Å at reactant).

The free energy barrier for TS1 with respect to the reactant is calculated to be 10.4 kcal/mol (20.7 kcal/mol with respect to Ca^{2+}-cluster, Table 6.7) in gas phase. Ba^{2+} polarizes the C5-O5 bond making C5 more positive and O5 more negative at this transition state. At TS1, the O16 of resulting formaldehyde forms a hydrogen bond with W362 not observed in Ca^{2+} case. The negative charge on O5 of PQQ as the reaction proceeds to INT1 is more electro stabilized by interaction with Ba^{2+} and W362, thereby lowering the energy barrier for this step compared to Ca^{2+} presence (Table 6.5). Like Step 1 for A-E, this reaction is also less endothermic (9.2 kcal/mol, 14.1 kcal/mol for Ca^{2+}-case, Table 6.6), because the energy of the first intermediate is lowered by 4.1 kcal/mol when Ba^{2+} is present compared to the Ca^{2+} case, relative to the reactant energy.

Reac   TS1   INT1
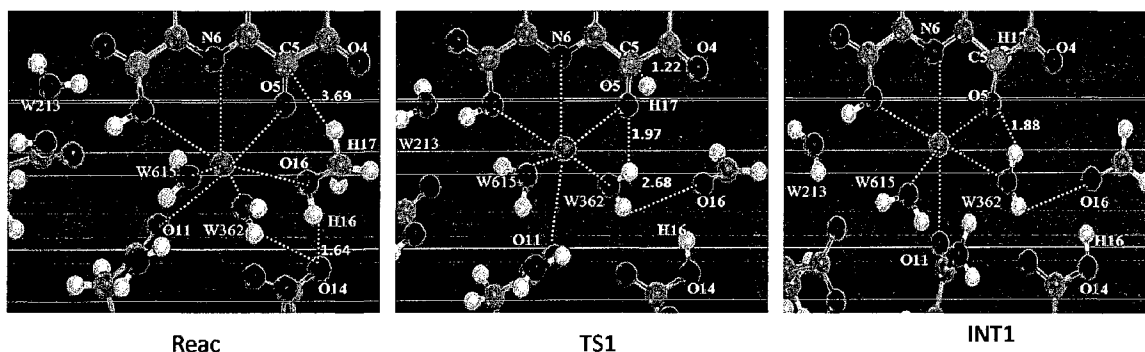
Figure 6.3 Geometry optimized structures involved in Step 1 of the methanol hydride-transfer oxidation mechanism with Ba^{2+} in the model.

Table 6.5 Comparison of selected parameters for TS1 of H-T.

Parameter	Ca^{2+}	Ba^{2+}
O14-H16, Å	1.00	1.05
C5-H17, Å	1.42	1.22
Ion-O5	2.60	2.42
W362-O5	2.58	1.97
W362-O16	3.02	2.68

6.2.2 Step 2: Proton Transfer from ASP303 to PQQ

The next step along the reaction profile consists of a proton transfer from ASP303 to the O5 of PQQ, thus resulting in the formation of a second intermediate (INT2). From our calculations, we found that the transition state for this step (TS2) shows an intermediate location of H16 on its way from O14 of ASP to the PQQ carbonyl oxygen O5, with H16-O5 = 1.30 Å and H16-O14 = 1.26 Å. The hydrogen bonding of W362 with respect to O5 of PQQ increases as this step proceeds.

Since the geometrical characteristics of TS2 are similar to those of INT1, a low energy barrier is anticipated for this step. There is not much change in the free energy barrier (~ 0.6 kcal/mol, Table 6.7) for this step in gas phase with respect to both ion clusters. This reaction is more exothermic by 5.4 kcal/mol for Ca^{2+}-containing case (Table 6.6).

6.2.3 Steps 3 and 4: Proton Transfer from PQQ to ASP303 (Step 3) and Back to PQQ (Step 4)

The enolization process of transferring the hydrogen (H17) from C5 of PQQ to C4 carbonyl oxygen (O4) involves the proposed Steps 3 and 4 of the methanol H-T mechanism. The third step involves the transfer of a proton (H17) from C5 to O14 of ASP303, emphasizing the role of this amino acid as the base catalyst.

For this step, the transition state (TS3) shows an intermediate location of H17 on its way from PQQ carbon C5 to the O14 of ASP303, with H17-C5 = 2.83 Å and H17-O14 = 2.65 Å. The hydrogen bonding of W362 with O5 of PQQ is completely lost by the end of this step. The free energy required for Step 3 is 5.5 kcal/mol, reduced by 7.3 kcal/mol with respect to the Ca^{2+}- case (Table 6.7). The energy of the third intermediate is almost the same in both cases (Table 6.6).

Through TS4, the final proton is transferred from O14 of ASP to negatively charged O4 of PQQ. During this final step, the distance O14-H17 has been increased from 1.02 (INT3) to 1.40 (TS4) to 1.72 (product) Å, and O4-H17 decreased from 1.67 (INT3) to 1.50 (TS4) to 1.01 (product) Å, respectively, indicating that PQQ is finally reduced. Throughout this reaction step, W362 and W615 maintain coordination with Ca^{2+} and W615, and W213 maintains hydrogen bonding with PQQ and GLU177, respectively. As observed for step 3, the free energy barrier is reduced by 5.4 kcal/mol for Ba^{2+}-case. This step is exothermic by approximately 6.0 kcal/mol in both cases (Table 6.6).

As we did for Ca^{2+} case, the free energy barrier for direct hydride transfer from C5 to O4 of PQQ was calculated to be 34.8 kcal/mol (45.4 kcal/mol for Ca^{2+} case), which is not at all possible kinetically. So the enolization process requires mediation by ASP303 in this case too.

Table 6.6 Reactant-relative free energies of the critical points along the PES of H-T tested with Model B + 3W in kcal/mol.

Point	Ca^{2+}	Ba^{2+}
Reac	0.0	0.0
TS1	20.7	10.4
INT1	14.1	9.2
TS2	18.6	12.7
INT2	8.7	8.7
TS3	21.5	14.2
INT3	6.1	5.8
TS4	15.8	9.7
Prod	-0.5	-4.5

The reactant-relative free energies of all stationary points along the PES for both ions with Model B + 3W for A-E and H-T are tabulated in Tables 6.3 and 6.6. As indicated earlier, the first step for both cases is less endothermic with Ba^{2+} in place. These reaction mechanisms were found to be more exothermic (by 4 kcal/mol) when investigated with Model B + 3W with Ba^{2+} than Ca^{2+} in the model.

The free energy barriers obtained for all models in gas phase and protein environment for H-T are well within the kinetic requirements when Ba^{2+} is present as shown in Table 6.7. The barrier for Step 1 is highest in Models A and B in gas phase and lowest in Model B + 3W. For all the models, Step 1 is found to be the rate-determining one as observed with Ca^{2+} in place for these models. As noted in A-E, negligible solvent effects and less barriers in case of Model B + 3W makes it a better one for analysis of this oxidation mechanism (same case with Ca^{2+} in the model).

Table 6.7 Free energy barriers for all the steps involved in H-T with Ba^{2+} in Model A (gas phase) and Model B (gas phase, solvation) in kcal/mol. Values in the parenthesis are for Ca^{2+} in the models.

	Model A (Gas Phase)	Model B (Gas Phase)	Model B (E=4)	Model B + 3W (Gas Phase)
Step 1	20.5 (29.2)	21.7 (32.8)	13.4 (27.0)	10.4 (20.7)
Step 2	6.1 (14.2)	7.9 (8.1)	7.8 (6.6)	3.5 (4.5)
Step 3	5.5 (15.0)	8.5 (15.4)	10.5 (11.5)	5.5 (12.8)
Step 4	10.8 (7.3)	5.1 (5.5)	10.2 (10.1)	2.7 (9.7)

6.3 Discussion and Summary

Methanol oxidation by a PQQ-containing MDH enzyme was investigated using a model cluster containing Ba^{2+} instead of Ca^{2+} at the generalized gradient approximation within the density functional theory formalism at the BLYP/DNP theory level. The two proposed mechanisms addition-elimination and hydride transfer were analyzed in detail. Qualitatively we observed same kind of intermediates and transition states associated with each step of proposed mechanisms (when compared to Ca^{2+}- cluster) with changes in geometry conformations and energy barriers particularly for the rate-determining steps. For both A-E and H-T, almost all barriers reduced in the presence of Ba^{2+} in the model irrespective of gas phase or presence of solvation, and they are kinetically possible when referred to the general kinetic requirements of an enzymatic catalytic process.

For A-E, the fastest one is Step 2 for any kind of model for both ions. For Model B in presence of water, the barriers for Steps 1 and 3 are 19.5 and 21.4 kcal/mol, respectively, for Ca^{2+} case making both of them rate-limiting, whereas for the Ba^{2+} case, the barriers for both steps are reduced by ~9 kcal/mol making the reaction more kinetically feasible. Thus the A-E mechanism seems to be more plausible with the Ba^{2+} ion in place than with Ca^{2+}.

For H-T the fastest one is Step 2, but the kinetically slower one is Step 1, which involves an hydride transfer to PQQ and a proton abstraction by ASP303 resulting in the formation of formaldehyde for all the models for both ions. For Model B + 3W, the barrier for Step 1 is reduced by 10.3 kcal/mol for the Ba^{2+} case making it more kinetically plausible than in the presence of Ca^{2+}. There is a change in the barriers for other steps in H-T compared to the Ca^{2+}-case, but not as distinctive as Step 1. This huge reduction in barriers for the rate-determining steps for both mechanisms is mainly due to very good stabilization of transition states corresponding to these steps with Ba^{2+} in place.

From experimental kinetic calculations of Goodwin et al. [52] the Gibbs free energy of activation for Ba^{2+}-MDH for the oxidation of methanol is 3.5 kcal/mol, less than 5 kcal/mol than Ca^{2+}-MDH. If we consider this free energy of activation as the free energy barrier for the rate-determining steps for proposed mechanisms, the observed reduction of barrier value in the presence of Ba^{2+} for A-E (8.2 kcal/mol) and H-T (10.3 kcal/mol) is almost twice as much the experimental free energy reduction.

CHAPTER 7

ALTERNATE OXIDATION MECHANISMS

BY MDH

7.1 Methanol A-E Versus H-T Electro-Oxidation Mechanisms by MDH

As we have seen from our energetic profile calculations on the two proposed mechanisms using the best model, Model B + 3W, the initial proton transfer to ASP303 and formation of hemiketal intermediate with C5 of PQQ (Step 1), and the conversion of INT2 to final products through TS3 (Step 3) are two rate-limiting steps for the A-E oxidation mechanism by MDH, whereas the proton and hydride transfers involved in Step 1 of the H-T mechanism make Step 1 the rate-determining according to the calculated free energy barriers. The free energy barriers for these rate-limiting steps of both mechanisms didn't compare well with the experimental free energy barrier for methanol oxidation by wild-type Ca^{2+}-MDH. So the idea here is to see whether the best model used to explore A-E and H-T does actually represent the MDH active site without any major error in the calculations or whether alternate mechanisms exist for oxidation of methanol by MDH. We attempted to look into different pathways for these proton and hydride transfers and whether these changes would affect the free energy barriers of rate-limiting steps using the best model, Model B + 3W.

7.2 Modified A-E Mechanism

Since both Steps 1 (18.9 kcal/mol) and 3 (20.8 kcal/mol) were found to be rate-limiting from our calculations on A-E, we tried modifying the Step 3 as shown in Figure7.1. According to the proposed step 3 of original A-E, there is cleavage of C_{met}-H17 bond and the H17 is transferred to O4 of PQQ with concomitant breakage of C5-O16 bond, resulting in the formation of formaldehyde.
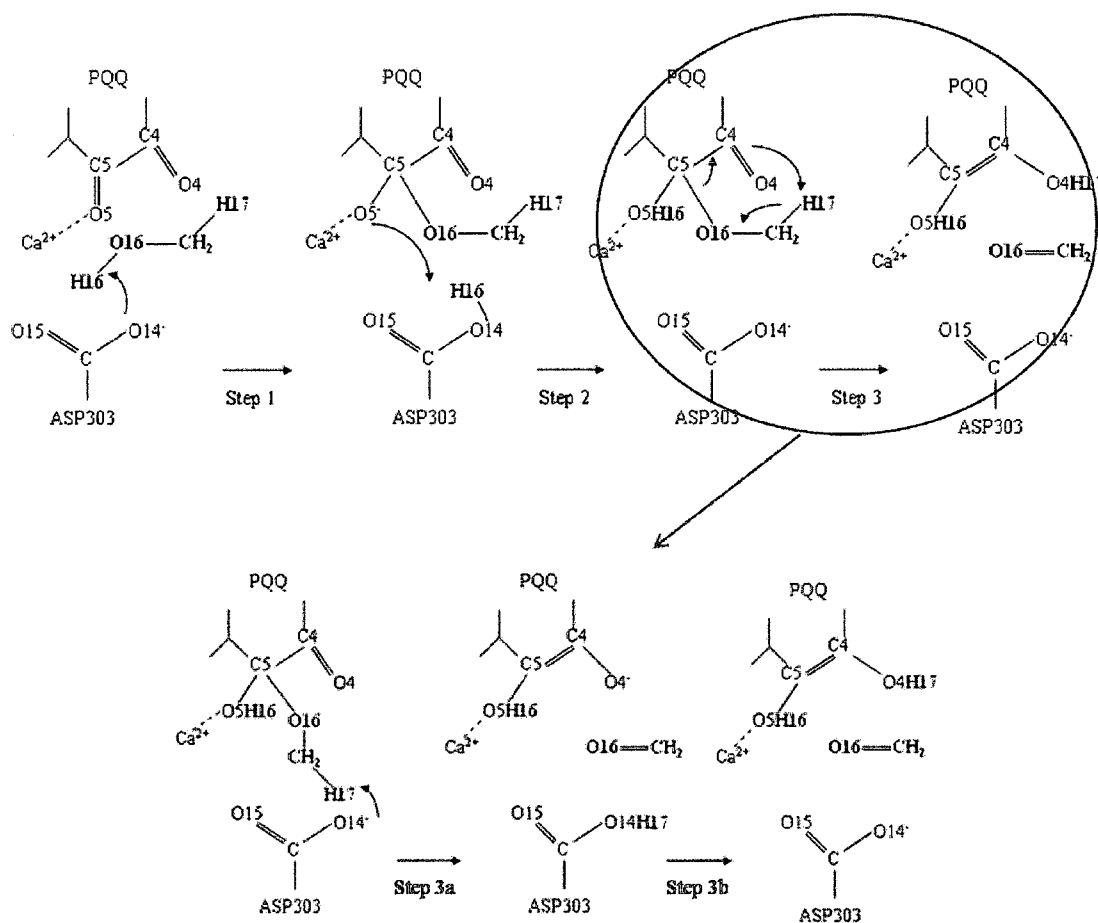
Figure 7.1 Modified A-E. Step 3 is divided into two steps 3a and 3b.

This step was considered to occur as two steps in our modified version (Figure 7.1). The first one involves the cleavage of the C_{met}-H17 bond, thereby transferring H17 to ASP303 in concert with breakage of C5-O16 bond resulting in the formation of

formaldehyde. The second one involves the transfer of proton H17 directly to O4 of PQQ thus getting PQQ reduced here. The assumption is that ASP303 plays a base catalyst role for this final proton transfer, which was not observed in the original A-E but confirmed from our calculations on the original H-T (Chapters 4 & 5). The original two steps (steps 1 &2) are the same as proposed in A-E. With Step 3 considered as two steps, the total number of steps for this modified mechanism is four.

As one can observe from Figure 7.2, the distance between O14 of ASP303 and H17 of the methoxide bonded to PQQ is 2.58 Å compared to O4-H17 distance of 2.51 Å at INT3a, showing that the ASP303 is in a good position to aid this transfer. The transition state TS3a shows the breaking of C5-O16 bond (3.47 Å) and also the transfer of H17 to O14 of ASP. The C_{met}-H17 bond length evolves from 1.10 (INT3a) to 1.70 (TS3a) to 2.58 (INT3b) and the corresponding H17-O14 distances from 2.58 to 1.53 and to 1.01 Å, respectively. So the formation of formaldehyde occurs by the end of this step. W362 maintains hydrogen bonding with ASP303 during the course of this reaction. The free energy required to overcome the transition state for this step is 6.0 kcal/mol with respect to INT3a. Energy of INT3b is lowered by 5.2 kcal/mol with respect to the reactant complex (Figure 7.3).
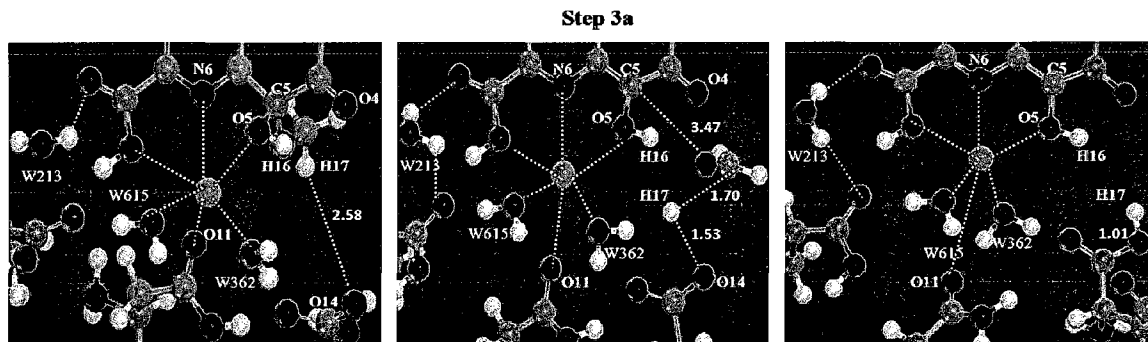
Step 3a

Figure 7.2 Reactive portions of geometry optimized structures involved in step 3a of modified A-E with Model B + 3W (formaldehyde not shown for clarity at INT3b). Distances are in Å.

Once Step 3a is completed, Step 3b should take place (Figure 7.1). The free energy of the intermediate formed by the end of Step 3a (INT3b) was observed to be exactly the same as the free energy of the third intermediate (INT3) from proposed H-T. Then this step (Step 3b) becomes nothing but the final step of the H-T mechanism (Step 4, Chapter 5), which involves the final proton transfer from O14 of ASP303 to O4 of PQQ, thus forming the final product. Step 4 of proposed H-T was already discussed in Chapter 5 for this particular model, and it is not shown here. The free energy barrier obtained for this step is 6.8 kcal/mol with respect to INT3b.

Figure 7.3 Potential energy surface (PES) for A-E and modified A-E by MDH active site Model B + 3W with Ca^{2+}. Reactant-relative energies calculated at the BLPY/DNP theory level are in kcal/mol.

As it can be observed from PES in Figure 7.3, the free energy barrier for Step 3 of original A-E was calculated to be 20.8 kcal/mol for this particular model. But from our modified A-E, if we add up the barriers for Steps 3a and 3b (6 and 6.8 kcal/mol, Figure 7.3), the final barrier is reduced by 8.0 kcal/mol. Also, both these steps combined is exothermic by 9 kcal/mol, similar to Step 3 of A-E.

7.2.1 Ca^{2+} Replaced by Ba^{2+} in the Model and Tested for Modified A-E

The ion is replaced with Ba^{2+} in the model and tested for the modified mechanism, and the reactant relative energies are tabulated below. The free energy barrier for Step 3 for original A-E with Ba^{2+} in place is found to be 13.2 kcal/mol. From modified A-E, the barriers for Steps 3a and 3b add up to 7.6 kcal/mol, reduced by 5.6 kcal/mol. This reduction is smaller compared to Ca^{2+} case (8.0 kcal/mol).

Table 7.1 Reactant-relative energies shown for Ba^{2+} in the model for original A-E (Step 3) and modified A-E (Steps 3a and 3b).

Point	Relative Energy	Point	Relative Energy
INT3	8.4	**INT3a**	8.4
TS3	21.6	**TS3a**	12.3
Prod	-0.7	**INT3b**	5.8
		TS3b	9.5
		Prod	-0.7

7.3 Modified H-T Mechanism (Two-Step H-T)

There is only one rate-determining step (Step 1, 19.7 kcal/mol) observed for the original H-T. We tried to modify this step by proposing that the hydride (H17) transfers directly to O4 instead of C5 of PQQ (Figure 7.4). This transfer allows the possibility to eliminate Steps 3 and 4 of the original proposed H-T, which involves the transfer of H17 from C5 to O14 of ASP303 and from ASP303 to O4 of PQQ. The initial proton abstraction (H16 to O14 of ASP303), which occurs in concert with hydride transfer, remains the same for Step 1. This transfer also allows the possibility for only two-step mechanism, where the second step involves the proton transfer (H16) from O14 of ASP303 to O5 of PQQ, thus getting PQQ reduced in this final step (Figure 7.4).
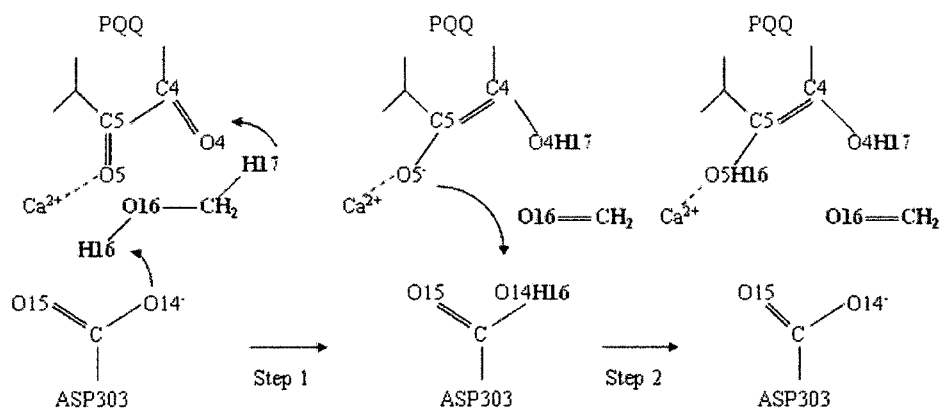
Figure 7.4 The alternate methanol "Two-Step hydride transfer" mechanism by MDH.

From the geometry optimized reactant complex shown in Figure 7.5, it can be observed that O4-H17 distance is 2.98 Å compared to C5-H17, which is 3.69 Å. This indicates that hydride transfer to O4 would be little easier compared to C5 of PQQ. The O14-H16 bond is formed in TS1a representing the first proton transfer to ASP303, and the O4-H17 and C_{met}-H17 distances are 1.32 and 1.50 Å, respectively. At this TS1a (Figure 7.5), the resulting formaldehyde is coordinated to Ca^{2+} (2.78 Å) and also hydrogen bonded to W362 (1.40 Å), which was not observed for TS1 of original H-T. At INT1a, the negatively charged O5 of PQQ is coordinated to the ion and W362. W362 maintains its hydrogen bonding with formaldehyde (1.75 Å) and O5 of PQQ, but formaldehyde loses its coordination with the ion (Figure 7.5).

Figure 7.5 Reactive portions of geometry optimized structures involved in Steps 1 and 2 of Two-Step H-T with Model B + 3W. Distances are in Å.

The free energy barrier for this transition state from the reactant complex is 11.4 kcal/mol compared to 19.7 kcal/mol, with respect to the first transition state for Step 1 of H-T (Figure 7.6). This reduction in the barrier can be due to the more stable transition state of this step as compared to TS1 of the original H-T as explained above. Also the energy of this intermediate, INT1a where O4-H17 bond is completely formed is lowered by 8.7 kcal/mol (Figure 7.6). The reaction is also less endothermic in this case (4.6 compared to 13.3 kcal/mol for Step 1 of H-T).

According to Step 2, the proton transfer from ASP303 to the PQQ is characterized by the second transition state (TS2a) where the O5-H16 and O14-H16 bond lengths are 1.50 and 1.75 Å, respectively (Figure 7.5). The hydrogen bonding of O5 and formaldehyde with W362 slowly starts deteriorating as the reaction proceeds to the final product. Once the proton is transferred to PQQ, W362 forms bonding with ASP303 at the product. The energetic expense of this proton transfer is 8.1 kcal/mol with respect to INT1a.

We observed that this second step can proceed in an alternative way. At INT1a, the hydrogen of W362 (H362) is 1.69 Å from O5 of PQQ, and oxygen (O362) is at a distance of 1.87 Å from H16 of ASP303. So this water molecule can mediate in the proton transfer between ASP303 and O5 of PQQ (Figure 7.5). A transition state is obtained for this step (TS2a`) where the H362 from W362 is transferred to O5 with concomitant transfer of H16 from ASP303 to O362. At this (TS2a`), O5-H362 is 1.32 and O362-H16 is 1.22 Å indicating that this transfer mediated by W362 could occur (Figure 7.5). The product obtained by these transfers looks similar to the original product with W362 forming hydrogen bonding with ASP303, and this product is more stable. The free energy barrier for this step is 6.2 kcal/mol, less by 2 kcal/mol than the direct proton transfer from ASP303 to O5 of PQQ (Figure 7.6).
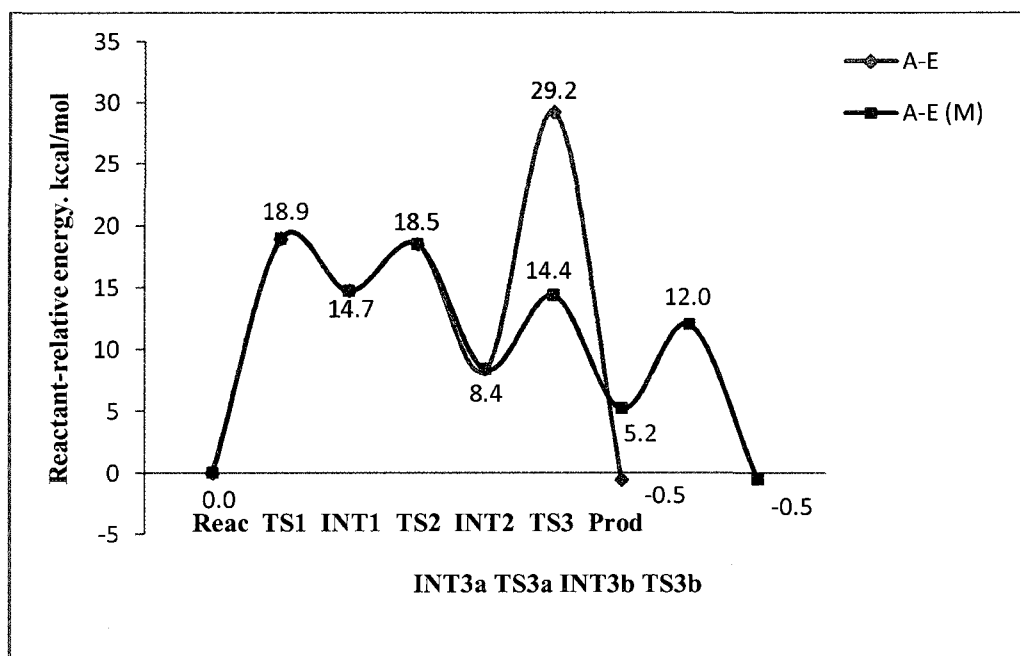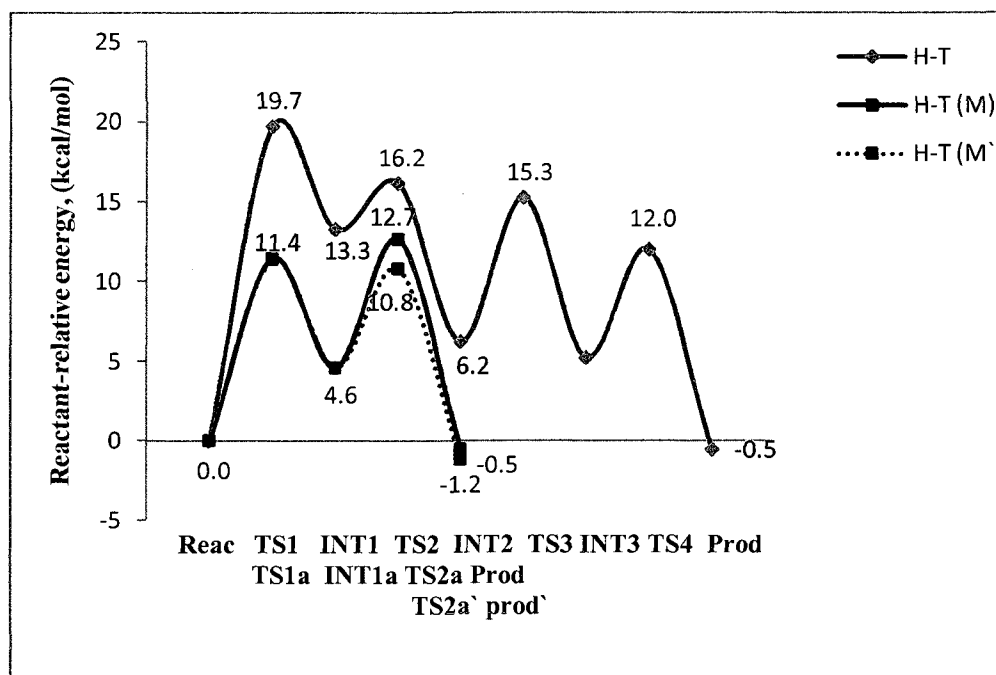
Figure 7.6 Potential energy surface (PES) for H-T and Two-Step H-T by MDH active site Model B + 3W. Reactant-relative energies calculated at the BLPY/DNP theory level are in kcal/mol.

7.3.1 Ca^{2+} Replaced by Ba^{2+} in the Model and Tested for Two-Step H-T

The Two-Step H-T was tested with Ba^{2+} in place in the model. As observed in case of Ca^{2+}, the free energy barrier for new TS1a with respect to reactant complex is reduced by 4.2 kcal/mol compared to original H-T. The energy of the new intermediate is also lowered by 4.6 kcal/mol. The free energy barrier for the second new transition state, TS2a, remains almost the same as previous H-T (Table 7.2). As observed in case of Ca^{2+}, alternate proton transfer mediated by W362 to O5 of PQQ reduced the energy barrier by only one kcal/mol and the energy of the alternate product is more stable.

Table 7.2 Reactant-relative energies shown for Ba^{2+} in the model for original H-T and Two-Step H-T. Values in parenthesis are for alternate proton transfer mediated by water.

Point	Relative Energy	Point	Relative Energy
Reac	0.0	**Reac**	0.0
TS1	10.4	**TS1a**	6.2
INT1	9.2	**INT1a**	4.6
TS2	12.6	**TS2a (TS2a`)**	8.2 (7.1)
INT2	8.7	**Prod (Prod`)**	-0.7(-0.9)
TS3	-----		
INT3	-----		
TS4	-----		
Prod	-0.7		

So our DFT calculations on the modified A-E and H-T mechanisms indicate that the free energy barriers for the rate-determining steps of the original A-E and H-T were reduced by a considerable value. The Step 3 barrier for the modified A-E was reduced by 8.0 and 5.6 kcal/mol when Ca^{2+} and Ba^{2+} are present in the model, respectively. The barrier for Step 1 for modified H-T (Two-Step H-T) was reduced by 8.3 and 4.2 kcal/mol with respect to Ca^{2+} and Ba^{2+} in the model.

The next step is to see whether we can validate the results obtained until now from quantum chemical DFT calculations on MDH active site models used to explore already proposed and suggested new mechanisms using density functional theory based molecular dynamics on a bigger active site model. The conformational changes in the active site of the enzyme can be explored using this technique.

7.4 Validation of MDH Enzyme Oxidation
Mechanisms Using DFT-MD

Classical MD simulations have been employed in the literature for determination of enzyme mechanisms and/or support for a particular one from two or three already proposed [49, 50, 87-89]. MD studies enhance the understanding of the role of the active site residues that are of fundamental importance for a better description of the catalytic mechanism. The motion of crystal waters can be observed from these studies, and in that way one can discover how they are interacting or forming hydrogen bonds with specific species during the simulation [49, 50, 87-89]. A high resolution X-ray crystal structure of the enzyme in the presence of substrate can be used as the starting coordinates for exploration of structure and enzyme mechanisms [49, 50, 87-89].

The idea here is to see whether density functional theory based molecular dynamics could validate the already proposed mechanisms or the suggested new ones proposed in this chapter. The differences between DFT-MD and classical MD are already discussed in the theoretical methods (Chapter 2).

7.4.1 Modeling Procedure Followed for
DFT-MD Calculations

The active site considered for conducting these calculations was taken from the recent 1.2 Å MDH crystal structure [32]. The model consisted of PQQ, Ca^{2+}, ASP303, GLU171, ASN261, and several other residues within a 15 Å radius from the Ca^{2+}. Also, all the crystal waters nearer the catalysis area and PQQ are considered. So this model represents a sphere (Figure 7.7) almost exactly as shown in Figure 1.1b in Chapter 1, where the interactions of active site residues from the 1.2 Å X-ray crystal structure were explained in detail. A hydrogen atom of each residue is kept frozen to prevent unrealistic movement of these residues during MD simulations. A methanol molecule is added to

this model in the same way as we did for DFT models to be proximal to C5 of PQQ and ASP303. This complete reactant complex is geometry optimized first at the BLYP/DNP level in the same way a molecular mechanics calculation is done on the initial structure to obtain a minimum energy structure for performing classical MD (Figure 7.7). Also a dielectric constant of 4 is applied during all DFT-MD calculations in the same way we did for the QM calculations for the neglected protein environment.
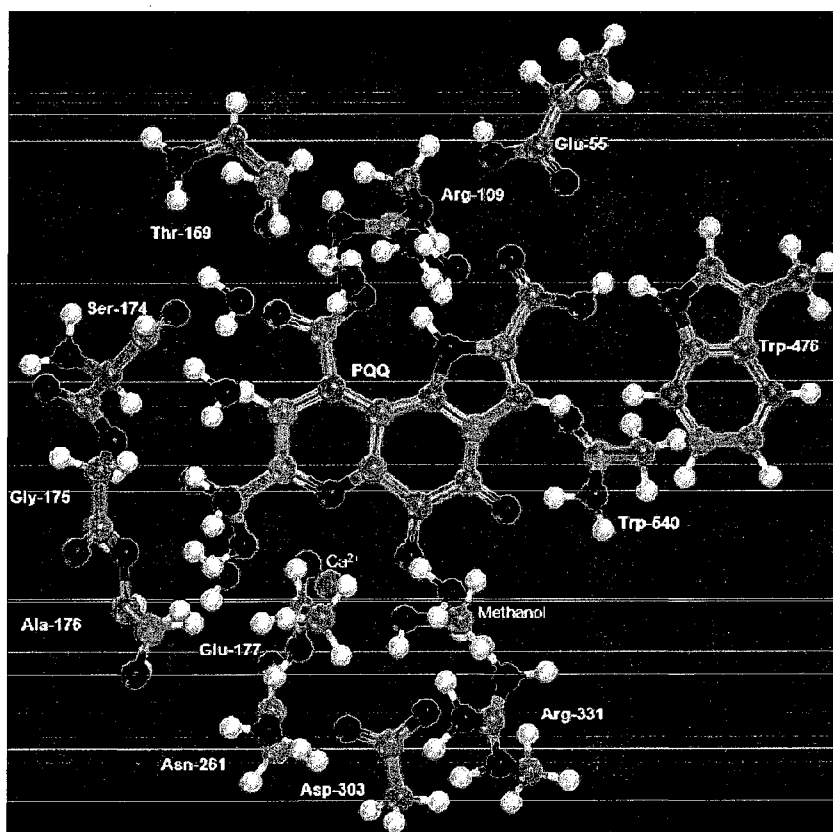
Figure 7.7 MDH active site model selected for DFT-MD calculations.

NVT dynamics was performed first on the reactant complex at room temperature (298.15 K) for 0.5 ps with a Nose-Hoover thermostat with a chain length of 5 (number of thermostats coupled to maintain target temperature in the ensemble) with a time step of 1fs. The final structure obtained after NVT dynamics is used as a starting structure for

NVE calculations at the elevated room temperature. Later NVE dynamics was ran for 1ps with a similar time step as a part of the production run. The important distances were taken after every 100 steps from the NVE dynamics simulation and plotted with respect to simulation time. Reference values for these plotted distances were taken from the minimum energy reactant complex obtained from QM calculations on Model B + 3W. This same procedure is repeated for all the necessary intermediates of the mechanisms proposed in the literature or by us to identify the possibility of reaction by looking at the crucial distance variations between the species during the simulation time.

7.4.1.1 Dynamics of the Reactant Complex

Only the reactive portion of the complex after NVT/NVE simulations is shown in the Figure 7.8 below. Ca^{2+} maintains its coordination with the nitrogen and oxygen atoms of PQQ, the carbonyl oxygen atoms of GLU177 and ASN261, and oxygen atom of water molecule W362. Coordination with W615 observed in QM calculations is not seen here. Also W615 and W213 maintain hydrogen bonding with respect to PQQ, PQQ and GLU177 respectively in accordance with the X-ray crystal structure during this MD simulation.
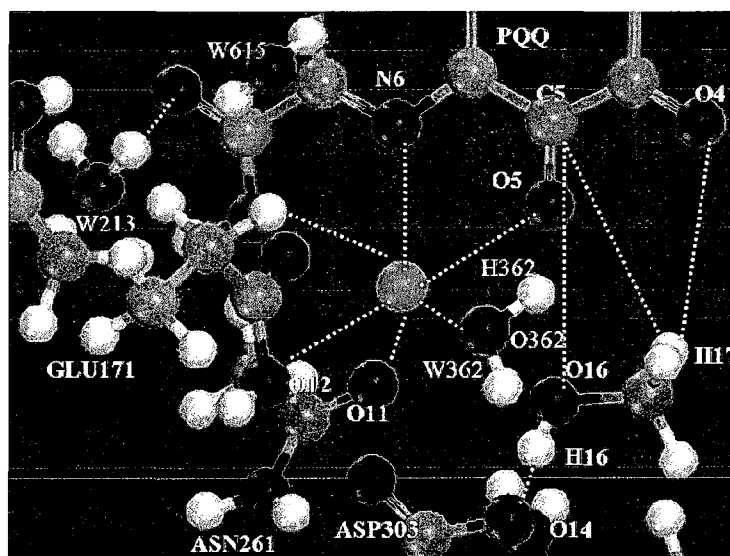
Figure 7.8 Reactive portion of the reactant complex after NVT/NVE simulations.

It has been suggested that ASP303 acts as the general base for initial proton abstraction from methanol (H16), which occurs in Step 1 of both A-E and H-T oxidation mechanisms from the reactant. From our NVE MD studies on reactant complex, we observed that O14-H16 distance (Figure 7.8) didn't vary that much with respect to the reference value (1.64 ± 0.21 Å, Figure 7.9), indicating that initial proton abstraction from methanol by ASP303 can be possible. The distance between C5 of PQQ and H17 of methanol, which corresponds to the hydride transfer and occurs in concert with proton abstraction in first step of H-T, is almost higher during the simulation time (0.12-1.03 Å) and keeps on increasing between 0.6-1ps than the reference value considered (C5-H17 is 3.69 Å from Model B + 3W, Figure 7.9). At the same time, the distance between H17 and O4 of PQQ is observed to decrease first but then maintains near the reference value (O4-H17 is 2.98 Å from Model B + 3W, +0.10-0.17 Å variation, Figure 7.9). This variation may indicate that hydride transfer from methanol to O4 of PQQ might be easier than to C5 of PQQ. This postulation by us was also supported from our free energy barrier

calculations corresponding to these transfers, 11.4 kcal/mol (first step of Two-Step H-T) compared to 19.7 kcal/mol with respect to the Step 1 of original H-T.
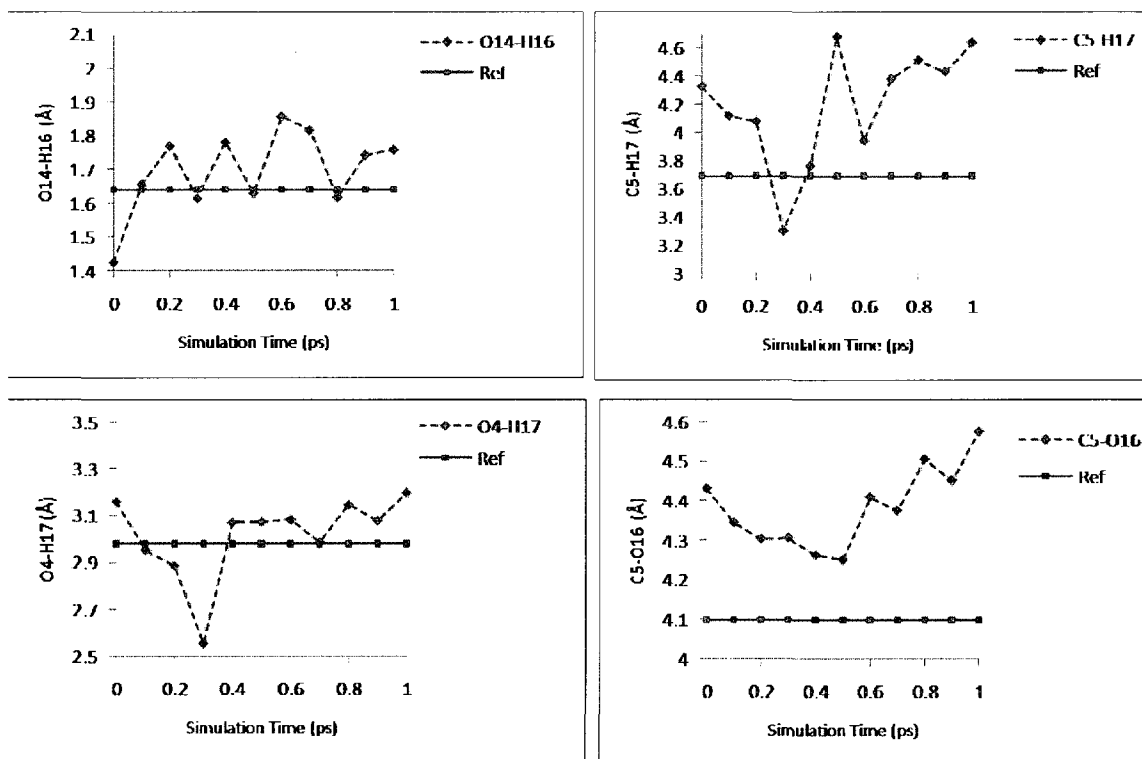
Figure 7.9 Time variation plots of various distances associated with Step 1 of both A-E and H-T.

Next, we observed the possibility of A-E mechanism from the NVT/NVE calculations on the reactant complex. For first step of A-E to occur, in concert with proton abstraction by Asp303, there should be a nucleophilic addition of methanol to C5 of PQQ. For this addition to occur, the methanol oxygen (O16) should be proximal to C5. From our MD calculations, the C5-O16 distance stays continuously higher than the reference and keeps on increasing as the simulation proceeds (C5-O16 is 4.10 Å from Model B + 3W,+0.1-0.6 Å variation, Figure 7.9). This distance is too high for the formation of the C5-O16 bond. Also, the energetic expense for this step to happen is

higher by almost 8 kcal/mol when compared to first step of two-step H-T from our QM calculations. So we can say that the chances of A-E reaction to occur are almost negligible when compared to our new proposed H-T.

7.4.1.2 Dynamics of the First Intermediate from our Two-Step H-T and Proposed H-T

At the intermediate (INT1a) from our Two-Step H-T, the hydride from methanol (H17) is to be completely transferred to O4 of PQQ in addition to the formation of O14-H16 bond indicating proton abstraction by ASP 303 and formation of formaldehyde. This intermediate should lead to the final product, where a proton transfer (H16) should occur from ASP303 to O5 of PQQ, thus getting PQQ reduced. From the NVT/NVE simulations, the distance between H16 from Asp303 to O5 of PQQ is observed to continuously stay above the reference distance (3.56 Å) throughout the simulation time (Figure 7.10).

However, W362 orients itself in such way between the ASP303 and O5 of PQQ (it maintains a hydrogen bond with oxyanion O5 throughout the simulation) that it can mediate this proton transfer. The hydrogen of this water (H362) is always below the reference distance of 1.69 Å from O5 of PQQ for most of the simulation. The same phenomenon is observed for the oxygen (O362) distance from H16 of ASP303 throughout the simulation (Figure 7.10). Even from our QM calculations, this process was observed to happen with a free energy barrier of 6.2 kcal/mol, less by 2 kcal/mol than the direct proton transfer from ASP303 to O5 of PQQ.

The difference between the above intermediate and first intermediate (INT1) of the original proposed H-T is the hydride (H17) transferred to C5 of PQQ (not to O4) resulting in formaldehyde formation. This INT1 should lead to the second one (INT2) in

the proposed H-T where the proton transfer occurs from ASP303 to O5 of PQQ. Dynamics were also performed on this INT1 to see whether W362 also plays a role here. We observed that O5-H16, H16-O362 and H362-O5 distances behave the same way with respect to their reference distances (not shown), thus postulating that proton transfer between ASP303 and O5 of PQQ can be mediated by W362.
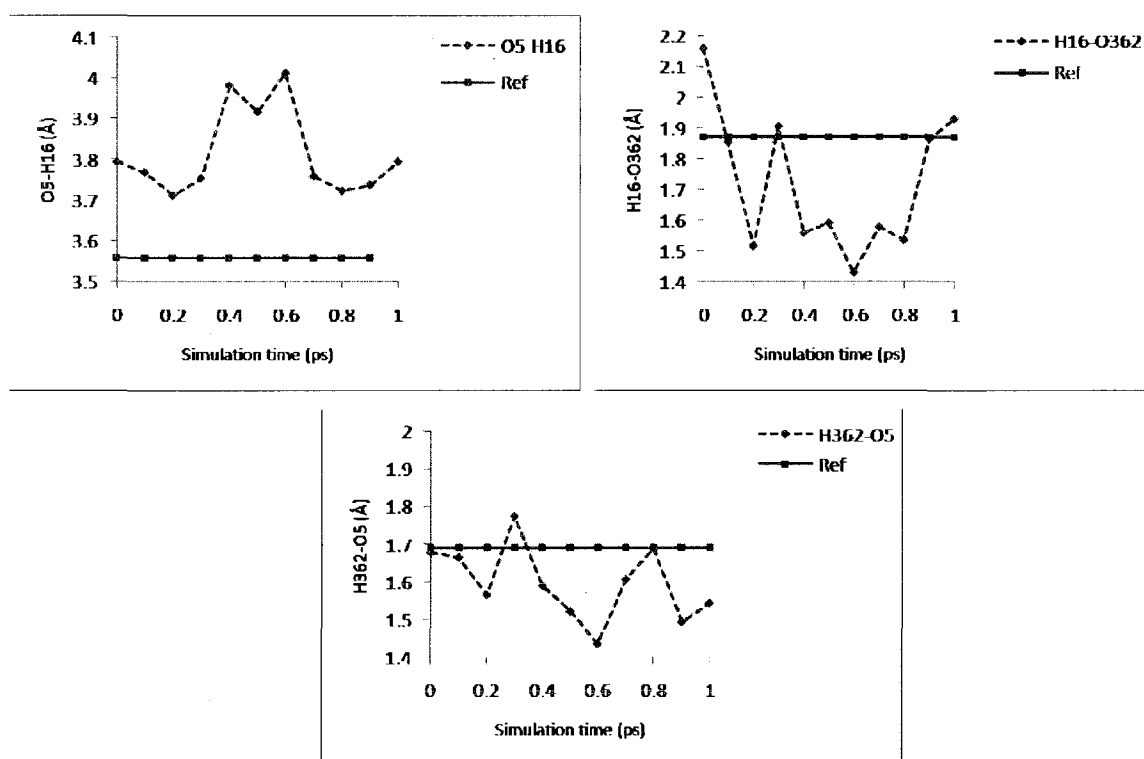
Figure 7.10 Time variation plots of various distances associated with Step 2 of both two-step H-T and original H-T.

7.4.1.3 Dynamics of the Second Intermediate from Proposed H-T

This intermediate (INT2) is formed when proton ASP303 is completely transferred to O5 of PQQ. H17 is already bonded to C5 of PQQ. This INT2 should lead to the final product by transfer of H17 to O4 of PQQ with mediation by ASP 303 as proposed in literature. NVT/NVE dynamics were performed on this INT2 to see whether

ASP303 is in a good position to act as a base catalyst for this transfer. Throughout the simulation time, the distance between H17 and O14 of ASP303 is far higher than the corresponding reference value (more than 3.0 Å, Figure 7.11). From this observations, we can say that ASP303 is not poised to assist in the migration of H17 to O4 of PQQ. So even if the hydride transfer (H17) is done to C5 of PQQ according to Step 1 of original H-T, this intermediate which comes along by the end of the second step is not in a suitable position for the final proton transfer to get PQQ reduced.
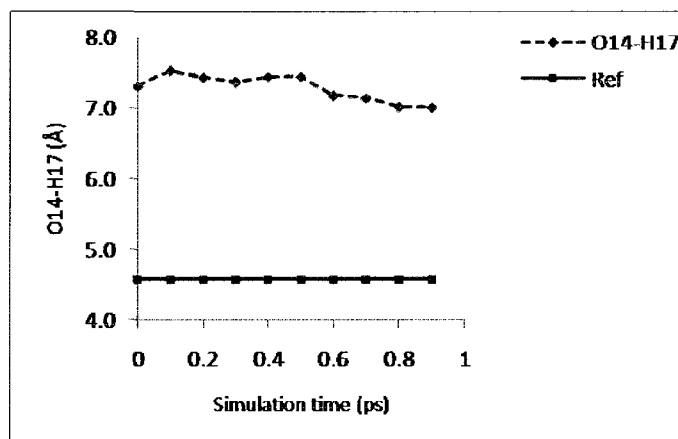
Figure 7.11 Time variation plots of O14-H17 associated with INT2 of H-T.

7.5 Discussion and Summary

In this chapter, alternate oxidation mechanisms by MDH were explored with Model B + 3W with respect to both ions. We proposed a modified A-E where the final step for proton transfer to get PQQ reduced can be mediated by the ASP303 base catalyst because of the low energy barrier associated with it. Even though the barrier for this modified step 3 is reduced comparatively, still the Step 1 is the same as original A-E, whose barrier is really high to be comparable to the experimental value (same case with Ba^{2+} presence in the model).

However, modifications to first step of original H-T resulted in our two-step H-T, where the barrier for the formation of formaldehyde is very much comparable (11.4 kcal/mol) to the experimental Gibbs energy of activation (8.5 kcal/mol). In case of Ba^{2+} presence during this mechanism, the free energy barrier is 6.2 kcal/mol which is comparable to free energy of activation for oxidation of methanol by Ba^{2+}-MDH (3.5 kcal/mol). The second step involving proton transfer in this Two-step H-T was observed to be mediated by a water molecule which was, to the best of our knowledge, held to be impossible in the literature.

Our DFT-MD investigations on the reactant complex, necessary intermediates with a bigger model also leads to the conclusion that oxidation of methanol by MDH is more likely to proceed through our Two-step hydride transfer mechanism compared to proposed A-E and H-T. This oxidation reaction is initiated by proton abstraction by ASP303 from methanol with concomitant transfer of hydride to O4 of PQQ with by-product formaldehyde formation. The final proton transfer to get PQQ reduced can be mediated by W362, which orients itself in such a way to help this transfer.

CHAPTER 8

CONCLUSIONS AND FUTURE WORK

8.1 Conclusions

This dissertation dealt with the investigations of the reaction mechanisms for the oxidation of methanol by methanol dehydrogenase (MDH) enzymes. Both addition-elimination (A-E) and hydride transfer (H-T) mechanisms were examined using models representing the MDH active site. The active site models of this enzyme were developed systematically in order to develop a detailed understanding of the reactions under consideration. Stationary points along the reaction paths were optimized and characterized, and potential energy surfaces for each mechanism for different models were obtained from quantum mechanical DFT calculations. The neglected protein environment of the MDH enzyme while constructing the models is considered by employing dielectric solvation on the optimized gas-phase geometries. By comparing the results of the calculations, like free energy barriers with available experimental data, the plausibility of the proposed and suggested new reaction mechanisms was judged. Finally, DFT based molecular dynamics were performed to validate/confirm the results obtained from QM calculations on a much bigger active site model. The important conclusions drawn from our calculations in this dissertation are

- Addition-elimination mechanism explored with MDH active site models

  - ➤ Solvation had more pronounced effect on the reaction mechanism energies tested with Models A, and B without water. So we can say that some groups which should be explicitly present to account for charge stabilization are absent. Step 1 is the slowest (rate-determining) and Step 2 is fastest in the gas phase and even in solvation of the three steps in A-E with these models. Steps 2 and 3 are plausible from their barriers, but the barrier for Step 1 is very high to be possible for a general enzymatic catalytic process.

  - ➤ Dielectric solvation didn't have much of an impact on the energetics of Model B with water as we observed for other two models. So, most of solvation to stabilize the charged species is already included explicitly in the model with the presence of water. In the gas phase, there is a major decrease in the free energy barrier for Step 1 (~10 kcal/mol), making it kinetically plausible in this case and a slight increase for Step 3 (~ 3.7 kcal/mol) compared to other two models.

  - ➤ A-E seems to be more plausible with all free energy barriers less than or nearer (~ 2 kcal/mol) to 18 kcal/mol when the MDH model consisted of PQQ; Ca^{2+}; ASP303; GLU171; ASN261; and three waters: W362, W615 and W213 (Model B + 3W).

  - ➤ From our calculations with Model B + 3W, Steps 1 and 3 were found to be rate-determining (Step 1, 19.5 kcal/mol and Step 3, 21.4 kcal/mol), whereas in literature only Step 3 was found to be rate-limiting.

➤ Comparison of our rate-determining steps free energy barriers with Gibbs energy of activation for oxidation of methanol by Ca^{2+}-MDH showed that they are higher by approximately 11-13 kcal/mol. This finding indicates that A-E may not be the mechanism under operation for oxidation of methanol.

- Hydride transfer mechanism explored with MDH active site models

  ➤ The energies and therefore the barriers obtained for this mechanism lowered in the presence of solvation for all steps for Model B without water, but the change is not that much as observed for Model A, thereby accounting for some explicit solvation. Also the barriers for all steps except Step 1 are favorable according to the general kinetic requirements for both these models.

  ➤ Solvation didn't have any major impact on the energies with Model B with water (same as in A-E) thereby confirming that all necessary groups for charge stabilization are accounted for in this model. Gas phase barrier for the Step 1 reduced hugely compared to Models A, and B without water making it kinetically plausible.

  ➤ Free energy barrier for Step 1 is observed to be the rate-limiting one with all models and kinetically plausible with only Model B + 3W, which is in accordance with the literature. However this barrier is higher by 9 kcal/mol with respect to barrier obtained from QM/MM calculations by Zhang et al.[51] and less by 11.6 kcal/mol than Leopoldini et al.[58] DFT calculations. Also it is higher by 12.2 kcal/mol than the Gibbs free energy barrier from experimental kinetics on methanol oxidation.

➢ The increase in barrier from H-T in our case can be related to same reason as observed from our A-E calculations: This H-T does not happen as proposed in literature for oxidation of methanol.

- Replacing Ca^{2+} with Ba^{2+} in the MDH active site models and exploring A-E and H-T

  ➢ For Model A with Ba^{2+} presence, dielectric solvation had pronounced effects on the energetics of all steps obtained from the gas phase as observed for this model with Ca^{2+}. For Model B, from gas phase and solvation calculations, it was observed that energetics were affected only for rate-determining steps in solvation. For Model B with three water molecules with Ba^{2+} in the model, calculations indicated that there was not much of a difference in the energetics (~ 2 kcal/mol) with solvation when compared to the gas phase as exactly found for Ca^{2+} in this model.

  ➢ When A-E is examined with all the models, the gas phase barriers obtained with Ba^{2+} in place are within or nearer to the general requirements of enzymes. However, the barriers for all steps are less in case of Model B + 3W, and negligible solvation effects makes it a better model compared to others. Steps 1 and 3 are observed to be rate-determining in this model (same as that with Ca^{2+}) but with reduced barriers (~ 9 kcal/mol) making them kinetically more feasible.

  ➢ For all models examined for H-T, Step 1 is found to be the rate-determining as observed with Ca^{2+} in place for these models. As noted in A-E, negligible solvent effects and less barriers in case of Model B + 3W makes it a better one for analysis of this oxidation mechanism (same case with Ca^{2+} in the

model). For Model B + 3W, the barrier for Step 1 is reduced by 10.3 kcal/mol for Ba^{2+} case.

> Reduction of barrier value in the presence of Ba^{2+} for A-E and H-T obtained with the best model is almost twice as much the experimental free energy reduction with Ba^{2+}-MDH.

- Modified A-E and two-step H-T from our DFT and DFT-MD calculations

  > Our DFT calculations on the modified A-E and H-T mechanisms indicate that the free energy barriers for the rate-determining steps of original A-E and H-T were reduced by a considerable value. The Step 3 barrier for modified A-E was reduced by 8.0 and 5.6 kcal/mol when Ca^{2+} and Ba^{2+} are present in the model, respectively. The barrier for Step 1 for modified H-T (2-step H-T) was reduced by 8.3 and 4.2 kcal/mol with respect to Ca^{2+} and Ba^{2+} in the model.

  > Even though the barrier for this modified Step 3 was reduced comparatively in modified A-E, still the Step 1 is the same as the original A-E, whose barrier is really high to be comparable to the experimental value (same case with Ba^{2+} presence in the model).

  > However, modifications to first step of original H-T resulted in our two-step H-T, where the barrier for the formation of formaldehyde is very much comparable (11.4 kcal/mol) to the experimental Gibbs energy of activation (8.5 kcal/mol). In case of Ba^{2+} presence during this mechanism, the free energy barrier is 6.2 kcal/mol, which is comparable to free energy of activation for oxidation of methanol by Ba^{2+}-MDH (3.5 kcal/mol). The second step involving

proton transfer in this Two-step H-T was observed to be mediated by a water molecule in the presence of both ions.

> DFT-MD investigations on the reactant complex and necessary intermediates associated with all mechanisms also lead us to the conclusion that oxidation of methanol by MDH has a greater probability of proceeding through our two-step hydride transfer mechanism compared to proposed A-E and H-T.

> From our DFT and DFT-MD calculations, we can say confidently that oxidation reaction of methanol is initiated by proton abstraction by ASP303 from methanol with concomitant transfer of hydride to O4 of PQQ with by-product formaldehyde formation. The final proton transfer to get PQQ reduced can be mediated by W362, which orients itself in such a way to help this transfer (Two-Step H-T).

Apart from the above conclusions concerning the specific reaction mechanisms, the overall results of this dissertation prove that the DFT methods, in conjunction with DFT-MD, are very useful tools in the study of enzyme reactions. The effectiveness of the use of relatively small active site models in the elucidation of reaction mechanisms is clearly demonstrated.

8.2 Future Work and Recommendations

8.2.1 Replacing the Ion and Repeating the Calculations

By using the best model from our calculations, methanol oxidation mechanisms (proposed and suggested new ones) by MDH can be explored with other divalent cations in the active site such as Sr^{2+} and Mg^{2+}. Free energy barriers obtained from the rate-limiting steps with these cations can be compared with the ones obtained with Ca^{2+} and

Ba^{2+} calculated barriers from this dissertation work. This comparison could help in determining whether these ion-modified MDH would be more/less active for the oxidation of methanol than Ba^{2+}-MDH as suggested in this work.

8.2.2 Electron Transport from MDH to Cytochrome C_L and to the Anode of Fuel Cell

The calculations in this dissertation are concentrated on analyzing only the methanol oxidation reactions, so the final product from the reactions contain PQQ in the reduced form ($PQQH_2$). In reality, after this, PQQ once again gets re-oxidized by transferring two electrons in sequential manner to its natural electron acceptor (mediator), Cytochrome C_L. The first electron transfer from $PQQH_2$ is supposed to take place in only one route, which involves $PQQH_2 \rightarrow$ disulphide bridge $\rightarrow$ Cys103 $\rightarrow$ W599 $\rightarrow$ W904 $\rightarrow$ cyctochrome C_L (Figure 8.1, solid arrows), and a second electron transfer can go through two ways, the first way from $PQQH \rightarrow$ disulphide bridge $\rightarrow$ Cys104 $\rightarrow$ Asp105 $\rightarrow$ Asn52 $\rightarrow$ Cyctochrome C_L (Figure 8.1, dotted arrows) or the second way from $PQQH \rightarrow$ disulphide bridge $\rightarrow$ Cys103 $\rightarrow$ W599 $\rightarrow$ W904 $\rightarrow$ cyctochrome C_L (just like first electron transfer) [32,39]. All these routes were only postulated, none was confirmed in the literature [32,39]. So future work can be concentrated on performing QM/MM calculations to study this electron transport process.

These hybrid QM/MM methods were shown capable of solving the Schrodinger equation on a selected active part of the enzyme, defined as the quantum region, describing its electronic structure under the polarization effects of the remainder of the protein environment defined by molecular mechanics. By selectively turning on and off different residues in the quantum region, the electron pathway for short-and large-range interactions can be obtained [90].

This novel methodology as proposed in the literature[90] consists of the following procedure. First the donor ($PQQH_2$) and acceptor (heme group of cytochrome C_L) molecules should be identified from the starting structure taken from high resolution X-ray crystal structure containing both MDH and cytochrome. Then parameters for both the donor and acceptor are set such that, oxidation states are matched [90]. By doing so, it can be postulated that the electron has already left the donor but has yet to arrive at the acceptor. This parameterization, consisting of a QM/MM calculation from which the electrostatic potential fitted charges are extracted, is important since the procedure continues by placing both the donor and the acceptor in the classical region (so, no electronic description of these residues exists in the quantum region) [90]. Instead, the focus will be on the 'transfer region' between them, the region that now contains the electron.
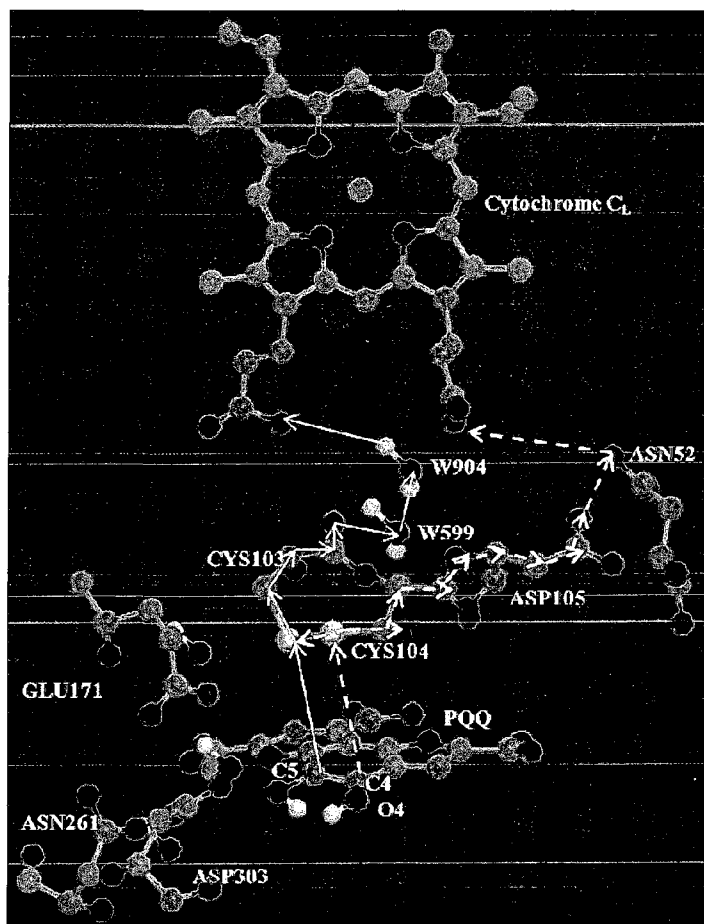
Figure 8.1 Electron transport process from PQQH$_2$ in MDH to cytochrome C$_L$ (only important portions of both MDH and cytochrome are shown). Disulphide bridge formed between Cys 103 and 104 is highlighted in yellow [32, 39].

A first iteration is performed at the QM/MM level by including the entire transfer region in the QM subsystem where this electron is added to the system and a doublet spin state is specified. Once the first receptor for this electron has been located from first iteration, we proceed to the second iteration by turning the first identified residue into the classical description (MM region), thus excluding it from the QM region. By excluding this residue, no electronic description of it is allowed; therefore, the additional electron within the system needs to find another host. For this reason, a search for second electron acceptor in the transfer region will be done. These iterations are continued until a direct

pathway connecting the donor and the acceptor was observed. Thus, this method consists in finding the residues with larger electron affinity in the transfer region, expecting that they will define an electron transfer pathway [90]. These whole procedure can be repeated for identifying the two sequential electron transfers from $PQQH_2$ in MDH to heme group in cytochrome C_L.

Once this electron transport to the cytochrome is essentially understood, then electron mediation from the cytochrome to the anode of the biofuel cell where this enzyme acts as an anodic catalyst can be analyzed. Cyclic voltammograms can be obtained with dynamic monte carlo (DMC) simulations at different temperature and pressure conditions where the anodic current is plotted as a function of applied voltage. All these proposed studies can further help in understanding the limitations and improving them to make this enzyme as a better catalyst for biofuel cell applications.

REFERENCES

[1].   N. M. Markovic and P. N. Ross, "Surface Science Studies of Model Fuel Cells Electrocatalysts," *Surface Science Reports*, vol. 286, pp. 1-113, 2002.

[2].   S. J. C. Cleghorn, X. Ren, T. E. Springer, M. S. Wilson, C. Zawodzinski, T. A. Zawodzinski and S. Gottesfeld, "PEM fuel cells for transportation and stationary power generation applications," *International Journal of Hydrogen Energy*, vol. 22, pp. 1137-1144, 1997.

[3].   M. Iwase and S. Kawatsu, presented at the First International Symposium on Proton Conducting Membrane Fuel Cells, Houston, 1995.

[4].   V. Mehta and J. S. Cooper, "Review and Analysis of PEM Fuel Cell Design and Manufacturing," *Journal of Power Sources*, vol. 114, pp. 32-53, 2003.

[5].   J. O. M. Bockris and S. U. M. Khan, *Surface electrochemistry: a molecular level approach*. New York: Plenum Press, 1993.

[6].   T. Rades, V. Y. Borokov, V. B. Kazansky, M. Polisset-Thfoin and J. Fraissard, "Diffuse reflectance IR study of CO adsorption on a bimetallic Pt-Pd catalyst supported on NaY zeolite. Evidence of alloy formation.," *Journal of Physical Chemistry*, vol. 100, pp. 16238-16241, 1996.

[7].   M. Fernandez-Garcia, J. A. Anderson and G. L. Halter, "Alloy Formation and Stability in Pd-Cu Bimetallic Catalysts," *Journal of Physical Chemistry*, vol. 100, pp. 16247-16254, 1996.

[8].   B. C. Beard and P. N. J. Ross, "The Structure and Activity of Pt-Co Alloys as Oxygen Reduction Electrocatalysts," *Journal of Electrochemical Society*, vol. 137, pp. 3368-3374, 1990.

[9].   N. Neergat, A. K. Shukla and K. S. Gandhi, "Platinum-Based Alloys As Oxygen-Reduction Catalysts for Solid-Polymer-Electrolyte Direct Methanol Fuel Cells," *Journal of Applied Electrochemistry*, vol. 31, pp. 373-378, 2001.

[10].   T. Toda, H. Igarashi and M. Watanabe, "Enhancement of the Electrocatalytic O_2 Reduction on Pt-Fe Alloys," *Journal of Electroanalytical Chemistry*, vol. 460, pp. 258-262, 1999.

[11]. T. Toda, H. Igarashi, H. Uchida and M. Watanabe, "Enhancement of the Electroreduction of Oxygen on Pt Alloys with Fe, Ni, and Co," *Journal of Electrochemical Society*, vol. 146, pp. 3750-3756, 1999.

[12]. S.-P. Huang, D. S. Mainardi and P. B. Balbuena, "Structure and Dynamics of Graphite-Supported Bimetallic Nanoclusters," *Surface Science*, vol. 545, pp. 163-179, 2003.

[13]. M. Koper, "A Lattice-Gas Model for Halide Adsorption on Single-Crystal Electrodes," *Journal of Electroanalytical Chemistry*, vol. 450, pp. 189-201, 1998.

[14]. V. Stamenkovic, N. M. Markovic and P. N. Ross, "Structure-relationships in electrocatalysis: oxygen reduction and hydrogen oxidation reactions on Pt(111) and Pt(100) in solutions containing chloride ions," *Journal of Electroanalytical Chemistry*, vol. 500, pp. 44-51, 2001.

[15]. N. M. Markovic, H. A. Gasteiger, B. N. Grgur and P. N. Ross, "Oxygen Reduction Reaction on Pt(111): Effects of Bromide," *Journal of Electroanalytical Chemistry*, vol. 467, pp. 157-163, 1999.

[16]. S.-P. Huang and P. B. Balbuena, "Platinum Nanoclusters on Graphite Substrates: A Molecular Dynamics Study," *Molecular Physics*, vol. 100, pp. 2165-2174, 2002.

[17]. S.-P. Huang and P. B. Balbuena, "Melting of bimetallic Cu-Ni nanoclusters," *Journal of Physical Chemistry B*, vol. 106, pp. 7225-7236, 2002.

[18]. N. Combe, P. Jensen and A. Pimpinelli, "Changing Shapes in the Nanoworld," *Physical Review Letters*, vol. 85, pp. 110-113, 2000.

[19]. M. Heinebrodt, N. Malinowski, F. Tast, W. Branz, I. M. l. Billas and T. P. Martin, "Bonding character of bimetallic clusters Au_nX_m (X = Al, In, Cs)," *Journal of Chemical Physics*, vol. 110, pp. 9915-9921, 1999.

[20]. T. Abe and M. Kaneko, "Reduction Catalysis by Metal Complexes Confined in a Polymer Matrix," *Progress in Polymer Science*, vol. 28, pp. 1441-1488, 2003.

[21]. A. A. Karyakin, S. V. Morozov, E. E. Karyakina, V. S.D., N. A. Zorin and S. Cosnier, "Hydrogen Fuel Electrode Based on Bioelectrocatalysis by the Enzyme Hydrogenase," *Electrochemistry Communications*, vol. 4, pp. 417-420, 2002.

[22]. A. Heller, "Miniature biofuel cells," *Physical Chemistry Chemical Physics*, vol. 6, pp. 209-216, 2004.

[23]. L. de la Garza, G. Jeong, P. Liddell, T. Sotomura, T. A. Moore, A. L. Moore and D. Gust, "Enzyme-Based Photoelectrochemical Biofuel Cell," *Journal of Physical Chemistry B*, vol. 107, pp. 10252-10260, 2003.

[24]. A. Heller, "Miniature Biofuel cells," *Journal of Physical Chemistry A*, vol. 6, pp. 209-216, 2004.

[25]. A. Pizzarielo, M. Stredansky and S. Miertus, "A Glucose/Hydrogen Peroxide Biofuel Cell That Uses Oxidase and Peroxidase as Catalysts by Composite Bulk-Modified Bioelectrodes Based on a Solid Binding Matrix," *Journal of Bioelectrochemistry*, vol. 56, pp. 99-105, 2002.

[26]. H. H. Kim, N. Mano, Y.Zhang and A.Heller, "A Miniature Membrane-Less Biofuel Cell Operating under Physiological Conditions at 0.5 V," *Journal of Electrochemical Society*, vol. 150, pp. 209-213, 2003.

[27]. X.C. Zhang, A. Ranta and A. Halme, "Direct methanol biocatalytic fuel cell—Considerations of restraints on electron transfer," *Journal of Biosensors and Bioelectronics*, vol. 21, pp. 2052-2057, 2006.

[28]. A. Pizzarielo, M. Stredansky and S. Miertus, "A Glucose/Hydrogen Peroxide Biofuel Cell That Uses Oxidase And Peroxidase as Catalysts by Composite Bulk-Modified Bioelectrodes Based on a Solid Binding Matrix," *Bioelectrochemistry*, vol. 56, pp. 99-105, 2002.

[29]. H. H. Kim, N. Mano, Y. Zhang and A. Heller, "A miniature Membrane-Less Biofuel Cell Operating Under Physiological Conditions at 0.5 V," *Journal of Electrochemical Society*, vol. 150, pp. A209-A213, 2003.

[30]. X-C. Zhang, A. Ranta and A. Halme, "Direct methanol biocatalytic fuel cell-Considerations of restraints on electron transfer.," *Biosensors and Bioelectronics*, vol. 45, pp. 2052-2057, 2006.

[31]. M. Ghosh, C. Anthony, K. Harlas, M. G. Goodwin and C. C. F. Blake, "The Refined Structure of the Quinoprotein Methanol Dehydrogenase from Methylobacterium Extorquens at 1.94 Å," *Structure (London)*, vol. 3, pp. 1771-1787, 1995.

[32]. P. A. Williams, L. Coates, F. Mohammed, R. Gill, P. T. Erskine, A. Coker, S. P. Wood, C. Anthony and J. B. Cooper, "The atomic resolution structure of methanol dehydrogenase from Methylobacterium extorquens," *Acta Crystallography Section D*, vol. D61, pp. 75-79, 2005.

[33]. S. White, G. Boyd, F. S. Mathews, Z. X. Xia, W. W. Dai, Y. S. Zhang and V. L. Davidson, "The Active Site Structure of Calcium Containing Methanol Dehydrogenase," *Journal of Biochemistry*, vol. 32, pp. 12955-12958, 1993.

[34]. Z. X. Xia, W. W. Dai, J. P. Xiong, Z. P. Hao, V. L. Davidson, S. White and F. S. Mathews, "The Three-Dimensional Structures of Methanol Dehydrogenase from Two Methylotrophic Bacteria at 2.6 Å Resolution," *Journal of Biological Chemistry*, vol. 267, pp. 22289-22297, 1992.

[35]. Z. X. Xia, Y. N. He, W. W. Dai, S. White, G. Boyd and F. S. Mathews, "Determination of Gene sequence and Three-dimensional Structure at 2.4 Å resolution of Methanol Dehydrogenase from *Methylophilus W3A1*," *Journal of Molecular Biology*, vol. 259, pp. 480-501, 1996.

[36]. Z. X. Xia, Y. N. He, W. W. Dai, S. White, G. Boyd and F. S. Mathews, "Detailed Active Site Configuration of a New Crystal Form of Methanol Dehydrogenase from Methylophilus W3a1 at 1.9 Å Resolution," *Biochemical Journal*, vol. 38, pp. 1214-1220, 1999.

[37]. C. Anthony, *Methanol Dehydrogenase, a PQQ-Containing Quinoprotein Dehydrogenase*. New York: Kluwer Academic/Plenum Publishers, 2000.

[38]. M. E. Lidstrom and L. Chistoserdova, "Plants in the Pink: Cytokinin Production by Methylobacterium," *Journal of Bacteriology*, vol. 184, pp. 1818, 2002.

[39]. C. Anthony and P. Williams, "The Structure and Mechanism of Methanol Dehydrogenase," *Biochimica. Biophysica. Acta*, vol. 1647, pp. 18-23, 2003.

[40]. P.R. Afolabi, K. Amaratunga, O. Majekodunmi, S. L. Dales, R. Gill, D. Thompson, J. B. Cooper, S. P. Wood, P. M. Goodwin and C. Anthony, "Site-Directed Mutagenesis and XRay-Crystallography of the PQQ-Containing Quinoprotein Methanol Dehydrogenase and Its Electron Acceptor, Cytochrome CL," *Biochemical Journal*, vol. 40, pp. 9799-9809, 2001.

[41]. J. Frank, S.H. van Krimpen, P.E.J.Verwiel, J.A. Jongejan and A.C. Mulder, "On the mechanism of inhibition of methanol dehydrogenase by cyclopropane-derived inhibitors," *European Journal of Biochemistry*, vol. 184, pp. 187-195, 1989.

[42]. A.J.J. Olsthoorn and J.A. Duine, "On the mechanism and specificity of the soluble, quinoprotein glucose dehydrogenase in the oxidation of aldose sugars.," *Biochemical Journal*, vol. 37, pp. 13854-13861, 1998.

[43]. J. Frank, M. Dijkstra, J.A. Duine and C. Balny, "Kinetic and spectral studies on the redox forms of methanol dehydrogenase from Hyphomicrobium X," *European Journal of Biochemistry*, vol. 174, pp. 331-338, 1988.

[44]. S. Itoh, H. Kawakami and S. Fukuzumi, "Model Studies on Calcium-Containing Quinoprotein Alcohol Dehydrogenases. Catalytic Role of Ca2+ for the Oxidation of Alcohols by Coenzyme PQQ (4,5 Dihydro-4,5-Dioxo-1h-Pyroolo[2,3-F]Quinoline-2,7,9-Tricarboxylic Acid)," *Journal of Biochemistry*, vol. 37, pp. 6562-6571, 1998.

[45]. S. Itoh, H. Kawakami and S. Fukuzumi, "Development of the Active Site Model for Calcium-Containing Quinoprotein Alcohol Dehydrogenases," *Journal of Molecular Catalysis B*, vol. 8, pp. 85-94, 2000.

[46]. A. Oubrie, H.J. Rozeboom, K.H. Kalk, A.J. Olsthoorn, J.A. Duine and B. W. Dijkstra, "Structure and mechanism of soluble quinoprotein glucose dehydrogenase," *EMBO Journal*, vol. 18, pp. 5187-5194, 1999.

[47]. A. Oubrie, H.J. Rozeboom, K.H. Kalk, E.J. Huizinga and B. W. Dijkstra, "Crystal structure of quinohemoprotein alcohol dehydrogenase from Comamonas testosteroni; structural basis for substrate oxidation and electron transfer," *Journal of Biological Chemistry*, vol. 277, pp. 3727-3732, 2002.

[48]. Y. J. Zheng and T. C.Bruice, "Conformation of Coenzyme Pyrroloquinoline Quinone and the Role of Ca2+ in the Catalytic Mechanism of Quinoprotein Methanol Dehydrogenase," *Proceedings of National Academy of Sciences*, vol. 94, pp. 11881-11886, 1996.

[49]. S. Y. Reddy, F. S. Mathews, Y. J. Zheng and T. C. Bruice, "Quinoprotein Methanol Dehydrogenase: A Molecular Dynamics Study and Comparison with Crystal Structure," *Journal of Molecular Structure*, vol. 655, pp. 269-277, 2003.

[50]. S. Y. Reddy and T. C.Bruice, "In-Silico Studies of the Mechanism of Methanol Oxidation by Quinoprotein Methanol Dehydrogenase," *Journal of American Chemical Society*, vol. 125, pp. 8141-8150, 2003.

[51]. X. Zhang, S. Y. Reddy and T. C. Bruice, "Mechanism of methanol oxidation by quinoprotein methanol dehydrogenase," *Proceedings of National Academy of Sciences*, vol. 104, pp. 745-749, 2007.

[52]. M. G. Goodwin and C. Anthony, "Characterization of a Novel Methanol Dehydrogenase Containing a Ba2+ Ion at the Active Site," *Biochemical Journal*, vol. 318, pp. 673-679, 1996.

[53]. C. W. M. Kay, B. Mennenga, H. Gorisch and R. Bittl, "Substrate binding in quinoprotein ethanol dehydrogenase from Pseudomonas aeruginosa studied by electron-nuclear double resonance," *Proceedings of the National Academy of Sciences of the United States of America*, vol. 103, pp. 5267-5272, 2006.

[54]. F. Himo, "Quantum chemical modeling of Enzyme active sites and reaction mechanisms," *Theoretical Chemistry Accounts*, vol. 116, pp. 232-240, 2006.

[55]. K. H. Hopmann and F. Himo, "Theoretical Study of the Full Reaction Mechanism of Human Soluble Epoxide Hydrolase," *Chemistry: A European Journal*, vol. 12, pp. 6898-6909, 2006.

[56]. K. H. Hopmann and F. Himo, "Quantum Chemical Modeling of the Dehalogenation Reaction of Haloalcohol Dehalogenase," *Journal of Chemical Theory and Computation*, vol. 4, pp. 1129-1137, 2008.

[57]. L. Noodleman, T. Lovell, W. Han, J. Li and F. Himo, "Quantum Chemical Studies of Intermediates and Reaction Pathways in Selected Enzymes and Catalytic Synthetic Systems," *Journal of Chemical Reviews*, vol. 104, pp. 459-508, 2004.

[58]. M. Leopoldini, N. Russo and M. Toscano, "The Preferred Reaction Path for the Oxidation of Methanol by PQQContaining Methanol Dehydrogenase: Addition–Elimination versus Hydride-Transfer Mechanism," *Chemistry: A European Journal*, vol. 13, pp. 2109-2117, 2007.

[59]. P. Velichkova and F. Himo, "Theoretical Study of the Methyl Transfer in Guanidinoacetate Methyltransferase," *Journal of Physical Chemistry B*, vol. 110, pp. 16-19, 2006.

[60]. R. Sevastik and F. Himo, "Quantum chemical modeling of enzymatic reactions: The case of 4-oxalocrotonate tautomerase," *Bioorganic Chemistry*, vol. 35, pp. 444-457, 2007.

[61]. R. Zhen Liao, J. Yu, F. M. Raushel and F. Himo, "Theoretical Investigation of the Reaction Mechanism of the Dinuclear Zinc Enzyme Dihydroorotase," *Chemistry: A European Journal*, vol. 14, pp. 4287-4292, 2008.

[62]. N. B. Idupulapati and D. S. Mainardi, "The Binding and Co-ordination of Ca^{2+} and Ba^{2+} in the Active Site of Methanol Dehydrogenase and interactions with Methanol," *Journal of Molecular Structure: TheoChem (in press)*, vol., pp. 2009.

[63]. T.K. Harris and V.L. Davidson, "Replacement of enzyme-bound calcium with strontium alters the kinetic properties of methanol dehydrohenase," *Biochemical Journal*, vol. 300, pp. 175-182, 1994.

[64]. F. Jensen, *Introduction to Computational Chemistry*. New York: Wiley & Sons, 2002.

[65]. A.R. Leach, *Molecular Modeling: principles and applications*. London: Prentice Hall, 2001.

[66]. E. lewars, *Introduction to the Theory and Applications of Molecular and Quantum Mechanics*. Norwell: Kluwer Academic Publications, 2003.

[67]. J. B. Foresman and A. Frisch, *Exploring Chemistry with Electronic Structure Methods*. Pittsburgh, PA: Gaussian,Inc, 1996.

[68]. W. J. Hehre, L. Radom, P. V. R. Schleyer and J. A.Pople, *Ab Initio Molecular Orbital Theory*. New York: Wiley & Sons, 1986.

[69]. C. J. Cramer, *Essentials of Computational Chemistry: Theories and Models*. West Sussex: Wiley & Sons, 2004.

[70]. P. Hohenberg and W. Kohn, "Inhomogeneous electron gas," *Physical Review B*, vol. 136, pp. 864-871, 1964.

[71]. W. Koch and M. C. Holthausen, *A Chemist's Guide to Density Functional Theory*. Wiley-CVH, 2001.

[72]. W. Kohn and L. J. Sham, "Self-consistent equations including exchange and correlation effects," *Physical Review A*, vol. 140, pp. 1133-1138, 1965.

[73]. J. P. Perdew, *Electronic Structure of Solids*. Berlin: Akademie Verlag, 1991.

[74]. J. P.Perdew, J. A Chevary, S. H.Vosko, K. A. Jackson, M. R. Pederson, D. J. Singh and C. Fiolhais, "Atoms, molecules, solids, and surfaces: applications of the generalized gradient approximation for exchange and correlation," *Physical Review B*, vol. 46, pp. 6671-6687, 1992.

[75]. R. M. Dreialer and E. K. U. Gross, *Density Functional Theory: An Approach to Quantum Many Body Problem*. Berlin: Springer, 1990.

[76]. Y. Wang, "Accurate and simple analytic representation of the electron-gas correlation energy," *Physical Review B*, vol. 45, pp. 13244-13249, 1992.

[77]. C. Lee, W. Yang and R. Parr, "Accurate and simple analytic representation of the electron-gas correlation energy," *Physical Review B: Condensed Matter*, vol. 37, pp. 786, 1998.

[78]. Accelrys Inc., Materials Studio (San Diego, 2006).

[79]. Accelrys Inc., DMOL^3 User Guide (San Diego, 2003).

[80]. M.E Grillo, N. Govind, G. Fitzgerald and K. B. Stark, "Computational Material Science with Materials Studio: Applications in Catalysis," *Lecture Notes in Physics*, vol. 642, pp. 202-227, 2004.

[81]. N. Govind, M. Petersen, G. Fitzgerald, D. King-Smith and J. Andzelm, " A generalized synchronous transit method for transition state location," *Computational Material Science*, vol. 28, pp. 250-258, 2003.

[82]. D. Marx and J. Hutter, "Ab initio molecular dynamics: Theory and Implementation," *Modern Methods and Algorithms of Quantum Chemistry*, vol. 1, pp. 301-449, 2000.

[83]. R. Cammi, B. Mennucci and J. Tomasi, *Journal of Physical Chemistry A*, vol. 103, pp. 9100, 1999.

[84]. R. Cammi, B. Mennucci and J. Tomasi, *Journal of Physical Chemistry A*, vol. 104, pp. 5631, 2000.

[85]. N. B. Idupulapati and D. S. Mainardi, "A DMOL^3 Study of the Methanol Addition-Elimination Oxidation Mechanism by Methanol Dehydrogenase Enzyme," *Molecular Simulation*, vol. 34, pp. 1057-1064, 2008.

[86]. N. B. Idupulapati and D. S. Mainardi, in *Modern Aspects of Electrochemistry, Volume 46: Advances in Electrocatalysis (in press)*, edited by P. B. Balbuena (Springer, 2008).

[87]. R. Zhu, F. Janetzko, Y. Zhang and D. Salahub, "Characterization of the active site of yeast RNA polymerase II by DFT and ReaxFF calculations," *Theoretical Chemistry Accounts*, vol. 120, pp. 479-489, 2008.

[88]. S.P. Huang, D. S. Mainardi and P. B. Balbuena, "Structure and Dynamics of Graphite-Supported Bimetallic Nanoclusters," *Journal of Surface Science*, vol. 545, pp. 163-179, 2003.

[89]. S.P. Huang and P. B. Balbuena, "Platinum nanoclusters on Graphite Substrates: A Molecular Dynamics Study," *Journal of Molecular Physics*, vol. 100, pp. 2165-2174, 2002.

[90]. V. Guallar and F. Wallrapp, "Mapping protein electron transfer pathways with QM/MM methods," *Journal of Royal Society Interface*, vol. 5, pp. 233-239, 2008.